Engineering Nanolayers for Localized Delivery of siRNA

by

Jonathan Ju-En Chou

B.S.E. Chemical and Biomolecular Engineering
University of Pennsylvania, Philadelphia, PA – 2014

SUBMITTED TO THE DEPARTMENT OF CHEMICAL ENGINEERING IN PARTIAL FULFILLMENT OF THE REQUIREMENTS FOR THE DEGREE OF

DOCTOR OF PHILOSOPHY IN CHEMICAL ENGINEERING
AT THE
MASSACHUSETTS INSTITUTE OF TECHNOLOGY

SEPTEMBER 2020

Signature of Author: _____
Department of Chemical Engineering
August 4, 2020

Certified by: _____
Paula T. Hammond
David H. Koch Professor of Chemical Engineering
Thesis Supervisor

Accepted by: _____
Patrick S. Doyle
Robert T. Haslam Professor of Chemical Engineering
Graduate Officer

Engineering Nanolayers for Localized Delivery of siRNA

by

Jonathan Ju-En Chou

Submitted to the Department of Chemical Engineering on August 4, 2020 in Partial Fulfillment of the Requirements for the Degree of Doctor of Philosophy in Chemical Engineering

Technical Summary

RNA interference (RNAi) is a promising technology for therapeutic application. The RNAi pathway involves sequence-specific gene silencing directed by RNA fragments of 21-23 nucleotides long known as short interfering RNA (siRNA). The great potential for siRNA to modulate gene expression has prompted research in treatment for diseases including inflammatory disorders, viral infections, and a host of cancers. Yet siRNA therapy is not without its challenges. Delivery barriers such as nuclease degradation, rapid clearance, cell membrane rejection, and lysosomal degradation must be overcome for effective siRNA therapy.

Local delivery of siRNA presents advantages including reducing off-target effects, increased efficacy at target site, and reduction in load requirements compared to systemic siRNA administration. Layer-by-layer (LbL) self-assembly technology is a promising method of nanolayer surface coating fabrication for the localized and controlled delivery of therapeutics. One area of particular interest for controlled localized siRNA delivery is the treatment of soft tissue wounds. Wound healing is a complex, multi-staged process wherein dysregulation in whichever healing phase may cause severe complications for patients.

Here we present the engineering of LbL thin films for localized delivery of siRNA. We design LbL films for release of multiple siRNAs. By tuning film architecture and incorporating barrier layers to prevent interlayer diffusion, we achieve sequential release of siRNA at physiological timescales relevant to a healing wound. To improve knockdown efficacy of released siRNA complexes, we investigate the assembly of a bilayer composed of siRNA and the polycation poly(β-amino ester) (PBAE). Through a fractional factorial design, we elucidate the effects of LbL assembly parameters on the resultant film's loading, composition, and *in vitro* efficacy. From these findings, we determine optimized assembly parameters for gene silencing.

Finally, we develop a mouse model for evaluating *in vivo* efficacy of LbL films assembled on sutures. Findings from a pilot study with our optimized films and recommendations for future studies are reported. This thesis work expounds the utility of LbL technology in assembling films for effective controlled localized siRNA delivery.

Thesis Supervisor: Paula T. Hammond
Title: Department Head, David H. Koch (1962) Professor in Engineering

THESIS SUPERVISOR

Paula T. Hammond, Ph.D.
David H. Koch Professor and Department Head of Chemical Engineering
Massachusetts Institute of Technology

THESIS COMMITTEE

Dr. Bradley D. Olsen, Ph.D.
Professor of Chemical Engineering
Massachusetts Institute of Technology

Dr. Sangeeta N. Bhatia, M.D., Ph.D.
John J. and Dorothy Wilson Professor of Health Sciences and Technology and of Electrical Engineering and Computer Science
Massachusetts Institute of Technology

Dr. Dennis P. Orgill, M.D., Ph.D.
Professor of Surgery
Harvard Medical School

For my family
My parents George and Michelle
My brothers Philip and Christian

Acknowledgements

This thesis would certainly not have been written without the support and encouragement from a great number of people. It would not be possible to name everyone who has played a role in my endeavors at MIT, but through the following acknowledgements, I would like to begin to express my gratitude.

My thesis advisor, Prof. Paula Hammond, thank you for your invaluable mentorship. You have been such an inspiration to me these past six years. You have challenged me to become an independent researcher. I will never forget your kindness, your enthusiasm, and your support.

My thesis committee, Profs. Bradley Olsen, Sangeeta Bhatia, and Dennis Orgill, thank you for your scientific support and advice. You have provided amazing insight into this work. Thank you for helping me think both critically in the fundamentals and big-picture in my research.

My fellow labmates in the Hammond Group, past and present, thank you for the support and insightful discussions. Steven Castleberry, thank you for helping me get started on this project and for your mentorship. Adam Berger, John Martin, Sheryl Wang, Maylin Howard, and Sarah Almofty, thank you for the valuable chats during our LbL subgroup meetings. Mohi Quadir, Mehdi Jorfi, Jason Kovacs, Jouha Min, Andreas Fall, Archana Boopathy, Anasuya Mandal, Santi Correa Echavarria, Connie Wu, Wade Wang, Brett Geiger, Natalie Boehnke, Apoorv Shanker, Sean Smith, Joelle Straehla, Antonio Barberio, Colin Bittner, Elad Deiss-Yehiely, Yanpu He, Celestine Hong, Stephanie Kong, and Brandon Johnston, thank you for your contributions to this work.

My undergraduate researchers, Jodie Tan and Sophia Chan, thank you for your help in this research. Your curiosity and enthusiasm in lab have been a great encouragement to me.

Lab managers and administrative staff, Xiuyun Hou, Liz Galoyan, Amy Tatem-Bannister, Donna Johnson, Marlisha McDaniels, and Josh Freedman, thank you so much for your helpful assistance during my PhD.

My family, my parents George and Michelle, my brothers Philip and Christian, thank you for your love. You bring so much joy and security in my life. This work is dedicated to you.

My GCC Class of 2014 brothers, Dan Nguyen, Ting Cho Lau, Dave Sawyers, Harry Choi, Jack Chen, Jeff Wen, Andrew Ellison, Chris Wang, and Bryant Andrews, thank you for your continued friendship. It means so much.

My Symphony Church community, thank you for exemplifying the love of Christ and being my spiritual family in Boston. Pastors Barry Kang, Shan Gian, Doug Tritton, Chan Park, and Michael Oh, thank for your leadership in serving. My brothers and coworkers in Christ, Rex Tzen and Kwadwo Owusu-Boaitey, thank you for your overwhelming support and encouragement during these years.

My partner, Elaine Choe, thank you for your gracious care and encouragement. Your loving support has seen me to the completion of this thesis.

My Lord and Savior, Jesus Christ, thank you for everything.

Table of Contents

List of Figures

Figure 2.4 Hierarchical Structure with [HMW Chitosan/Laponite]$_{40}$ Barrier. (a) Schematic of LbL architecture for staggered release. The bottom film consists of 25 tetralayers of chitosan (15 kDa), siRNA, Poly 2, and laponite clay. The barrier film consists of 40 bilayers of high molecular weight chitosan (350 kDa) and laponite clay. The top film consists of 25 tetralayers of chitosan (15 kDa), siRNA, Poly 2, and dextran sulfate. (b) Release Profile of siRNAs. Cumulative release of siRNA is reported in percentages. With this architecture, siRNA2 (green) is readily released while siRNA1 (brown) exhibits a slower sustained release. Error bars represent standard deviation.

Figure 2.5 Hierarchical Structure without Barrier. (a) Schematic of LbL architecture for staggered release. The bottom film consists of 25 tetralayers of chitosan (15 kDa), siRNA, Poly 2, and laponite clay. The top film consists of 25 tetralayers of chitosan (15 kDa), siRNA, Poly 2, and dextran sulfate. (b) Release Profile of siRNAs. Cumulative release of siRNA is reported in percentages. With this architecture, siRNA2 (green) is still readily released while siRNA1 (brown) exhibits a slower sustained release. Error bars represent standard deviation.

Figure 2.6 Graphene Oxide Barrier Layers. Cumulative siRNA release profiles, schematic representation, and SEM imaging of (a) [GO-NH_2/Laponite]$_{10}$, (b) [Chitosan/Lap-GO Hybrid], and (c) [GO-NH_2/GO]$_{10}$. Apart from the barrier layers, the architecture is the same for each group: [Chitosan/siRNA2/Poly2/Dextran Sulfate]$_{25}$ on the top and [Chitosan/siRNA1/Poly2/Laponite]$_{25}$ on the bottom. Cumulative release of siRNA is reported in percentages. Release of siRNA1 is in brown, release of siRNA2 is in green. Error bars represent standard deviation. Scale bar is 5 μm for SEM images.

Figure 2.7 [GO-NH_2/Laponite]$_{10}$ Barrier Layer. (a) Schematic of LbL architecture with [GO-NH_2/Laponite]$_{10}$ barrier layer. (b) Day-by-day release plot of siRNA in μg/cm^2. Error bars represent standard deviation.

Figure 3.1 Layer-by-layer coating of suture and the parameters varied. (a) Schematic representation of dip LbL assembly for coating Vicryl 3-0 suture with [PBAE/siRNA] bilayers. (b) Cross-section depiction of a suture coated with 3 bilayers. Films assembled in this study consisted of 15 bilayers. (c) List of parameters varied in the fractional factorial design. The pH (pH 4.5 – pH 6.0) of the entire process, ionic strength (150 mM – 250 mM) and PBAE concentration (0.5 mg/mL – 2.0 mg/mL) of the PBAE bath, and the siRNA concentration (20 μg/mL – 30 μg/mL) of the siRNA bath were varied. Parameters are color coded to reference the affected steps: black for the entire process, red for the PBAE bath, and blue for the siRNA bath. Wash baths and the siRNA bath were buffered to 10 mM Sodium Acetate.

Figure 3.2 Standard Least Squares Fit of Parameters on Response Variables. A standard least squares fit was performed on the average values from each run for (a) PBAE loading, (b) siRNA loading, and (c) PBAE:siRNA w/w ratio. “Actual by Predicted” plots are shown with R^2 and p-values reported. The coefficients for each parameter were normalized by the range tested and p-values are reported. Parameter terms with correlation p-values < 0.05 are highlighted; significant

positive coefficients are highlighted in red, negative coefficients are highlighted in blue. Error bars represent standard deviation.

Figure 3.3 Bubble plot of *in vitro* knockdown by PBAE loading and siRNA loading. Resulting GFP knockdown data of all LbL films are represented with siRNA loading on the x-axis and PBAE loading on the y-axis. Each biological replicate is included as its own data point. LbL coated sutures that effected greater knockdown are represented with larger bubbles. The knockdown is also color coded with high knockdown in red and low knockdown in blue. Sutures that produce the greatest knockdown are seen to have the greatest siRNA loading. Sutures with high siRNA loading show greater knockdown if they also have high PBAE loading.

Figure 3.4 Knockdown comparison of optimized formulation vs. runs with neighboring conditions. The optimized LbL parameters of pH 6, ionic strength of 150 mM, PBAE concentration of 1.0 mg/mL, and siRNA concentration of 30 μg/mL was found to achieve *in vitro* knockdown of 47%. Run 6 (37% knockdown) and Run 10 (2% knockdown) from the fractional factorial design both neighbor these conditions with a single parameter varied. Colors denote high (red), moderate (yellow), and low (blue) values of parameters within the experimental range of the design.

Figure 3.5 Knockdown of LbL films with optimized parameters. As the number of bilayers is increased to 30, over 80% of siRNA knockdown is achieved.

Figure 4.1 Synthesis of Poly 2-30%C3OH-DETA. Poly 2 was constructed with 30% feed of 3-amino-1-propanol. It was then endcapped with diethylenetriamine.

Figure 4.2 (a) Schematic of $[P2C3OHD/siRNA]_{30}$ assembly on Vicryl sutures. (b) *In Vitro* knockdown of GFP from sutures with the $[P2C3OHD/siRNA]_{30}$ film relative to treatment of uncoated suture. Error bars represent standard deviation.

Figure 4.3 Implantation of LbL Coated Suture in Mice. Mice were shaved and suture entrance and exit points were marked. LbL coated suture was implanted in the subcutaneous space and tissue glue was used to secure the suture.

Figure 4.4 *In Vivo* GFP Fluorescence (a) GFP Fluorescence Imaging of Mice Treated with siRNA Coated Sutures. IVIS was used to image GFP fluorescence at 465 ex / 540 em. Images were taken pre-implantation, post-implantation, and then daily for three days. Regions of interest (ROI) were drawn to cover the area around the sutures. Coated sutures were implanted on the left; uncoated sutures were implanted on the right. Representative mice from each treatment group are presented. (b) Average radiant efficiency of GFP over time. Radiant efficiency was averaged over both left and right ROIs for each mouse. Data for mice treated with suture coated with GFP-targeting siRNA (siGFP) are shown in green. Data for mice treated with negative control siRNA (siCon) are shown in black. Error bars represent standard error.

Figure 4.5 In Vivo Release of Fluorescently Tagged siRNA. Negative control siRNA tagged with Alexa Fluor 647 was imaged at 640 ex / 700 em. Images taken immediately post implantation (left) reveal retention of siRNA on the suture after the procedure was performed. Images taken on Day 1 (right) show that near complete release of siRNA is released within 24 hours from implantation.

Figure A.1 Validation of siRNAs for Dual-Reporter MDA-MB-435 Cells siRNAs for GFP and RFP were validated for the cell line. Treatment of a single siRNA resulted in the exclusive knockdown of the corresponding reporter gene. Treatment with both siRNAs resulted in knockdown of both reporter genes.

Figure A.2 Confocal Imaging of LbL Treated Cells. HeLa cells expressing d2eGFP were exposed to PLGA sutures coated with a $[\text{Poly 2/siRNA}]_{30}$ LbL coating. The nuclei is stained in blue with Hoechst. The GFP is shown in green. The siRNA is labeled with Alexa-Fluor 647 and is shown in red. The punctate fluorescence suggests the siRNA is trapped in endosomes.

Figure A.3 Effect of Replenishing siRNA on Concentration in Bath Over Dipping Process. The concentration of the siRNA bath was monitored over the course of bilayer coating of $[\text{Poly 2/siRNA}]_{30}$ on PLGA sutures. The amount of siRNA added was predetermined in an estimate to bring the concentration back to the initial level of approximately 18 μg/mL. There appears to be a first order decrease in the concentration for each case.

Figure A.4 Effects of Replenishing siRNA on siRNA Loading and Effecting Knockdown (a) siRNA loading generally increases as the number of replenishments increases. Approximately 4 μg/cm loading is achieved when siRNA is replenished four times throughout LbL coating. (b) The film that resulted in the greatest GFP knockdown is when siRNA is replenished once, midway through dipping. Almost 20% knockdown is achieved with this film.

Figure A.5 Effect of Number of Pieces of Suture on GFP Knockdown. HeLa cells were treated with sutures coated with $[\text{Poly 2/siRNA}]_{30}$ bilayers. The siRNA bath was replenished midway through the dipping process. Generally, as the number of pieces of suture applied to each well increases, the GFP knockdown increases. Over 25% knockdown was achieved with 5 pieces of suture.

Figure B.1 Micro BCA Assay for PBAE Quantitation. Serial two-fold dilutions of PBAE were made with siRNA (red squares) and without siRNA (blue triangles). The Micro BCA assay was performed following manufacturer's instructions. The linear regressions (represented by dashed lines) show that the presence of siRNA does not affect Micro BCA assay readings. We found that the Micro BCA assay can be appropriately repurposed to quantify PBAE loading in the LbL film.

Figure B.2 Ribogreen Assay for siRNA Quantitation. Standard curves with known siRNA amounts were made with PBAE (red squares) and without PBAE (blue triangles). The Ribogreen assay was performed following manufacturer's instructions. Without modification (a), the presence of PBAE

quenches the Ribogreen fluorescent signal considerably. To address the quenching, the PBAE was hydrolyzed as detailed in the experimental section. After hydrolysis of the PBAE (b), interference from the PBAE is shown to be minimized.

Figure B.3 Gating Strategy for Flow Cytometry

Figure B.4 pH Titration of PBAE. 10.1 mg PBAE was dissolved at 1 mg/mL in water with 75 μL of 1 M HCl. 0.1 N NaOH was used for titration. The pKa of the PBAE was found to be 7.4.

Figure B.5 Standard Least Squares Fit on Knockdown. A standard least squares fit was performed for *in vitro* knockdown with (a) assembly parameters as explanatory variables and (b) PBAE loading, siRNA loading, and w/w ratio as explanatory variables. "Actual by Predicted" plots are shown with R^2 and p-values reported. The coefficients for each parameter were normalized by the ranges of the explanatory variables and p-values are reported. No significant parameter terms were identified for either regression (correlation p-value < 0.05). Error bars represent standard deviation.

Figure B.6 Polyplex transfection studies. Polyplexes were formed by mixing PBAE and siRNA together at predetermined ratios. HeLa cells expressing d2e-GFP were treated with polyplexes. Flow cytometry was performed three days after treatment. (a) NucBlue assay was used to measure viability. (b) Alexa Fluor 647-labeled siRNA was used to track siRNA uptake. (c) GFP-targeting siRNA was used in studies of siRNA knockdown efficacy. Untreated cells served as negative controls. For positive controls, cells were treated with siRNA + Lipofectamine RNAiMAX.

Figure C.1 GFP Knockdown of [P2C3OHD/siRNA] vs. [Poly 2/siRNA] The [Poly 2/siGFP] coated suture was able to effect approximately 20% knockdown. The [P2C3OHD/siGFP] suture was able to effect approximately 50% knockdown. Error bars represent standard error.

Figure C.2 GFP Knockdown from [P2C3OHD/siRNA] Film from Various Substrates. The [P2C3OHD/siGFP] bilayer was constructed on Vicryl Rapide Suture, Webcryl suture, PDS II suture, PLGA strips, and Tegaderm. Knockdown ranges from 10% to 50%. The distinct abilities to effect knockdown indicates that the substrate may have an effect on transfection. Error bars represent standard error.

Figure C.3 Analysis of P2C3OHD siRNA Polyplexes (a) Zeta potential vs. P2C3OHD to siRNA weight ratio plot. Generally, as the weight ratio of P2C3OHD to siRNA increases, the zeta potential increases. As the weight ratio increases above 10, the zeta potential levels off around +22 mV. (b) GFP Knockdown vs. P2C3OHD to siRNA weight ratio plot. As the weight ratio increases, greater knockdown is effected. The knockdown efficiency starts to level off after above a weight ratio of 10. Error bars represent standard deviation.

Figure C.4 Knockdown by Varying Suture Number and Bilayers. The [P2C3OHD/siGFP] bilayer was constructed on size 5-0 Vicryl Rapide Suture. The concentration of the P2C3OHD bath was

1 mg/mL, the concentration of the siRNA was 20 μg/mL. The dipping pH was 6.0 and the concentration of buffer in the PBAE bath was 150 mM. The number of sutures applied to each well and the number of bilayers coated were varied. Knockdown was normalized to cells treated with uncoated suture. Error bars represent standard error.

Figure C.5 Loading on Sutures of Varying Sizes and Varied Bilayers The [P2C3OHD/siGFP] bilayer was constructed on size 5-0 Vicryl Rapide Suture and size 0 Vicryl Suture. The concentration of the P2C3OHD (PBAE) bath was 1 mg/mL, the concentration of the siRNA was 20 μg/mL. The dipping pH was 6.0 and the concentration of buffer in the PBAE bath was 150 mM. PBAE and siRNA loading were measured with BCA assay and fluorescence reading respectively.

List of Tables

CHAPTER 1.
Introduction

1.1 siRNA as a Therapeutic

RNA interference (RNAi) involves the silencing of genes and was first discovered by Fire and Mello in 1998[1]. The RNAi pathway can be described as follows: long double-stranded RNA is cleaved into fragments of 21-23 nucleotides long by the enzyme Dicer[2]. These fragments, known as short interfering RNA (siRNA), are then incorporated into the RNA-induced silencing complex (RISC)[3]. The siRNA is then unwound into two strands: the passenger strand and the guide strand. The passenger strand is then degraded and the guide strand directs the complex to seek out mRNA of complementary sequence[4]. The complex then cleaves the mRNA between bases 10 and 11 relative to the 5' end of the guide strand[5]. This process is depicted in Figure 1.1. Utilizing this endogenous mechanism, siRNA may be synthetically produced and introduced to cells to achieve sequence-specific gene knockdown[6].

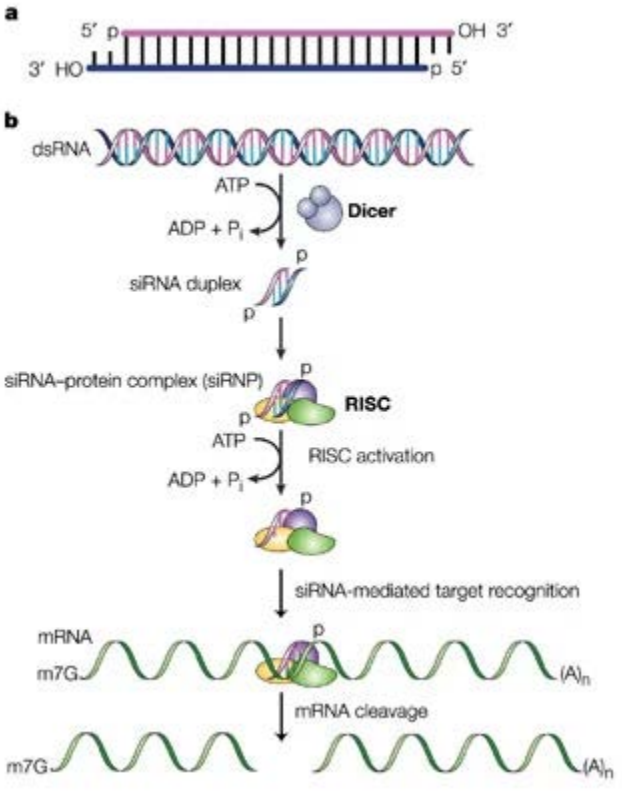

Figure 1.1 (a) Structure of siRNA; (b) siRNA pathway. Adapted by permission from Springer Nature[7].

The ability to theoretically target and knock down expression of any protein of choice without concerns of integration and modification to the host DNA presents exciting opportunities for siRNA as a therapeutic. The great potential of siRNA has prompted research in treatment for diseases including inflammatory disorders, viral infections, and a host of cancers[8]. The FDA approval of the siRNA therapeutic Onpattro™ (patisiran) to Alnylam Pharmaceuticals, Inc. in 2018[9] has generated even more excitement in this field.

1.2 Barriers to siRNA Delivery

To take full advantage of siRNA therapy, barriers in delivery must be addressed. When administered intravenously, naked siRNA is prone to nuclease degradation, rapid clearance, and rejection by the cell membrane due to its negative charge[10]. While this prompts the use of delivery vehicles, care must be taken in design to avoid phagocytosis by macrophages and monocytes[11]. Once in the cell, siRNA must escape the endosome to reach the cytosol, where all the RNAi machinery is located[12]. If endosomal escape does not occur, the siRNA would be subject to lysosomal degradation. If the siRNA reaches the cytoplasm, dissociation from any carrier system is necessary to allow incorporation of siRNA with RISC.

1.3 Approaches to siRNA Delivery

One approach to improving siRNA delivery efficacy is chemical modification of the siRNA molecule. These efforts include ribose modifications, phosphate backbone modifications, nucleobase and sugar modifications, and modifications to the termini and conjugate groups[13]. An example of chemical modification is 2'-*O*-methylation, which has been shown to reduce immune system activation through the Toll-like receptor 7 pathway and confer endonuclease resistance[14,15].

Among the first vehicles studied for siRNA delivery are viral vectors. Vectors including retrovirus, adenovirus, adeno-associated virus, herpes virus, pox virus, human foamy virus, and lentivirus have been developed for gene therapy[16]. Studies have shown efficient and stable siRNA expression and consequent knockdown through retroviral[17] and lentiviral[18] vector delivery. While efficient, many safety concerns for viral delivery exist. Risks associated with viral vectors include inflammation due to immunogenicity, insertional mutagenesis, and activation of proto-oncogenes[19].

A common approach to address the challenges in siRNA administration is nonviral nanoparticle delivery. A nanoparticle delivery vehicle works to protect siRNA from nuclease

degradation and immune response activation. Ligands may be attached to the nanoparticles for targeted delivery. Physicochemical characteristics that affect nanoparticle delivery efficacy of siRNA include shape, size, surface properties, thermal stability, quality control, and siRNA loading efficiency[20]. Nanoparticles may be generally categorized into one of two types: soft/organic nanoparticles or hard/inorganic nanoparticles. Soft/organic nanoparticles include liposomes, dendrimers, and polymer nanoparticles. Hard/inorganic nanoparticles include nanotubes, gold nanoparticles, quantum dots, and nanodiamonds[21].

The most common nanoparticle vehicle systems are lipid-based; lipid nanoparticles comprise a majority of siRNA nanoparticles in Phase I clinical trials[22]. Cationic lipids interact with the anionic siRNA through electrostatic interactions to form lipoplexes[23]. The lipoplexes may take the structural form of multilamellar or unilamellar liposomes. Intracellular uptake and endosomal escape of the lipid-siRNA nanoparticle are facilitated by the cationic lipid[24]. However, innate immune responses have been often observed after administration of lipid nanoparticles[25]. Efforts to reduce inflammatory responses have included coating the nanoparticle surface with polyethylene glycol (PEG)[26]. Nonetheless, off-target accumulation of lipid nanoparticles is often seen in the liver and failure to mitigate accumulation may lead to severe toxicity[27].

Polymer-based nanoparticles are another widely investigated method of siRNA delivery. Cationic polymers with either linear or branched structures are able to bind and condense siRNA into stabilized nanoparticles for transfection[28]. The positive charge of the polymers is proposed to facilitate endosomal escape by the ‘proton-sponge’ effect[29]. Polyethyleneimine (PEI) is a widely studied polymer for siRNA delivery. Both linear PEI (LPEI) and branched PEI (BPEI) have been used for siRNA administration[30], though BPEI has been shown to exhibit greater toxicity[31]. Other polymer systems have also been developed in efforts to address biocompatibility, including cyclodextrin[32], poly(lactic-co-glycolic acid) (PLGA)[33], and poly(β-amino esters) (PBAE)[34].

1.4 Local Delivery of siRNA

While intravenous delivery of siRNA nanoparticles has its benefits, localized administration of siRNA is advantageous in reducing off-target effects and increasing gene knockdown efficacy at the target site[35]. Furthermore, the increase of efficacy leads to reduction in load requirements and thus a reduction in production cost of the therapeutic. Though some diseases will require systemic delivery, local delivery may be optimal for a variety of pathologies[36]. Research has revealed promise of local siRNA delivery for application in bone repair, muscle

regeneration, inflammation, and fibrosis mitigation[37]. Local delivery strategies that have been investigated include loading of siRNA in microparticles, scaffolds, hydrogels, electrospun fibers, and surface coatings[37].

Microparticles containing siRNA are generally prepared using a double emulsion technique, followed by solvent extraction. The porosity and size of the microparticles can be tuned to optimize injectability, tissue retention, and siRNA release[38,39]. Nonetheless, there are key concerns in designing microparticle systems. For example, changes in pH have been shown to significantly impact microparticle behavior and release[40].

Natural and synthetic polymers have been explored for fabrication of scaffolds for local siRNA delivery. Naturally-derived polymers, such as collagen, have been used for their inherent cell-adhesion and enzymatic degradation properties[41,42]. Synthetic materials, such as PLGA, have been investigated for nucleic acid delivery as they offer greater control over scaffold properties, including degradation rate and mechanical stiffness[43]. A major obstacle to be addressed in scaffold delivery is the loss of siRNA bioactivity during incorporation into the scaffold[44,45]. Hydrogels are a subclass of scaffolds characterized by significant water content. Studies have demonstrated tunable and sustained release of siRNA from hydrogels composed of natural[46] and synthetic polymers[47].

Biomimetic nano-fibers may be formed by the electrospinning of various polymers[48]. Encapsulation of siRNA into electrospun fibers has been shown to achieve sustained release and transfection[49]. The incorporation of commercial transfection reagents improve efficacy of siRNA-loaded electrospun fibers, yet significant toxicity is associated with these agents.

1.5 Layer-by-Layer Self-Assembly

Of the local delivery strategies explored, layer-by-layer (LbL) self-assembly technology for formulating surface coatings stands out. LbL technology enables the assembly of multilayer coatings by the alternating deposition of components with complementary interactions (Figure 1.2). The assembly of LbL films is typically driven by electrostatic interactions between compounds of opposite charge. Other interactions that may drive LbL assembly include hydrophobic, van der Waals, hydrogen bonding, host-guest, covalent bonding, and biospecific interactions[50].

The LbL assembly process typically occurs under aqueous assembly conditions. The technology obviates the use of harsh solvents, temperatures, ionic strengths, and pH values. This

is advantageous for biomedical applications as the mild assembly conditions permit the conformal coating of medically relevant substrates with small molecules and biologics while maintaining the structural integrity of the substrates[51,52]. Multilayer films are typically assembled via dipping, spraying, and spin coating methods, although other methods such as 3D printing and micropatterning have also been investigated[53–56].

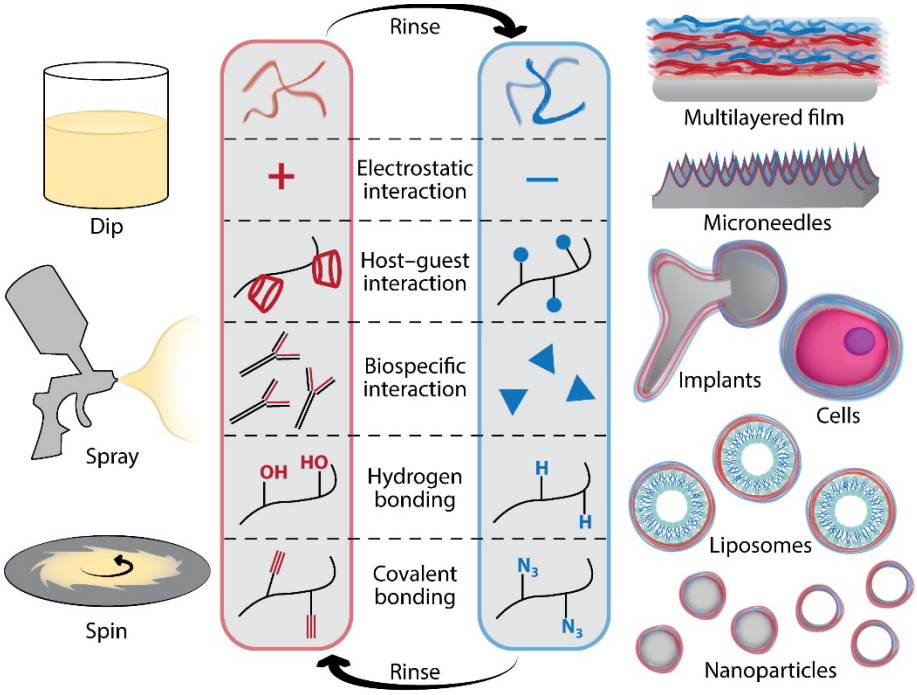

Figure 1.2 (Left) Schematic of common LbL Approaches, (middle) common interactions exploited in LbL self-assembly, and (right) examples of substrates coated for biomedical applications. Adapted by permission from Annual Reviews, Inc.[62]

Studies have shown that LbL assembly conditions affect the growth and stability of constructed multilayers. Assembly parameters including temperature[57], ionic strength[58], pH[59], molecular weight[60], species concentration[58], incubation time[61], and assembly method[54] have been investigated to have effects on film assembly and behavior. An understanding of assembly conditions and their effects on LbL film formulation is vital for designing optimized films for therapeutic application.

The LbL technique presents many advantages for drug delivery. Substrates including bandages[63], textiles[64], implants[65], nanoparticles[66], and cells[67] have been coated with LbL films for therapeutic use. Therapies including antibiotics[68], anti-inflammatory drugs[69], growth factors[70], and nucleic acids[71] have been incorporated into LbL films. High drug loadings may be achieved due to multivalent interactions, and loading may be tuned by adjusting the number of layers assembled.

LbL films have also exhibited advantages in protecting cargo from degradation[72] and enhancing shelf-life[73], while showing minimal toxicity[74].

1.6 LbL Assembly for Controlled Localized Drug Delivery

A notable feature of LbL technology is its potential in controlled localized drug delivery. Drug release from LbL films may be dictated by swelling, dissolution, or degradation of the film, as well as diffusion of the therapeutic[62]. Reports have shown that drug release kinetics from LbL films may be modulated through various methods, including changing film thickness[75] and tuning the film degradation rate[76]. LbL technology also presents the ability to deliver and tune the release of multiple drugs by taking advantage of the modular assembly process of the multilayer films[77]. The use of barrier layers[78] and covalent modification[79] have shown promise in stratifying release kinetics of multi-drug delivery.

1.7 Wound Healing Process

The following section is reproduced and adapted by permission from Mary Ann Liebert, Inc.[80]

An area of particular interest for controlled localized drug delivery is the treatment of soft tissue wounds. Soft tissue wounds encompass a broad category of injuries, varying in severity and prevalence[81–83]. They range from simple cuts and burns to chronic ulcers, major traumatic injuries, and burn wounds. Wound healing is an intricate network of interactions between multiple cell types, growth factors, and cytokines. The normal course of wound healing has classically been organized into three overlapping stages: inflammation, proliferation, and remodeling (Figure 1.3).

The role of the inflammatory phase is to contain damage and eliminate pathogens. Inflammation typically lasts for a few days, but may persist up to 2 weeks[84]. Release of the neuropeptide substance P from the peripheral nerves in a wound leads to increased vascular permeability, and various chemoattractants are released, allowing an influx of neutrophils and monocytes[85,86]. Throughout the course of the inflammatory phase, monocytes mature into macrophages[87]. Macrophages of the inflammatory phenotype (M1) work to remove bacteria and debris[88]. Once the wound is free of foreign material, macrophages polarize toward the anti-inflammatory (M2) state to resolve the inflammatory phase[89].

The proliferative phase is marked by fibroplasia with fibrous tissue deposition, reepithelialization, angiogenesis, and nerve regeneration[90]. Proliferation starts approximately 2–3

days after injury[84]. Fibroblasts migrate into the wound area to initiate production of collagen[91]. Keratinocytes begin to proliferate, covering the wound and initiating wound closure[92]. Vascularization is initiated as proangiogenic factors, including vascular endothelial growth factor (VEGF), fibroblast growth factor 2 (FGF-2), and platelet-derived growth factor (PDGF), are released[93]. Schwann cells work to regrow injured nerves[94]. The proliferative stage typically lasts up to a few weeks.

The remodeling phase begins 2–3 weeks after injury and can last for months. During the remodeling phase, vascularization is reduced and collagenases break down granulation tissue. Collagen type I is synthesized as collagen type III degrades[95]. The wound tissue matures and is restored to a functional state.

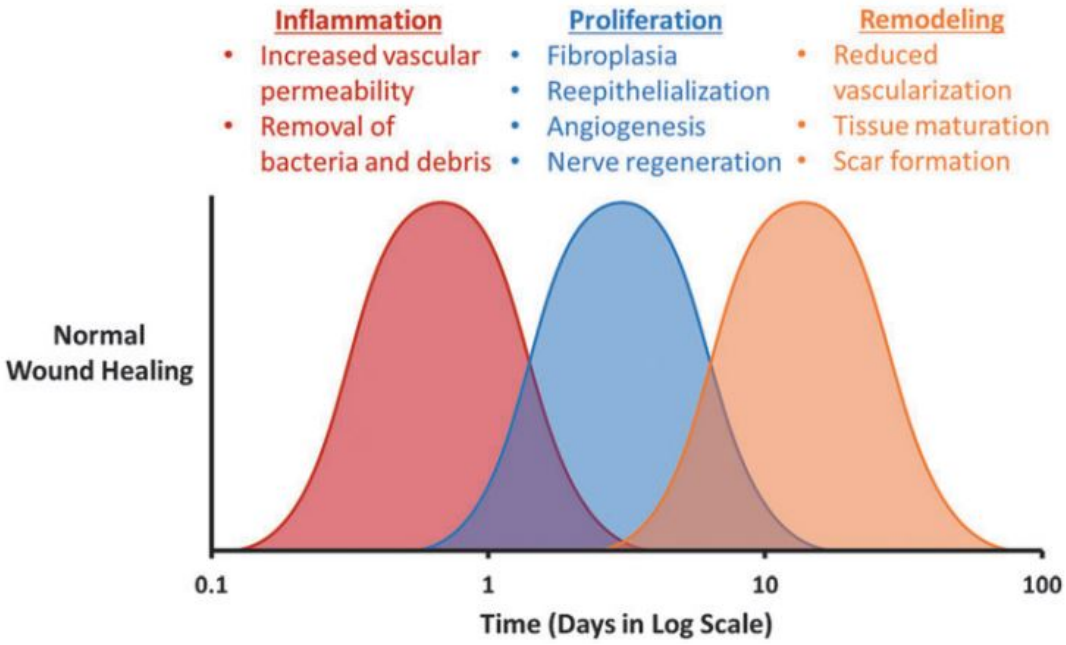

Figure 1.3 The wound healing process is classically organized into three overlapping stages: inflammation, proliferation, and remodeling. Adapted by permission from Mary Ann Liebert, Inc.[80]

1.8 Dysregulated Wound Healing

Dysregulation within the wound healing cascade can lead to severe complications for patients. If dysregulation occurs within inflammation or proliferation stages, deficient healing may result, leading to venous ulcers, diabetic ulcers, or pressure sores[96]. Fibrosis and scarring may occur when the remodeling phase is dysregulated[96].

Patients with type two diabetes mellitus often display symptoms of poorly vascularized and neuropathic extremities[97]. This significantly contributes to delays in wound healing. Once a wound is created, chronic inflammation leads to increased inflammatory cytokine expression,

increased proteolytic activity, and decreased growth factor signaling[98]. Diabetes is rising in prevalence, estimated at about 12-14% in the United States[99]. Among diabetes patients, the lifetime risk of developing foot ulcers is estimated to be 15%[100]. The estimated Medicare cost is $28.1-96.8 billion each year for chronic wounds, and $18.7 billion for diabetic foot ulcers[101,102].

Burns are another example of wounds that result in poor healing outcomes. Damage caused by burns often leads to dysregulation of the healing process, resulting in excessive deposition of the ECM, decreased vascularity, and formation of highly fibrotic scars[103]. Fibrotic scarring may lead to physical deformities and extensive pain. Additionally, contractions resulting from fibrosis can limit flexibility and function[104]. In the United States, burn injuries requiring medical treatment affect nearly half a million people each year[105].

1.9 Controlled Drug Delivery for Wound Healing

Due to the sequential nature of the wound healing process, controlled drug delivery may hold promise for modulating the wound environment to promote healing. Studies have shown that deficient healing is associated with the upregulation of specific factors including matrix metallopeptidase 9 (MMP-9), prolyl hydroxylase domain protein 2 (PHD2), and tumor necrosis factor alpha (TNF-α) especially in the early stages of inflammation and proliferation. Inhibition of these factors have been shown to enhance wound closure[106–108]. Dysregulation in the later phase of remodeling may lead to fibrosis and scarring, which are associated with upregulation of factors such as connective tissue growth factor (CTGF), transforming growth factor beta (TGF-β), and tissue inhibitor of metalloproteinase (TIMP). Inhibition of these factors have been shown to result in reduced scar height and area[109–111]. Reports have also highlighted the temporal effects of these treatments, later inhibition of CTGF and TGF-β have shown greater reduction of scarring compared to early treatments[109,112]. These findings warrant the development of temporally controlled multi-therapy treatments to address dysregulation in wound healing.

1.10 Scope and Outline of Thesis

The work presented in this thesis describes the development of LbL films for the therapeutic delivery of siRNA. In this first chapter, we provide the background information that motivated our studies. The potential of siRNA therapy is described, and LbL technology is presented as a promising tool in formulation of surface coatings for controlled localized drug

delivery. The wound healing process is summarized and presented as an application in which controlled delivery of multiple siRNAs is advantageous.

In Chapter 2, we describe our results in the development of LbL films for simultaneous delivery of multiple siRNAs with temporal control. We investigate how the composition of siRNA-containing multilayers and barrier layers affect release kinetics for staggered delivery of siRNA.

In Chapter 3, we describe our efforts in optimizing the LbL assembly process to construct siRNA films for maximal knockdown efficacy. A fractional factorial design was implemented to determine effects of assembly parameters on film composition and efficacy. The effects were corroborated with theory and assembly parameters were optimized for the construction of a film exhibiting impressive knockdown efficacy, greater than seen in our lab previously.

In Chapter 4, we detail our preliminary *in vivo* experiments. We describe our efforts in developing a simple mouse model for verification of siRNA film efficacy *in vivo* without the confounding factors associated with a wound environment. We present findings from our pilot study which show potential of our system, warranting further development.

In Chapter 5, we summarize the findings described in this thesis. Conclusions and future directions of this research are presented.

1.11 References

(1) Fire, A.; Xu, S.; Montgomery, M. K.; Kostas, S. A.; Driver, S. E.; Mello, C. C. Potent and Specific Genetic Interference by Double-Stranded RNA in Caenorhabditis Elegans. *Nature* **1998**, *391* (6669), 806–811. https://doi.org/10.1038/35888.

(2) Bernstein, E.; Caudy, A. A.; Hammond, S. M.; Hannon, G. J. Role for a Bidentate Ribonuclease in the Initiation Step of RNA Interference. *Nature* **2001**, *409* (6818), 363–366. https://doi.org/10.1038/35053110.

(3) Rand, T. A.; Ginalski, K.; Grishin, N. V.; Wang, X. Biochemical Identification of Argonaute 2 as the Sole Protein Required for RNA-Induced Silencing Complex Activity. *PNAS* **2004**, *101* (40), 14385–14389. https://doi.org/10.1073/pnas.0405913101.

(4) Ameres, S. L.; Martinez, J.; Schroeder, R. Molecular Basis for Target RNA Recognition and Cleavage by Human RISC. *Cell* **2007**, *130* (1), 101–112. https://doi.org/10.1016/j.cell.2007.04.037.

(5) Rand, T. A.; Petersen, S.; Du, F.; Wang, X. Argonaute2 Cleaves the Anti-Guide Strand of SiRNA during RISC Activation. *Cell* **2005**, *123* (4), 621–629. https://doi.org/10.1016/j.cell.2005.10.020.

(6) Elbashir, S. M.; Harborth, J.; Lendeckel, W.; Yalcin, A.; Weber, K.; Tuschl, T. Duplexes of 21-Nucleotide RNAs Mediate RNA Interference in Cultured Mammalian Cells. *Nature* **2001**, *411* (6836), 494–498. https://doi.org/10.1038/35078107.

(7) Dykxhoorn, D. M.; Novina, C. D.; Sharp, P. A. Killing the Messenger: Short RNAs That Silence Gene Expression. *Nature Reviews Molecular Cell Biology* **2003**, *4* (6), 457–467. https://doi.org/10.1038/nrm1129.

(8) Chakraborty, C.; Sharma, A. R.; Sharma, G.; Doss, C. G. P.; Lee, S.-S. Therapeutic MiRNA and SiRNA: Moving from Bench to Clinic as Next Generation Medicine. *Molecular Therapy - Nucleic Acids* **2017**, *8*, 132–143. https://doi.org/10.1016/j.omtn.2017.06.005.

(9) Commissioner, O. of the. FDA approves first-of-its kind targeted RNA-based therapy to treat a rare disease https://www.fda.gov/news-events/press-announcements/fda-approves-first-its-kind-targeted-rna-based-therapy-treat-rare-disease (accessed May 25, 2020).

(10) Whitehead, K. A.; Langer, R.; Anderson, D. G. Knocking down Barriers: Advances in SiRNA Delivery. *Nat Rev Drug Discov* **2009**, *8* (2), 129–138. https://doi.org/10.1038/nrd2742.

(11) Alexis, F.; Pridgen, E.; Molnar, L. K.; Farokhzad, O. C. Factors Affecting the Clearance and Biodistribution of Polymeric Nanoparticles. *Mol. Pharm.* **2008**, *5* (4), 505–515. https://doi.org/10.1021/mp800051m.

(12) Oliveira, S.; van Rooy, I.; Kranenburg, O.; Storm, G.; Schiffelers, R. M. Fusogenic Peptides Enhance Endosomal Escape Improving SiRNA-Induced Silencing of Oncogenes. *Int J Pharm* **2007**, *331* (2), 211–214. https://doi.org/10.1016/j.ijpharm.2006.11.050.

(13) Selvam, C.; Mutisya, D.; Prakash, S.; Ranganna, K.; Thilagavathi, R. Therapeutic Potential of Chemically Modified SiRNA: Recent Trends. *Chemical Biology & Drug Design* **2017**, *90* (5), 665–678. https://doi.org/10.1111/cbdd.12993.

(14) Judge, A. D.; Bola, G.; Lee, A. C. H.; MacLachlan, I. Design of Noninflammatory Synthetic SiRNA Mediating Potent Gene Silencing in Vivo. *Molecular Therapy* **2006**, *13* (3), 494–505. https://doi.org/10.1016/j.ymthe.2005.11.002.

(15) Vornlocher, H.-P.; Hadwiger, P.; Zimmermann, T. S.; Manoharan, M.; Rajeev, K. G.; Roehl, I.; Akinc, A. Nuclease Resistant Double-Stranded Ribonucleic Acid. WO2005115481A2, December 8, 2005.
(16) Huang, Y.; Liu, X.; Dong, L.; Liu, Z.; He, X.; Liu, W. Development of Viral Vectors for Gene Therapy for Chronic Pain. *Pain Res Treat* **2011**, *2011*. https://doi.org/10.1155/2011/968218.
(17) Barton, G. M.; Medzhitov, R. Retroviral Delivery of Small Interfering RNA into Primary Cells. *PNAS* **2002**, *99* (23), 14943–14945. https://doi.org/10.1073/pnas.242594499.
(18) Rubinson, D. A.; Dillon, C. P.; Kwiatkowski, A. V.; Sievers, C.; Yang, L.; Kopinja, J.; Rooney, D. L.; Zhang, M.; Ihrig, M. M.; McManus, M. T.; Gertler, F. B.; Scott, M. L.; Van Parijs, L. A Lentivirus-Based System to Functionally Silence Genes in Primary Mammalian Cells, Stem Cells and Transgenic Mice by RNA Interference. *Nature Genetics* **2003**, *33* (3), 401–406. https://doi.org/10.1038/ng1117.
(19) David, R. M.; Doherty, A. T. Viral Vectors: The Road to Reducing Genotoxicity. *Toxicol Sci* **2017**, *155* (2), 315–325. https://doi.org/10.1093/toxsci/kfw220.
(20) Young, S. W. S.; Stenzel, M.; Jia-Lin, Y. Nanoparticle-SiRNA: A Potential Cancer Therapy? *Critical Reviews in Oncology/Hematology* **2016**, *98*, 159–169. https://doi.org/10.1016/j.critrevonc.2015.10.015.
(21) Tatiparti, K.; Sau, S.; Kashaw, S. K.; Iyer, A. K. SiRNA Delivery Strategies: A Comprehensive Review of Recent Developments. *Nanomaterials* **2017**, *7* (4), 77. https://doi.org/10.3390/nano7040077.
(22) Forbes, D. C.; Peppas, N. A. Oral Delivery of Small RNA and DNA. *Journal of Controlled Release* **2012**, *162* (2), 438–445. https://doi.org/10.1016/j.jconrel.2012.06.037.
(23) Schroeder, A.; Levins, C. G.; Cortez, C.; Langer, R.; Anderson, D. G. Lipid-Based Nanotherapeutics for SiRNA Delivery. *J Intern Med* **2010**, *267* (1), 9–21. https://doi.org/10.1111/j.1365-2796.2009.02189.x.
(24) Lin, Q.; Chen, J.; Zhang, Z.; Zheng, G. Lipid-Based Nanoparticles in the Systemic Delivery of SiRNA. *Nanomedicine* **2013**, *9* (1), 105–120. https://doi.org/10.2217/nnm.13.192.
(25) Sakurai, H.; Kawabata, K.; Sakurai, F.; Nakagawa, S.; Mizuguchi, H. Innate Immune Response Induced by Gene Delivery Vectors. *Int J Pharm* **2008**, *354* (1–2), 9–15. https://doi.org/10.1016/j.ijpharm.2007.06.012.
(26) Chono, S.; Li, S.-D.; Conwell, C. C.; Huang, L. An Efficient and Low Immunostimulatory Nanoparticle Formulation for Systemic SiRNA Delivery to the Tumor. *Journal of Controlled Release* **2008**, *131* (1), 64–69. https://doi.org/10.1016/j.jconrel.2008.07.006.
(27) Zatsepin, T. S.; Kotelevtsev, Y. V.; Koteliansky, V. Lipid Nanoparticles for Targeted SiRNA Delivery – Going from Bench to Bedside. *Int J Nanomedicine* **2016**, *11*, 3077–3086. https://doi.org/10.2147/IJN.S106625.
(28) Tan, S. J.; Kiatwuthinon, P.; Roh, Y. H.; Kahn, J. S.; Luo, D. Engineering Nanocarriers for SiRNA Delivery. *Small* **2011**, *7* (7), 841–856. https://doi.org/10.1002/smll.201001389.
(29) Akhtar, S.; Benter, I. F. Nonviral Delivery of Synthetic SiRNAs in Vivo. *J Clin Invest* **2007**, *117* (12), 3623–3632. https://doi.org/10.1172/JCI33494.
(30) Richards Grayson, A. C.; Doody, A. M.; Putnam, D. Biophysical and Structural Characterization of Polyethylenimine-Mediated SiRNA Delivery in Vitro. *Pharm Res* **2006**, *23* (8), 1868–1876. https://doi.org/10.1007/s11095-006-9009-2.
(31) Williford, J.-M.; Wu, J.; Ren, Y.; Archang, M. M.; Leong, K. W.; Mao, H.-Q. Recent Advances in Nanoparticle-Mediated SiRNA Delivery. *Annual Review of Biomedical*

Engineering **2014**, *16* (1), 347–370. https://doi.org/10.1146/annurev-bioeng-071813-105119.
(32) Heidel, J. D.; Yu, Z.; Liu, J. Y.-C.; Rele, S. M.; Liang, Y.; Zeidan, R. K.; Kornbrust, D. J.; Davis, M. E. Administration in Non-Human Primates of Escalating Intravenous Doses of Targeted Nanoparticles Containing Ribonucleotide Reductase Subunit M2 SiRNA. *PNAS* **2007**, *104* (14), 5715–5721. https://doi.org/10.1073/pnas.0701458104.
(33) Singha, K.; Namgung, R.; Kim, W. J. Polymers in Small-Interfering RNA Delivery. *Nucleic Acid Therapeutics* **2011**, *21* (3), 133–147. https://doi.org/10.1089/nat.2011.0293.
(34) Tzeng, S. Y.; Hung, B. P.; Grayson, W. L.; Green, J. J. Cystamine-Terminated Poly(Beta-Amino Ester)s for SiRNA Delivery to Human Mesenchymal Stem Cells and Enhancement of Osteogenic Differentiation. *Biomaterials* **2012**, *33* (32), 8142–8151. https://doi.org/10.1016/j.biomaterials.2012.07.036.
(35) Haussecker, D. Current Issues of RNAi Therapeutics Delivery and Development. *Journal of Controlled Release* **2014**, *195*, 49–54. https://doi.org/10.1016/j.jconrel.2014.07.056.
(36) Weiser, J. R.; Saltzman, W. M. Controlled Release for Local Delivery of Drugs: Barriers and Models. *Journal of Controlled Release* **2014**, *190*, 664–673. https://doi.org/10.1016/j.jconrel.2014.04.048.
(37) Sarett, S. M.; Nelson, C. E.; Duvall, C. L. Technologies for Controlled, Local Delivery of SiRNA. *Journal of Controlled Release* **2015**, *218*, 94–113. https://doi.org/10.1016/j.jconrel.2015.09.066.
(38) Klose, D.; Siepmann, F.; Elkharraz, K.; Krenzlin, S.; Siepmann, J. How Porosity and Size Affect the Drug Release Mechanisms from PLGA-Based Microparticles. *International Journal of Pharmaceutics* **2006**, *314* (2), 198–206. https://doi.org/10.1016/j.ijpharm.2005.07.031.
(39) Mountziaris, P. M.; Sing, D. C.; Chew, S. A.; Tzouanas, S. N.; Lehman, E. D.; Kasper, F. K.; Mikos, A. G. Controlled Release of Anti-Inflammatory SiRNA from Biodegradable Polymeric Microparticles Intended for Intra-Articular Delivery to the Temporomandibular Joint. *Pharm Res* **2011**, *28* (6), 1370–1384. https://doi.org/10.1007/s11095-010-0354-9.
(40) Zhu, X.; Lu, L.; Currier, B. L.; Windebank, A. J.; Yaszemski, M. J. Controlled Release of NFκB Decoy Oligonucleotides from Biodegradable Polymer Microparticles. *Biomaterials* **2002**, *23* (13), 2683–2692. https://doi.org/10.1016/S0142-9612(01)00409-4.
(41) Place, E. S.; Evans, N. D.; Stevens, M. M. Complexity in Biomaterials for Tissue Engineering. *Nature Materials* **2009**, *8* (6), 457–470. https://doi.org/10.1038/nmat2441.
(42) Viñas-Castells, R.; Holladay, C.; di Luca, A.; Díaz, V. M.; Pandit, A. Snail1 Down-Regulation Using Small Interfering RNA Complexes Delivered through Collagen Scaffolds. *Bioconjugate Chem.* **2009**, *20* (12), 2262–2269. https://doi.org/10.1021/bc900241w.
(43) Salvay, D. M.; Zelivyanskaya, M.; Shea, L. D. Gene Delivery by Surface Immobilization of Plasmid to Tissue-Engineering Scaffolds. *Gene Therapy* **2010**, *17* (9), 1134–1141. https://doi.org/10.1038/gt.2010.79.
(44) Nelson, C. E.; Gupta, M. K.; Adolph, E. J.; Shannon, J. M.; Guelcher, S. A.; Duvall, C. L. Sustained Local Delivery of SiRNA from an Injectable Scaffold. *Biomaterials* **2012**, *33* (4), 1154–1161. https://doi.org/10.1016/j.biomaterials.2011.10.033.
(45) Andersen, M. Ø.; Howard, K. A.; Paludan, S. R.; Besenbacher, F.; Kjems, J. Delivery of SiRNA from Lyophilized Polymeric Surfaces. *Biomaterials* **2008**, *29* (4), 506–512. https://doi.org/10.1016/j.biomaterials.2007.10.003.

(46) Nguyen, K.; Dang, P. N.; Alsberg, E. Functionalized, Biodegradable Hydrogels for Control over Sustained and Localized SiRNA Delivery to Incorporated and Surrounding Cells. *Acta Biomaterialia* **2013**, *9* (1), 4487–4495. https://doi.org/10.1016/j.actbio.2012.08.012.
(47) Andersen, M. Ø.; Le, D. Q. S.; Chen, M.; Nygaard, J. V.; Kassem, M.; Bünger, C.; Kjems, J. Spatially Controlled Delivery of SiRNAs to Stem Cells in Implants Generated by Multi-Component Additive Manufacturing. *Advanced Functional Materials* **2013**, *23* (45), 5599–5607. https://doi.org/10.1002/adfm.201300832.
(48) Ma, P. X. Biomimetic Materials for Tissue Engineering. *Advanced Drug Delivery Reviews* **2008**, *60* (2), 184–198. https://doi.org/10.1016/j.addr.2007.08.041.
(49) Chen, M.; Gao, S.; Dong, M.; Song, J.; Yang, C.; Howard, K. A.; Kjems, J.; Besenbacher, F. Chitosan/SiRNA Nanoparticles Encapsulated in PLGA Nanofibers for SiRNA Delivery. *ACS Nano* **2012**, *6* (6), 4835–4844. https://doi.org/10.1021/nn300106t.
(50) Borges, J.; Mano, J. F. Molecular Interactions Driving the Layer-by-Layer Assembly of Multilayers. *Chem. Rev.* **2014**, *114* (18), 8883–8942. https://doi.org/10.1021/cr400531v.
(51) Saurer, E. M.; Jewell, C. M.; Roenneburg, D. A.; Bechler, S. L.; Torrealba, J. R.; Lynn, D. M. Polyelectrolyte Multilayers Promote Stent-Mediated Delivery of DNA to Vascular Tissue. *Biomacromolecules* **2013**, *14* (5), 1696–1704. https://doi.org/10.1021/bm4005222.
(52) Shukla, A.; Fang, J. C.; Puranam, S.; Hammond, P. T. Release of Vancomycin from Multilayer Coated Absorbent Gelatin Sponges. *Journal of Controlled Release* **2012**, *157* (1), 64–71. https://doi.org/10.1016/j.jconrel.2011.09.062.
(53) Izquierdo, A.; Ono, S. S.; Voegel, J.-C.; Schaaf, P.; Decher, G. Dipping versus Spraying: Exploring the Deposition Conditions for Speeding Up Layer-by-Layer Assembly. *Langmuir* **2005**, *21* (16), 7558–7567. https://doi.org/10.1021/la047407s.
(54) Kharlampieva, E.; Kozlovskaya, V.; Chan, J.; Ankner, J. F.; Tsukruk, V. V. Spin-Assisted Layer-by-Layer Assembly: Variation of Stratification as Studied with Neutron Reflectivity. *Langmuir* **2009**, *25* (24), 14017–14024. https://doi.org/10.1021/la9014042.
(55) Andres, C. M.; Kotov, N. A. Inkjet Deposition of Layer-by-Layer Assembled Films. *J. Am. Chem. Soc.* **2010**, *132* (41), 14496–14502. https://doi.org/10.1021/ja104735a.
(56) Yang, S. Y.; Rubner, M. F. Micropatterning of Polymer Thin Films with PH-Sensitive and Cross-Linkable Hydrogen-Bonded Polyelectrolyte Multilayers. *J. Am. Chem. Soc.* **2002**, *124* (10), 2100–2101. https://doi.org/10.1021/ja017681y.
(57) Salomäki, M.; Vinokurov, I. A.; Kankare, J. Effect of Temperature on the Buildup of Polyelectrolyte Multilayers. *Langmuir* **2005**, *21* (24), 11232–11240. https://doi.org/10.1021/la051600k.
(58) Dubas, S. T.; Schlenoff, J. B. Factors Controlling the Growth of Polyelectrolyte Multilayers. *Macromolecules* **1999**, *32* (24), 8153–8160. https://doi.org/10.1021/ma981927a.
(59) Bieker, P.; Schönhoff, M. Linear and Exponential Growth Regimes of Multilayers of Weak Polyelectrolytes in Dependence on PH. *Macromolecules* **2010**, *43* (11), 5052–5059. https://doi.org/10.1021/ma1007489.
(60) Porcel, C.; Lavalle, Ph.; Decher, G.; Senger, B.; Voegel, J.-C.; Schaaf, P. Influence of the Polyelectrolyte Molecular Weight on Exponentially Growing Multilayer Films in the Linear Regime. *Langmuir* **2007**, *23* (4), 1898–1904. https://doi.org/10.1021/la062728k.
(61) Selin, V.; Ankner, J. F.; Sukhishvili, S. A. Nonlinear Layer-by-Layer Films: Effects of Chain Diffusivity on Film Structure and Swelling. *Macromolecules* **2017**, *50* (16), 6192–6201. https://doi.org/10.1021/acs.macromol.7b01218.

(62) Alkekhia, D.; Hammond, P. T.; Shukla, A. Layer-by-Layer Biomaterials for Drug Delivery. *Annual Review of Biomedical Engineering* **2020**, *22* (1), null. https://doi.org/10.1146/annurev-bioeng-060418-052350.
(63) Castleberry, S. A.; Almquist, B. D.; Li, W.; Reis, T.; Chow, J.; Mayner, S.; Hammond, P. T. Self-Assembled Wound Dressings Silence MMP-9 and Improve Diabetic Wound Healing In Vivo. *Advanced Materials* **2016**, *28* (9), 1809–1817. https://doi.org/10.1002/adma.201503565.
(64) Truong-Phuoc, L.; Christoforidis, K. C.; Vigneron, F.; Papaefthimiou, V.; Decher, G.; Keller, N.; Keller, V. Layer-by-Layer Photocatalytic Assembly for Solar Light-Activated Self-Decontaminating Textiles. *ACS Appl. Mater. Interfaces* **2016**, *8* (50), 34438–34445. https://doi.org/10.1021/acsami.6b12585.
(65) Jia, Z.; Xiu, P.; Roohani-Esfahani, S.-I.; Zreiqat, H.; Xiong, P.; Zhou, W.; Yan, J.; Cheng, Y.; Zheng, Y. Triple-Bioinspired Burying/Crosslinking Interfacial Coassembly Strategy for Layer-by-Layer Construction of Robust Functional Bioceramic Self-Coatings for Osteointegration Applications. *ACS Appl. Mater. Interfaces* **2019**, *11* (4), 4447–4469. https://doi.org/10.1021/acsami.8b20429.
(66) Correa, S.; Boehnke, N.; Deiss-Yehiely, E.; Hammond, P. T. Solution Conditions Tune and Optimize Loading of Therapeutic Polyelectrolytes into Layer-by-Layer Functionalized Liposomes. *ACS Nano* **2019**, *13* (5), 5623–5634. https://doi.org/10.1021/acsnano.9b00792.
(67) Liu, T.; Wang, Y.; Zhong, W.; Li, B.; Mequanint, K.; Luo, G.; Xing, M. Biomedical Applications of Layer-by-Layer Self-Assembly for Cell Encapsulation: Current Status and Future Perspectives. *Advanced Healthcare Materials* **2019**, *8* (1), 1800939. https://doi.org/10.1002/adhm.201800939.
(68) Chuang, H. F.; Smith, R. C.; Hammond, P. T. Polyelectrolyte Multilayers for Tunable Release of Antibiotics. *Biomacromolecules* **2008**, *9* (6), 1660–1668. https://doi.org/10.1021/bm800185h.
(69) Smith, R. C.; Riollano, M.; Leung, A.; Hammond, P. T. Layer-by-Layer Platform Technology for Small-Molecule Delivery. *Angewandte Chemie International Edition* **2009**, *48* (47), 8974–8977. https://doi.org/10.1002/anie.200902782.
(70) Shah, N. J.; Macdonald, M. L.; Beben, Y. M.; Padera, R. F.; Samuel, R. E.; Hammond, P. T. Tunable Dual Growth Factor Delivery from Polyelectrolyte Multilayer Films. *Biomaterials* **2011**, *32* (26), 6183–6193. https://doi.org/10.1016/j.biomaterials.2011.04.036.
(71) Saurer, E. M.; Jewell, C. M.; Kuchenreuther, J. M.; Lynn, D. M. Assembly of Erodible, DNA-Containing Thin Films on the Surfaces of Polymer Microparticles: Toward a Layer-by-Layer Approach to the Delivery of DNA to Antigen-Presenting Cells. *Acta Biomaterialia* **2009**, *5* (3), 913–924. https://doi.org/10.1016/j.actbio.2008.08.022.
(72) Lin, M.; Gao, Y.; Diefenbach, T. J.; Shen, J. K.; Hornicek, F. J.; Park, Y. I.; Xu, F.; Lu, T. J.; Amiji, M.; Duan, Z. Facial Layer-by-Layer Engineering of Upconversion Nanoparticles for Gene Delivery: Near-Infrared-Initiated Fluorescence Resonance Energy Transfer Tracking and Overcoming Drug Resistance in Ovarian Cancer. *ACS Appl. Mater. Interfaces* **2017**, *9* (9), 7941–7949. https://doi.org/10.1021/acsami.6b15321.
(73) Shukla, A.; Puranam, S.; Hammond, P. T. Vancomycin Storage Stability in Multilayer Thin Film Coatings for On-Demand Care. *Journal of Biomaterials Science, Polymer Edition* **2012**, *23* (15), 1895–1902. https://doi.org/10.1163/156856211X598256.
(74) Choi, K. Y.; Correa, S.; Min, J.; Li, J.; Roy, S.; Laccetti, K. H.; Dreaden, E.; Kong, S.; Heo, R.; Roh, Y. H.; Lawson, E. C.; Palmer, P. A.; Hammond, P. T. Binary Targeting of SiRNA

to Hematologic Cancer Cells In Vivo Using Layer-by-Layer Nanoparticles. *Advanced Functional Materials* **2019**, *29* (20), 1900018. https://doi.org/10.1002/adfm.201900018.
(75) Pérez-Anes, A.; Gargouri, M.; Laure, W.; Van Den Berghe, H.; Courcot, E.; Sobocinski, J.; Tabary, N.; Chai, F.; Blach, J.-F.; Addad, A.; Woisel, P.; Douroumis, D.; Martel, B.; Blanchemain, N.; Lyskawa, J. Bioinspired Titanium Drug Eluting Platforms Based on a Poly-β-Cyclodextrin–Chitosan Layer-by-Layer Self-Assembly Targeting Infections. *ACS Appl. Mater. Interfaces* **2015**, *7* (23), 12882–12893. https://doi.org/10.1021/acsami.5b02402.
(76) Guo, X.; Carter, M. C. D.; Appadoo, V.; Lynn, D. M. Tunable and Selective Degradation of Amine-Reactive Multilayers in Acidic Media. *Biomacromolecules* **2019**, *20* (9), 3464–3474. https://doi.org/10.1021/acs.biomac.9b00756.
(77) Min, J.; Choi, K. Y.; Dreaden, E. C.; Padera, R. F.; Braatz, R. D.; Spector, M.; Hammond, P. T. Designer Dual Therapy Nanolayered Implant Coatings Eradicate Biofilms and Accelerate Bone Tissue Repair. *ACS Nano* **2016**, *10* (4), 4441–4450. https://doi.org/10.1021/acsnano.6b00087.
(78) Min, J.; Braatz, R. D.; Hammond, P. T. Tunable Staged Release of Therapeutics from Layer-by-Layer Coatings with Clay Interlayer Barrier. *Biomaterials* **2014**, *35* (8), 2507–2517. https://doi.org/10.1016/j.biomaterials.2013.12.009.
(79) Wood, K. C.; Chuang, H. F.; Batten, R. D.; Lynn, D. M.; Hammond, P. T. Controlling Interlayer Diffusion to Achieve Sustained, Multiagent Delivery from Layer-by-Layer Thin Films. *Proceedings of the National Academy of Sciences* **2006**, *103* (27), 10207–10212. https://doi.org/10.1073/pnas.0602884103.
(80) Berger, A. G.; Chou, J. J.; Hammond, P. T. Approaches to Modulate the Chronic Wound Environment Using Localized Nucleic Acid Delivery. *Advances in Wound Care* **2020**. https://doi.org/10.1089/wound.2020.1167.
(81) Dryden, M. S. Complicated Skin and Soft Tissue Infection. *J Antimicrob Chemother* **2010**, *65* (suppl_3), iii35–iii44. https://doi.org/10.1093/jac/dkq302.
(82) Gurtner, G. C.; Werner, S.; Barrandon, Y.; Longaker, M. T. Wound Repair and Regeneration. *Nature* **2008**, *453* (7193), 314–321. https://doi.org/10.1038/nature07039.
(83) Janis, J. E.; Kwon, R. K.; Lalonde, D. H. A Practical Guide to Wound Healing. *Plastic and Reconstructive Surgery* **2010**, *125* (6). https://doi.org/10.1097/PRS.0b013e3181d9a0d1.
(84) Li, J.; Chen, J.; Kirsner, R. Pathophysiology of Acute Wound Healing. *Clinics in Dermatology* **2007**, *25* (1), 9–18. https://doi.org/10.1016/j.clindermatol.2006.09.007.
(85) Richardson, J. D.; Vasko, M. R. Cellular Mechanisms of Neurogenic Inflammation. *The Journal of pharmacology and experimental therapeutics* **2002**, *302* (3), 839–845. https://doi.org/10.1124/jpet.102.032797.
(86) Suvas, S. Role of Substance P Neuropeptide in Inflammation, Wound Healing, and Tissue Homeostasis. *The Journal of Immunology* **2017**, *199* (5), 1543–1552. https://doi.org/10.4049/jimmunol.1601751.
(87) Soehnlein, O.; Lindbom, L. Phagocyte Partnership during the Onset and Resolution of Inflammation. *Nature Reviews Immunology* **2010**, *10*, 427–439. https://doi.org/10.1038/nri2779.
(88) Weiss, G.; Schaible, U. E. Macrophage Defense Mechanisms against Intracellular Bacteria. *Immunol Rev* **2015**, *264* (1), 182–203. https://doi.org/10.1111/imr.12266.

(89) Ferrante, C. J.; Leibovich, S. J. Regulation of Macrophage Polarization and Wound Healing. *Adv Wound Care (New Rochelle)* **2012**, *1* (1), 10–16. https://doi.org/10.1089/wound.2011.0307.
(90) Cañedo-Dorantes, L.; Cañedo-Ayala, M. Skin Acute Wound Healing: A Comprehensive Review https://www.hindawi.com/journals/iji/2019/3706315/ (accessed Nov 26, 2019). https://doi.org/10.1155/2019/3706315.
(91) Greaves, N. S.; Ashcroft, K. J.; Baguneid, M.; Bayat, A. Current Understanding of Molecular and Cellular Mechanisms in Fibroplasia and Angiogenesis during Acute Wound Healing. *Journal of Dermatological Science* **2013**, *72* (3), 206–217. https://doi.org/10.1016/j.jdermsci.2013.07.008.
(92) Rousselle, P.; Braye, F.; Dayan, G. Re-Epithelialization of Adult Skin Wounds: Cellular Mechanisms and Therapeutic Strategies. *Adv. Drug Deliv. Rev.* **2019**, *146*, 344–365. https://doi.org/10.1016/j.addr.2018.06.019.
(93) Eelen Guy; de Zeeuw Pauline; Simons Michael; Carmeliet Peter. Endothelial Cell Metabolism in Normal and Diseased Vasculature. *Circulation Research* **2015**, *116* (7), 1231–1244. https://doi.org/10.1161/CIRCRESAHA.116.302855.
(94) Zochodne, D. W. The Challenges and Beauty of Peripheral Nerve Regrowth. *J. Peripher. Nerv. Syst.* **2012**, *17* (1), 1–18. https://doi.org/10.1111/j.1529-8027.2012.00378.x.
(95) Olczyk, P.; Mencner, Ł.; Komosinska-Vassev, K. The Role of the Extracellular Matrix Components in Cutaneous Wound Healing https://www.hindawi.com/journals/bmri/2014/747584/ (accessed Nov 26, 2019). https://doi.org/10.1155/2014/747584.
(96) O'Kane, S.; Ferguson, M. W. J. Transforming Growth Factor Bs and Wound Healing. *The International Journal of Biochemistry & Cell Biology* **1997**, *29* (1), 63–78. https://doi.org/10.1016/S1357-2725(96)00120-3.
(97) Davis, F. M.; Kimball, A.; Boniakowski, A.; Gallagher, K. Dysfunctional Wound Healing in Diabetic Foot Ulcers: New Crossroads. *Curr Diab Rep* **2018**, *18* (1), 2. https://doi.org/10.1007/s11892-018-0970-z.
(98) Barrientos, S.; Stojadinovic, O.; Golinko, M. S.; Brem, H.; Tomic-Canic, M. PERSPECTIVE ARTICLE: Growth Factors and Cytokines in Wound Healing. *Wound Repair and Regeneration* **2008**, *16* (5), 585–601. https://doi.org/10.1111/j.1524-475X.2008.00410.x.
(99) Menke, A.; Casagrande, S.; Geiss, L.; Cowie, C. C. Prevalence of and Trends in Diabetes Among Adults in the United States, 1988-2012. *JAMA* **2015**, *314* (10), 1021–1029. https://doi.org/10.1001/jama.2015.10029.
(100) Singh, N.; Armstrong, D. G.; Lipsky, B. A. Preventing Foot Ulcers in Patients With Diabetes. *JAMA* **2005**, *293* (2), 217–228. https://doi.org/10.1001/jama.293.2.217.
(101) Nussbaum, S. R.; Carter, M. J.; Fife, C. E.; DaVanzo, J.; Haught, R.; Nusgart, M.; Cartwright, D. An Economic Evaluation of the Impact, Cost, and Medicare Policy Implications of Chronic Nonhealing Wounds. *Value in Health* **2018**, *21* (1), 27–32. https://doi.org/10.1016/j.jval.2017.07.007.
(102) Sen, C. K. Human Wounds and Its Burden: An Updated Compendium of Estimates. *Advances in Wound Care* **2019**, *8* (2), 39–48. https://doi.org/10.1089/wound.2019.0946.
(103) Xue, M.; Jackson, C. J. Extracellular Matrix Reorganization During Wound Healing and Its Impact on Abnormal Scarring. *Adv Wound Care (New Rochelle)* **2015**, *4* (3), 119–136. https://doi.org/10.1089/wound.2013.0485.

(104) Aarabi, S.; Longaker, M. T.; Gurtner, G. C. Hypertrophic Scar Formation Following Burns and Trauma: New Approaches to Treatment. *PLOS Medicine* **2007**, *4* (9), e234. https://doi.org/10.1371/journal.pmed.0040234.

(105) Gibran, N. S.; Wiechman, S.; Meyer, W.; Edelman, L.; Fauerbach, J.; Gibbons, L.; Holavanahalli, R.; Hunt, C.; Keller, K.; Kirk, E.; Laird, J.; Lewis, G.; Moses, S.; Sproul, J.; Wilkinson, G.; Wolf, S.; Young, A.; Yovino, S.; Mosier, M. J.; Cancio, L. C.; Amani, H.; Blayney, C.; Cullinane, J.; Haith, L.; Jeng, J. C.; Kardos, P.; Kramer, G.; Lawless, M. B.; Serio-Melvin, M. L.; Miller, S.; Moran, K.; Novakovic, R.; Potenza, B.; Rinewalt, A.; Schultz, J.; Smith, H.; Dylewski, M.; Wibbenmeyer, L.; Bessey, P. Q.; Carter, J.; Gamelli, R.; Goodwin, C.; Graves, T.; Hollowed, K.; Holmes, J.; Noordenbas, J.; Nordlund, M.; Savetamal, A.; Simpson, P.; Traber, D.; Traber, L.; Nedelec, B.; Donelan, M.; Baryza, M. J.; Bhavsar, D.; Blome-Eberwein, S.; Carrougher, G. J.; Hickerson, W.; Joe, V.; Jordan, M.; Kowalske, K.; Murray, D.; Murray, V. K.; Parry, I.; Peck, M.; Reilly, D.; Schneider, J. C.; Ware, L.; Singer, A. J.; Boyce, S. T.; Ahrenholz, D. H.; Chang, P.; Clark, R. A. F.; Fey, R.; Fidler, P.; Garner, W.; Greenhalgh, D.; Honari, S.; Jones, L.; Kagan, R.; Kirby, J.; Leggett, J.; Meyer, N.; Reigart, C.; Richey, K.; Rosenberg, L.; Weber, J.; Wiggins, B. American Burn Association Consensus Statements. *Journal of Burn Care & Research* **2013**, *34* (4), 361–385. https://doi.org/10.1097/bcr.0b013e31828cb249.

(106) Gao, M.; Nguyen, T. T.; Suckow, M. A.; Wolter, W. R.; Gooyit, M.; Mobashery, S.; Chang, M. Acceleration of Diabetic Wound Healing Using a Novel Protease–Anti-Protease Combination Therapy. *PNAS* **2015**, *112* (49), 15226–15231. https://doi.org/10.1073/pnas.1517847112.

(107) Takeda, Y.; Costa, S.; Delamarre, E.; Roncal, C.; Leite de Oliveira, R.; Squadrito, M. L.; Finisguerra, V.; Deschoemaeker, S.; Bruyère, F.; Wenes, M.; Hamm, A.; Serneels, J.; Magat, J.; Bhattacharyya, T.; Anisimov, A.; Jordan, B. F.; Alitalo, K.; Maxwell, P.; Gallez, B.; Zhuang, Z. W.; Saito, Y.; Simons, M.; De Palma, M.; Mazzone, M. Macrophage Skewing by Phd2 Haplodeficiency Prevents Ischaemia by Inducing Arteriogenesis. *Nature* **2011**, *479* (7371), 122–126. https://doi.org/10.1038/nature10507.

(108) Ashcroft, G. S.; Jeong, M.-J.; Ashworth, J. J.; Hardman, M.; Jin, W.; Moutsopoulos, N.; Wild, T.; McCartney-Francis, N.; Sim, D.; McGrady, G.; Song, X.; Wahl, S. M. Tumor Necrosis Factor-Alpha (TNF-α) Is a Therapeutic Target for Impaired Cutaneous Wound Healing. *Wound Repair and Regeneration* **2012**, *20* (1), 38–49. https://doi.org/10.1111/j.1524-475X.2011.00748.x.

(109) Sisco, M.; Kryger, Z. B.; O'Shaughnessy, K. D.; Kim, P. S.; Schultz, G. S.; Ding, X.-Z.; Roy, N. K.; Dean, N. M.; Mustoe, T. A. Antisense Inhibition of Connective Tissue Growth Factor (CTGF/CCN2) MRNA Limits Hypertrophic Scarring without Affecting Wound Healing in Vivo. *Wound Repair and Regeneration* **2008**, *16* (5), 661–673. https://doi.org/10.1111/j.1524-475X.2008.00416.x.

(110) Shah, M.; Foreman, D. M.; Ferguson, M. W. Neutralising Antibody to TGF-Beta 1,2 Reduces Cutaneous Scarring in Adult Rodents. *Journal of Cell Science* **1994**, *107* (5), 1137–1157.

(111) Wang, P.; Jiang, L.-Z.; Xue, B. Recombinant Human Endostatin Reduces Hypertrophic Scar Formation in Rabbit Ear Model through Down-Regulation of VEGF and TIMP-1. *African Health Sciences* **2016**, *16* (2), 542–553. https://doi.org/10.4314/ahs.v16i2.23.

(112) Lu, L.; Saulis, A. S.; Liu, W. R.; Roy, N. K.; Chao, J. D.; Ledbetter, S.; Mustoe, T. A. The Temporal Effects of Anti-TGF-B1, 2, and 3 Monoclonal Antibody on Wound Healing

and Hypertrophic Scar Formation. *Journal of the American College of Surgeons* **2005**, *201* (3), 391–397. https://doi.org/10.1016/j.jamcollsurg.2005.03.032.

CHAPTER 2.

Modulating Sequential Release of siRNA from Layer-by-Layer Films

2.1 Introduction

Layer-by-layer (LbL) self-assembly is a versatile technology, widely utilized in fabricating surface coatings[1]. The LbL technique typically involves the alternating deposition of components with opposite charge, resulting in the assembly of multilayer coatings. Complementary interactions, other than electrostatic, used for LbL assembly include hydrophobic, van der Waals, hydrogen bonding, host-guest, covalent bonding, and biospecific interactions[2]. The LbL assembly method has been implemented in coating substrates such as bandages[3], textiles[4], and implants[5] for therapeutic application. Many efforts have been made in exploiting this technology to incorporate a range of drugs, including antibiotics[6], anti-inflammatory therapies[7], growth factors[8], and nucleic acids[9], into thin-film surface coatings for local delivery.

The modular assembly process allows for incorporation of multiple drugs within a single film. Researchers have investigated different methods of stratifying the release profiles of individual therapies from a multi-drug film. Studies have shown that sequential deposition of drug-containing films on a substrate may provide some level of stratification[10], but incorporating a barrier layer to prevent interlayer diffusion of the drugs results in greater staggering of release[10,11]. Studies have also shown that release profiles of different drugs within a single film may be controlled without the use of barrier layers by incorporating polymers of different degradation rates into respective film layers[12].

The ability to tune the individual release of multiple therapies from a LbL film finds promise for a variety of applications. The process of soft tissue wound healing occurs over the course of three sequential stages: inflammation, proliferation, and remodeling[13]. Within each stage of wound healing, different cell types and signaling molecules are present to create a microenvironment unique to aiding the healing process. Timed release of specific therapeutics according to the sequential course of wound healing may be critical to the efficacy of a combination drug coating[14]. Bone repair is another promising application for tunable multi-drug delivery. Similar to soft tissue wound healing, bone repair is a multistep process involving migration, proliferation, differentiation, and activation of multiple cell types[15].

Here we investigate the assembly of LbL films incorporating multiple siRNAs for controlled local delivery. Tuned sequential delivery of siRNAs may prove advantageous for applications such as dysregulated wound healing, in which treatment must align with temporal fluctuations of the wound microenvironment[14]. In this chapter, we present our developments in stratifying release profiles of two distinct siRNAs within a single LbL film. We study the effects of film composition on release profiles of siRNA. Furthermore, we demonstrate the ability of various barrier layers to modulate sequential release.

2.2 Materials and Methods

2.2.1 Materials

Qiagen AllStars Neg. Alexa Fluor 647-labeled siRNA and Alexa Fluor 546-labeled siRNA were purchased from Qiagen (Valencia, CA). Linear poly(ethyleneimine) (LPEI) (25 kDa), dextran sulfate (DS) (500 kDa), low molecular weight (LMW) chitosan (15 kDa), high molecular weight (HMW) chitosan (350 kDa), graphene oxide (GO), and amine functionalized graphene oxide (GO-NH_2) were purchased from Sigma Aldrich (St. Louis, MO). Laponite was purchased from Southern Clay Products (Gonzales, TX). The poly(β-amino ester) Poly 2 was synthesized as previously described[16]. Sodium acetate buffer (1 M, pH 4.5) was purchased from Alfa Aesar (Haverhill, MA). Phosphate buffered saline (PBS) solution was purchased from Invitrogen (Carlsbad, CA). RNase free UltraPure water was purchased from Life Technologies (Carlsbad, CA).

2.2.2 Preparation of Solutions

Solutions of LMW chitosan, HMW chitosan, GO, GO-NH_2 were prepared at 1 mg/mL. Solutions of LPEI, DS, Poly 2, and laponite were prepared at 2 mg/mL. Solutions of siRNA were prepared at 20 μg/mL. The Lap-GO hybrid solution was prepared as a mixture of 5 mg/mL laponite and 1 mg/mL GO. The solutions of LMW Chitosan, HMW Chitosan, GO-NH_2, Poly 2, and LPEI were prepared in RNase free UltraPure water buffered to 20 mM with pH 4.5 sodium acetate solution. The solutions of DS and siRNA were prepared in RNase free water buffered to 10 mM with pH 4.5 sodium acetate solution. The solutions of GO, laponite, and Lap-GO hybrid were prepare in RNase free water without buffer. The GO, GO-NH_2, and Lap-GO hybrid solutions were sonicated for an hour before use in film assembly. Solutions of LMW chitosan, HMW chitosan, LPEI, DS, Poly 2, and laponite were filtered through a 0.2 μm cellulose acetate filter.

2.2.3 Layer-by-layer Film Preparation

Silicon substrates were first cleaned in ethanol and rinsed with water. The silicon was subject to oxygen plasma treatment for 10 minutes on high setting in a plasma cleaner (PDC-32G, Harrick, USA). The silicon was then immediately immersed in a LPEI solution for a minimum of two hours before LbL assembly with a Carl Zeiss HMS-DS50 stainer (Oberkochen, Germany). Each LbL formulation was built upon 10 base layers of [LPEI/DS]. The base layer was assembled through alternating adsorption steps of LPEI and DS. These adsorption steps were 10 minutes long each. Two wash steps (30 seconds each with agitation) took place between each adsorption step.

LbL films were consequently assembled according to their specific architecture. The adsorption step for each component was 10 minutes long, except for adsorption of siRNA which was 15 minutes. For tetralayer assembly, one wash step (1 minute with agitation) took place between each adsorption step. For barrier bilayer assembly, two wash steps (30 seconds each with agitation) took place between each adsorption step. This discrepancy was due to limited space in the slide stainers. RNase free water was used for wash steps; if the following adsorption step was prepared with sodium acetate buffer, the preceding wash steps were prepared with buffer accordingly. Generally, the first deposited tetralayer was constructed with Alexa Fluor 546-labeled siRNA (referred to in the Results and Discussion section as siRNA1). For dual release films, Alexa Fluor 647-labeled siRNA was incorporated in the second tetralayer formulation (referred to as siRNA2).

2.2.4 Characterization of siRNA Loading and Release

After assembly of the LbL films, the coated silicon chips were incubated at 37°C in microcentrifuge tubes filled with preheated PBS. Every 24 hours, coated substrates were transferred to new tubes of preheated PBS and incubated at 37°C. Release samples were kept in a -20°C freezer until quantification. Film release was carried out for up to 21 days. Quantification of siRNA in the release samples was performed with a fluorescence plate reader. Alexa Fluor 546-labeled siRNA was quantified with 540/575 ex/em wavelengths. Alexa Fluor 647-labeled siRNA was quantified with 640/675 ex/em wavelengths. Standard curves were employed to quantify siRNA in the samples.

*Note: It was discovered years later after these studies that complexation to polycations in fact quenches the fluorescent signal of siRNA. While the reported siRNA loadings in this chapter may be lower than the amount actually incorporated, we believe the relative amounts (ie.

cumulative release curves represented as percentages) are fairly accurate as complexation would affect each reading in the construction of these plots. To achieve more accurate quantification of fluorescent siRNA, we recommend mixing the releasate samples in high concentration salt solutions (eg. 3 M NaCl) to dissociate any complexes before using the plate reader to measure siRNA concentration.

2.2.5 Characterization of Barrier Layer Surface Morphology

Silicon chips were prepared as previously described with 10 base layers of [LPEI/DS]. Barrier layers that incorporated GO and/or GO-NH_2 were assembled directly on these substrates, forgoing the deposition of tetralayers. Samples were sputter coated with gold before SEM analysis with a JEOL 6700F scanning electron microscope.

2.3 Results and Discussion

2.3.1 Incorporating siRNA into Layer-by-Layer Films

We first investigated the construction of an LbL film for the incorporation and release of a single siRNA. We assembled tetralayer films on top of silicon chips by alternating deposition of chitosan (15 kDa), siRNA, Poly 2, and laponite clay (Figure 2.1a). This film is represented as $[\text{Chitosan/siRNA/Poly 2/Laponite}]_x$ where 'x' denotes the number of architectural repeats. This nomenclature will be used throughout this thesis. Chitosan is a positively charged biocompatible polysaccharide derived from the shells of crustaceans, such as crabs and shrimp, and has been shown to promote wound healing by inducing hemostasis[17]. It also has been widely reported in literature for use in siRNA delivery[18–20]. Poly 2 is a type of poly(β-amino ester) (PBAE), a synthetic polycation known for its biocompatibility as well as its efficacy in gene delivery[21]. Laponite clay is a negatively charged disk-shaped synthetic silicate that has been shown to support tissue regeneration[22,23]. It has been used in drug delivery for its ability to modulate release properties due to its capacity for intercalation[24,25].

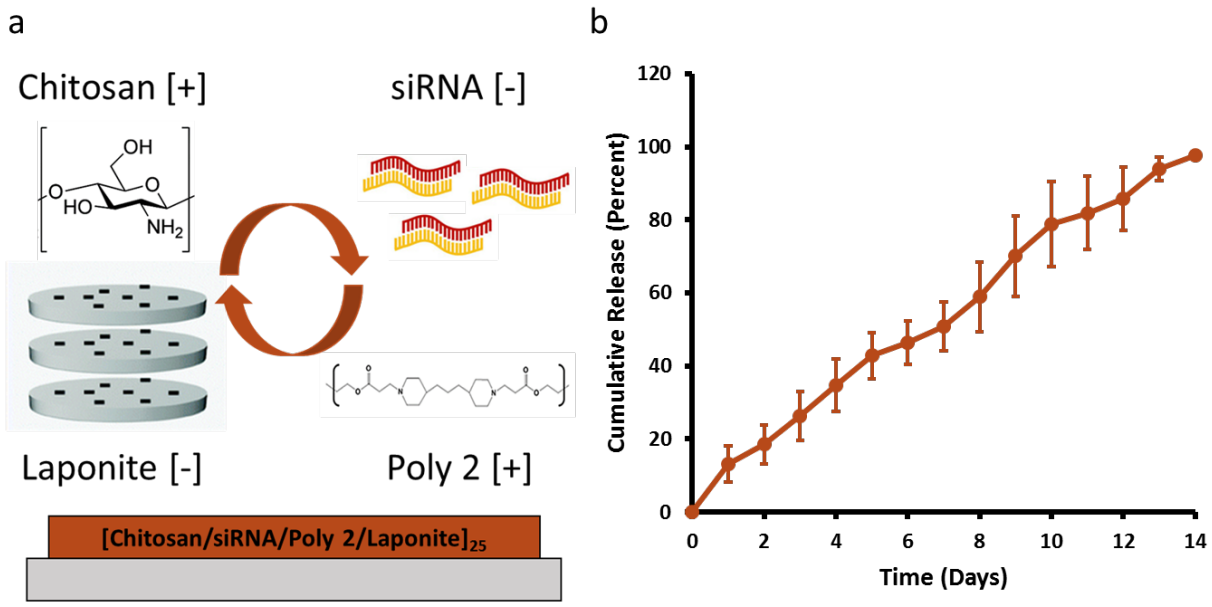

Figure 2.1 [Chitosan/siRNA/Poly 2/Laponite] Tetralayer Film for siRNA Delivery. (a) Schematic of assembly process for [Chitosan/siRNA/Poly 2/Laponite] tetralayer films. Chitosan (15 kDa) and laponite clay were prepared at a 1 mg/mL concentration. The siRNA solution was prepared at a 20 µg/mL concentration. Poly 2 was prepared at a 2 mg/mL concentration. The chitosan, siRNA, and Poly 2 solutions were prepared in deionized water that was buffered to 10 mM with pH 4.5 sodium acetate buffer. The laponite clay solution was prepared without buffer at a pH of 8.0. Wash steps occurred between each deposition step. (b) Cumulative siRNA release curve for 25 tetralayers of [Chitosan/siRNA/Poly 2/Laponite] LbL film. Sustained release is seen over the course of two weeks. siRNA release was performed in PBS at 37°C. Release was quantified with a plate reader using fluorescently labeled siRNA. Error bars represent standard deviation.

The assembly of this tetralayer film was found to incorporate approximately 15 µg/cm^2 of siRNA on the silicon substrate. This architecture also demonstrated sustained release of siRNA for up to two weeks in phosphate buffered saline (PBS) maintained at 37°C (Figure 2.1b). The tetralayer film was found to be a suitable basis for further investigation into constructing dual siRNA films due to its physiologically relevant timescale of drug release.

2.3.2 Initial Efforts in Modulating Sequential Release

Once we had achieved sustained release of a single siRNA from this tetralayer architecture, we investigated the effects of depositing a film of the same composition on top of the original film. The siRNA in this second layer was labeled with a different fluorescent dye to distinguish the siRNAs during quantification for characterization of release kinetics. This dual siRNA film was investigated to determine if a simple stacking of the architecture would induce sequential release. Figure 2.2a depicts the schematic of this film with 'siRNA1' referring to the siRNA deposited first and 'siRNA2' referring to the second deposited siRNA.

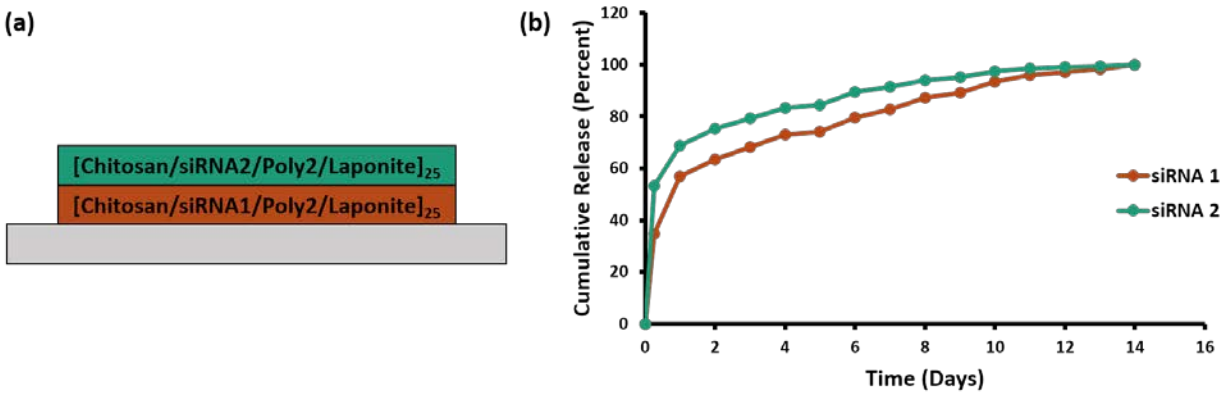

Figure 2.2 Simple Stacked [Chitosan/siRNA/Poly 2/Laponite] Tetralayer Film. (a) Schematic representation of LbL architecture for dual siRNA release. (b) Cumulative siRNA release over time in percentages. siRNA release was performed in PBS at 37°C. Twenty five repeats of the tetralayer containing siRNA1 are deposited first (brown) followed by 25 repeats of the tetralayer containing siRNA2 (green). siRNA1 and siRNA2 refer siRNAs tagged with different fluorescent dyes. The color representations of siRNA correspond to the colors of the curves in the cumulative release plot.

The release curves of this film show that no appreciable delay of release of siRNA1 is achieved (Figure 2.2b). The two siRNAs exhibit similar release profiles. Interestingly, the release profiles of both siRNAs show faster release compared to the single siRNA film in Figure 2.1. Over 50% of each siRNA is released within the first day of incubation in PBS, while it takes approximately four days for 50% release from the single siRNA formulation. The comparable release rates of the two siRNAs and the quicker release suggest that interlayer diffusion of siRNAs and film rearrangement occur during film assembly.

2.3.3 [Chitosan/Laponite] Barrier Layers

To achieve greater distinction in release of dual siRNA films, we investigated various barrier layers for preventing interlayer diffusion. The first barrier layer formulation we looked into was the bilayer consisting of chitosan and laponite clay. The addition of laponite clay barrier layers would increase tortuosity of diffusion paths within LbL films due to their high aspect ratios[26]. This barrier layer formulation was previously reported to show success in achieving staggered release of bone morphogenetic protein-2 (rhBMP-2) and gentamicin (GS) by blocking diffusion-based release and preventing interlayer diffusion[11]. The formulation was chosen to be studied first as both components of the bilayer were already used in the siRNA-containing tetralayers.

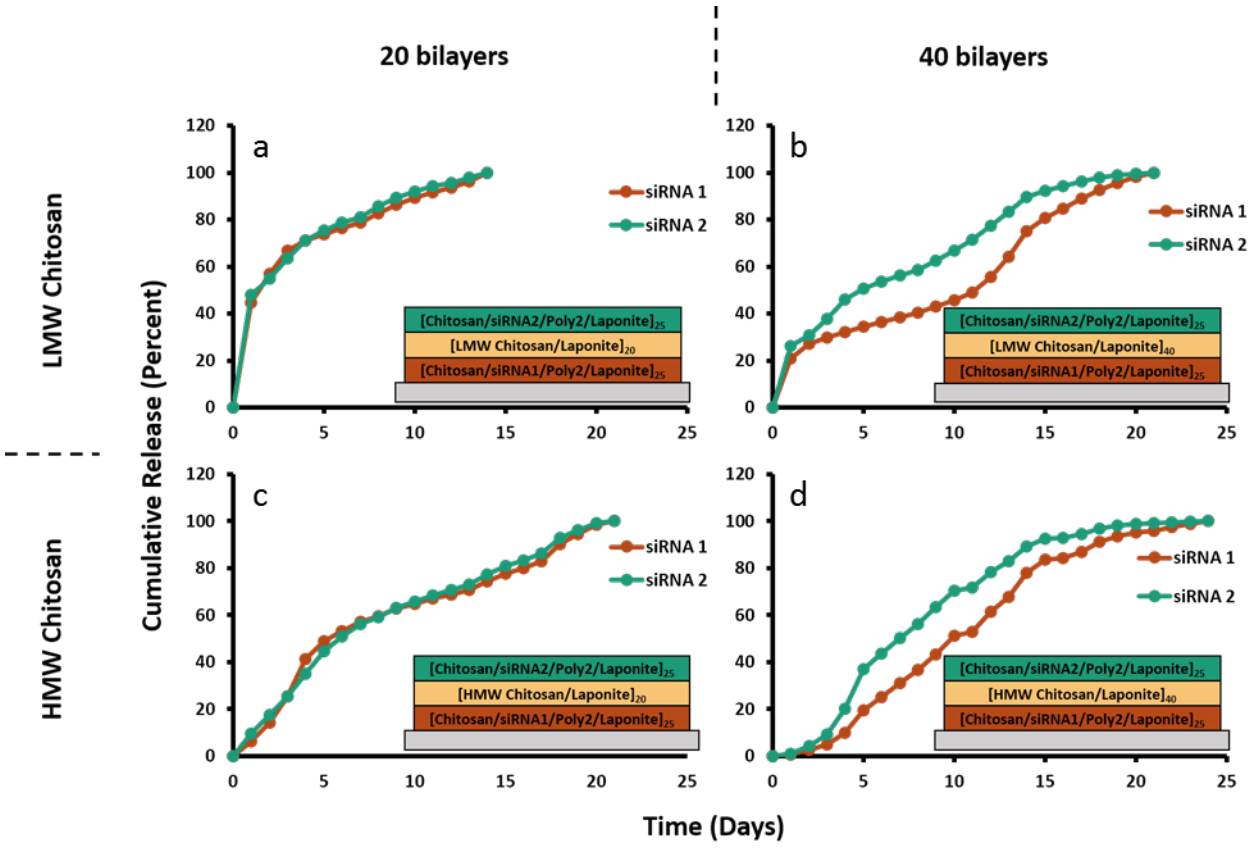

Figure 2.3 Release Profiles of Films with [Chitosan/Laponite] Barrier. Within each film, barrier layers were deposited between two sets of [Chitosan/siRNA/Poly 2/Laponite]$_{25}$ tetralayers with siRNA1 (brown) beneath and siRNA2 (green) on top. Barrier layers studied consisted of (a) 20 bilayers of [LMW Chitosan/Laponite], (b) 40 bilayers of [LMW Chitosan/ Laponite], (c) 20 bilayers of [HMW Chitosan/Laponite], and (d) 40 bilayers of [HMW Chitosan/Laponite]. Cumulative release is reported over time in percentages. Films with 40 bilayers of barrier exhibit a clear stagger of release compared to films with 20 bilayers. Films that incorporate high molecular weight chitosan into the barrier exhibit a greater suppression of release compared to films that incorporate low molecular weight chitosan.

We investigated a variety of films in which [Chitosan/Laponite] bilayers were deposited between the siRNA-containing tetralayers (Figure 2.3). Particularly, we studied the impact that the number of barrier layers and the molecular weight of chitosan have on stratifying siRNA release. Barriers of 20 bilayers and 40 bilayers were introduced into films. Barrier layers were constructed with low molecular weight (LMW) chitosan (15 kDa) and high molecular weight (HMW) chitosan (350 kDa).

While none of the formulations produced an appreciable stagger in release of siRNAs, they provide insight on the effects of number of bilayers and molecular weight. Films with 20 barrier bilayers exhibited no distinction in siRNA release curves across both molecular weights of chitosan tested. This suggests that with 20 bilayers, the barrier layer is not sufficient to prevent interlayer diffusion; rearrangement of the film during LbL assembly and diffusion of siRNA results

in siRNA1 and siRNA2 releasing at the same rate. Nonetheless, slight distinction in release profiles of the siRNAs is achieved with 40 barrier bilayers in formulations of both LMW and HMW chitosan. This indicates the addition of bilayers was able to deter interlayer diffusion of the siRNA in some extent.

The effects of using HMW chitosan as opposed to LMW chitosan can also be appreciated. When HMW chitosan is incorporated into the barrier layer, release of siRNA is seen to be slower and more sustained. This is apparent in formulations with both 20 bilayers and 40 bilayers of barrier. The suppression of release kinetics suggests that chitosan of higher molecular weight increases the durability of the LbL film, decreasing the rate of its degradation.

2.3.4 Hierarchical Structure for Sequential Release

From the [Chitosan/Laponite] barrier films studied, we found that the barrier consisting of 40 bilayers with HMW chitosan achieved the most significant delay in release of siRNA1. Nonetheless, the release of siRNA2 was also found to be dampened. We hypothesize this may be due to rearrangement of the film during assembly and laponite clay from the barrier layer diffusing into the siRNA2-containing tetralayer. In efforts to achieve greater stratification in release of the siRNAs, we endeavored to tune the composition of the top siRNA2 tetralayer for quicker release while maintaining the [HMW Chitosan/Laponite]$_{40}$ barrier layer and [Chitosan/siRNA1/Poly 2/ Laponite]$_{25}$ bottom tetralayer. The hypothesized result would be a quicker release of siRNA2, followed by the delayed release of siRNA1 as seen in Figure 2.3d.

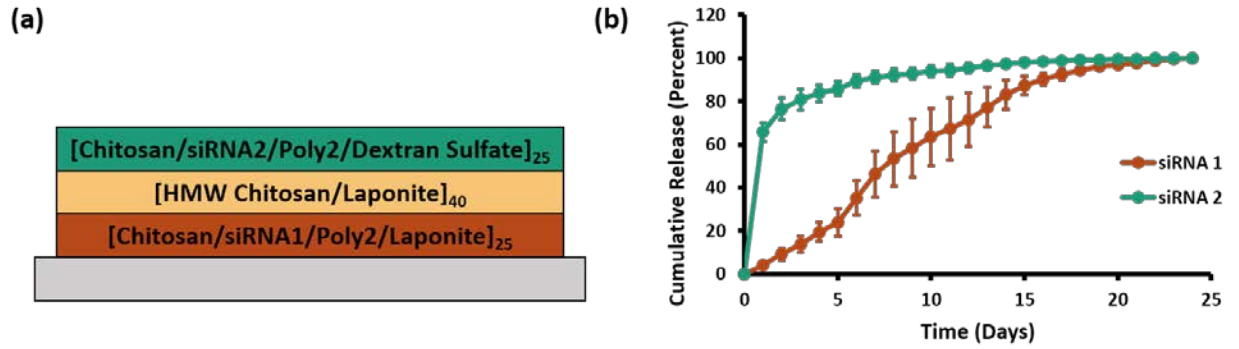

Figure 2.4 Hierarchical Structure with [HMW Chitosan/Laponite]$_{40}$ Barrier. (a) Schematic of LbL architecture for staggered release. The bottom film consists of 25 tetralayers of chitosan (15 kDa), siRNA, Poly 2, and laponite clay. The barrier film consists of 40 bilayers of high molecular weight chitosan (350 kDa) and laponite clay. The top film consists of 25 tetralayers of chitosan (15 kDa), siRNA, Poly 2, and dextran sulfate. (b) Release Profile of siRNAs. Cumulative release of siRNA is reported in percentages. With this architecture, siRNA2 (green) is readily released while siRNA1 (brown) exhibits a slower sustained release. Error bars represent standard deviation.

To achieve a more rapid release of siRNA2 from the top tetralayer, we replaced the laponite clay with dextran sulfate in the architecture (Figure 2.4a) as laponite was thought to be the component that contributed the most to slow release. Dextran sulfate is an anionic polysaccharide commonly used in LbL formulations[27–29]. As hypothesized, siRNA2 is readily released from the film while the release of siRNA1 is dampened (Figure 2.4b). The stratification is prominent; within 5 days, approximately 80% of siRNA2 is released, whereas only about 20% of siRNA1 from the film is released. The film exhibits sustained release of siRNA1, and after two weeks approximately 80% of siRNA1 is released.

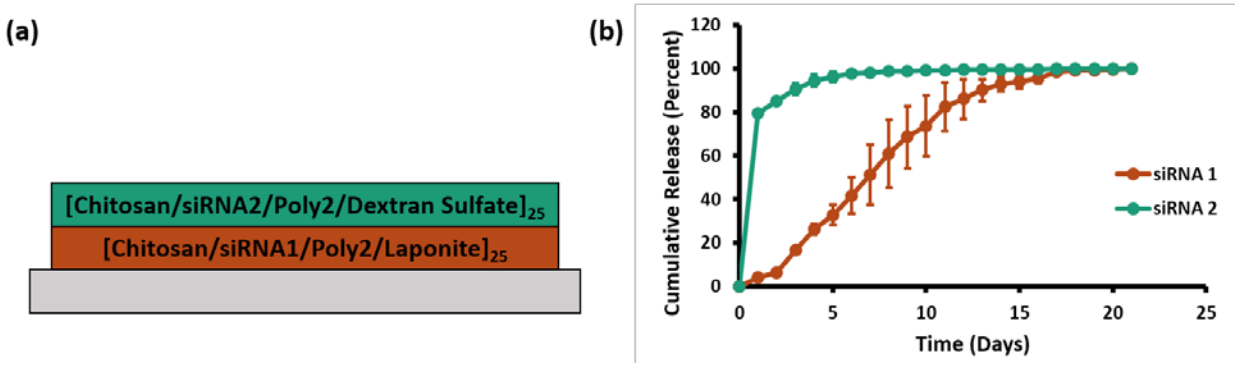

Figure 2.5 Hierarchical Structure without Barrier. (a) Schematic of LbL architecture for staggered release. The bottom film consists of 25 tetralayers of chitosan (15 kDa), siRNA, Poly 2, and laponite clay. The top film consists of 25 tetralayers of chitosan (15 kDa), siRNA, Poly 2, and dextran sulfate. (b) Release Profile of siRNAs. Cumulative release of siRNA is reported in percentages. With this architecture, siRNA2 (green) is still readily released while siRNA1 (brown) exhibits a slower sustained release. Error bars represent standard deviation.

The stark effect of replacing laponite with dextran sulfate in the top siRNA2 tetralayer led us to investigate the effects of removing the [HMW Chitosan/Laponite]$_{40}$ barrier layer from this film to determine how much of an effect the barrier truly had. The [Chitosan/siRNA1/Poly 2/Laponite]$_{25}$ tetralayers were deposited first, followed by [Chitosan/siRNA2/Poly 2/Dextran Sulfate]$_{25}$ (Figure 2.5a). The cumulative release curves (Figure 2.5b) reveal stratification of siRNA release similar to that of the film with the [HMW Chitosan/Laponite]$_{40}$ barrier layer. Here, within 5 days, approximately 95% of siRNA 2 is released, and about 30% of siRNA1 is released. Sustained release of siRNA1 still occurs, and after two weeks approximately 90% of siRNA1 is released.

The study of this LbL architecture reveals that sequential siRNA release is indeed achievable without the need of a barrier layer to block interlayer diffusion. By tuning the composition of the two siRNA-containing tetralayers, stratification of release is possible. Here, the [HMW Chitosan/Laponite]$_{40}$ barrier layers show little effect on modulating release kinetics.

2.3.5 Graphene Oxide as a Barrier Layer Component

To increase control in modulating sequential release of siRNA, we investigated the use of high aspect ratio graphene oxide (GO) as a barrier layer component. GO has been found to have a potent thrombogenic effect observed both *in vitro* and *in vivo*[30], which may prove advantageous in the context of wound healing. A study by Hong et al. showed that barrier layers of alternating amine-functionalized GO (GO-NH_2) and GO were able to delay the release of protein ovalbumin. They were able to tune delay of ovalbumin release from 30 to 90 days from an LbL film by varying the number of bilayers of functionalized GO[31].

Furthermore, research has shown that GO has notable interactions with laponite clay. Chouhan et al. presents a method for the formation of a Laponite-GO hybrid from a highly stable aqueous dispersion in the ratio Lap:GO of 10:1[32]. [GO/Laponite] films have been previously investigated as a multilayer coating for reducing oxygen permeability due to the high aspect ratio of the two components creating tortuous pathways in the gas barrier[33].

Three different barrier layers containing GO and/or GO-NH_2 were investigated: [GO-NH_2/ Laponite]$_{10}$, [Chitosan/Lap-GO Hybrid]$_{10}$, and [GO-NH_2/GO]$_{10}$. The "Lap-GO Hybrid" component consisted of a 5 to 1 weight ratio mixture of laponite to graphene oxide. These barrier films were deposited between the bottom slow-release [Chitosan/siRNA1/Poly 2/Laponite]$_{25}$ and the top quick-release [Chitosan/siRNA2/Poly 2/Dextran Sulfate]$_{25}$ tetralayers (Figure 2.6).

The three different barrier layer formulations each exhibited distinct effects in modulating sequential release of siRNA. The [GO-NH_2/Laponite]$_{10}$ barrier (Figure 2.6a) was found to induce a somewhat sustained release of siRNA2. Approximately 50% of siRNA2 is released in the first day, followed by a steady release of the rest of the load over the course of a week. The release of the bottom siRNA1 was delayed. Only 20% is eluted during the first week. The release rate increases in the second week, with near complete elution by day 14.

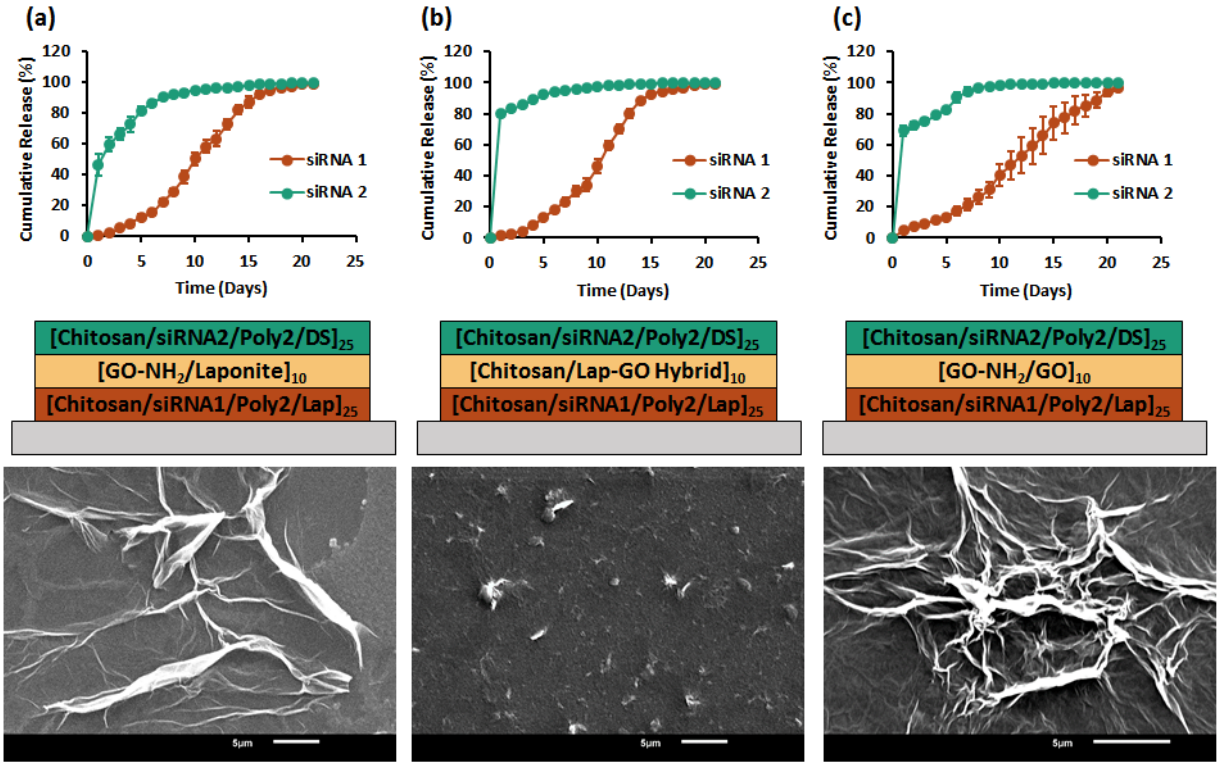

Figure 2.6 Graphene Oxide Barrier Layers. Cumulative siRNA release profiles, schematic representation, and SEM imaging of (a) [GO-NH_2/Laponite]$_{10}$, (b) [Chitosan/Lap-GO Hybrid], and (c) [GO-NH_2/GO]$_{10}$. Apart from the barrier layers, the architecture is the same for each group: [Chitosan/siRNA2/Poly2/Dextran Sulfate]$_{25}$ on the top and [Chitosan/siRNA1/Poly2/Laponite]$_{25}$ on the bottom. Cumulative release of siRNA is reported in percentages. Release of siRNA1 is in brown, release of siRNA2 is in green. Error bars represent standard deviation. Scale bar is 5 µm for SEM images.

The [Chitosan/Lap-GO Hybrid]$_{10}$ barrier (Figure 2.6b) resulted in the greatest burst release of siRNA2 with 80% released in the first day. Most of the siRNA2 load is subsequently released over the first week. The release of the bottom siRNA1 is similar to the previous film with [GO-NH_2/Laponite]$_{10}$ barrier. Approximately 20% of siRNA1 is released during the first week, followed by steady release of the rest during the second week.

The incorporation of [GO-NH_2/GO]$_{10}$ barrier (Figure 2.6c) in the LbL film produced burst release of siRNA2 with 70% released in the first day. This is followed by sustained release of the rest of siRNA2 over the first week. This barrier film had the greatest effect on the elution of the bottom siRNA1. Similar to the previous two films, approximately 20% siRNA1 is released over the first week. However, with this particular barrier formulation, subsequent release of siRNA1 is sustained out to three weeks.

Scanning electron microscopy (SEM) imaging of the barrier layers provides insight to the interactions of the different components. While faint in the image of the [Chitosan/Lap-GO Hybrid]$_{10}$ barrier, the web-like sheets of GO are prominent in the images of the [GO-NH_2/ Laponite]$_{10}$ barrier and [GO-NH_2/GO]$_{10}$ barrier. Laponite clay platelets can be recognized in the SEM image of the [GO-NH_2/Laponite]$_{10}$ barrier.

Table 2.1 siRNA Loadings of Hierarchical LbL Films. Films were constructed with [Chitosan/siRNA1/Poly 2/Laponite]$_{25}$ tetralayer deposited first. Barrier layers (if applicable) were deposited next. [Chitosan/siRNA2/Poly2/Dextran Sulfate]$_{25}$ were then deposited. siRNA loadings were quantified by fluorescence readings of the distinctly labeled siRNAs. Loadings are reported as mean ± standard deviation.

Barrier Layer Formulation	siRNA1 Loading (μg/cm^2)	siRNA2 Loading (μg/cm^2)
No barrier	4.57 ± 0.08	2.72 ± 0.29
[GO-NH_2/Laponite]$_{10}$	7.94 ± 1.23	3.40 ± 1.13
[Chitosan/Lap-GO Hybrid]$_{10}$	4.46 ± 0.79	4.69 ± 0.22
[GO-NH_2/GO]$_{10}$	6.65 ± 1.07	5.37 ± 1.45

A comparison of the siRNA loadings within these films in Table 2.1 reveal noteworthy trends. The siRNA loadings for both siRNA1 and siRNA2 are generally greater in formulations with barrier layers compared to the formulation without a barrier. This suggests that siRNA may be diffusing out of the film during assembly of the formulation without a barrier. We hypothesize that the incorporation of barrier layers stabilize the films, preventing leakage of underlying siRNA1 while promoting retention of deposited siRNA2 on top. Barrier layers thus potentially serve not only to modulate stratification of release, but also to increase overall siRNA loading through film stabilization.

The deposition of the [GO-NH_2/Laponite]$_{10}$ and [GO-NH_2/GO]$_{10}$ barrier layers appear to provide greater retention of siRNA1 compared to the [Chitosan/Lap-GO Hybrid]$_{10}$ barrier. This phenomenon correlates with the presence of web-like sheets in the SEM images in Figure 2.6, suggesting that formation of these sheets prevent diffusion of siRNA1 even during film assembly.

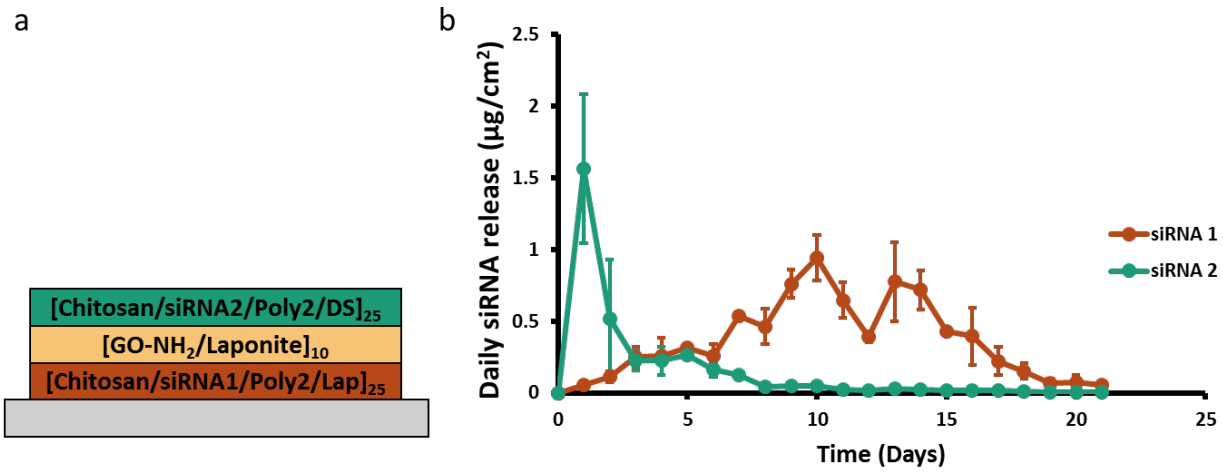

Figure 2.7 [GO-NH_2/Laponite]$_{10}$ Barrier Layer. (a) Schematic of LbL architecture with [GO-NH_2/Laponite]$_{10}$ barrier layer. (b) Day-by-day release plot of siRNA in µg/cm^2. Error bars represent standard deviation.

Of the three GO-containing barrier layers investigated, the [GO-NH_2/Laponite]$_{10}$ formulation is of particular interest. This LbL formulation was found to release siRNA2 in a more sustained manner compared to the other films. A daily release plot (Figure 2.7) depicts sustained release of siRNA2 over the course of a week after an initial burst release on day 1. Release of siRNA1 is minimal during the first week, and then increases on day 8 with sustained release for approximately 10 days afterward. The modulation of siRNA2 release by this barrier is suspected to be a result of laponite clay from the barrier diffusing into the top tetralayer during assembly. The absence of this phenomenon in the formulation with the [Chitosan/Lap-GO Hybrid]$_{10}$ barrier may be due to various reasons. It may be possible that stronger electrostatic interactions between GO and laponite in the hybrid mixture restrict the diffusion of laponite into the siRNA2 tetralayer.

2.4 Conclusions

In this work, we describe our efforts in developing LbL films for sequential release of distinct siRNAs. We began this work with investigation of the tetralayer [Chitosan/siRNA/Poly 2/Laponite]$_{25}$ for release of a single siRNA from silicon chips. This film was found to exhibit sustained release of siRNA over approximately two weeks. The subsequent deposition of tetralayers of the same formulation with distinctly tagged siRNA did not result in stratification of siRNA release. The deposition of barrier layers consisting of [Chitosan/Laponite] bilayers in between the two tetralayers was investigated. Subtle effects of chitosan molecular weight and number of barrier layers were identified but stratification of release profiles was not achieved by these barrier formulations.

Replacing laponite with dextran sulfate in the top tetralayer formulation was found to produce prominent separation of release profiles without the need of barrier layers. The top siRNA2 exhibited a burst release of 80% followed by a sustained release for a week. The bottom siRNA1 had a steady release over the course of two weeks.

The investigation of incorporating barrier layers composed with GO and/or GO-NH_2 yielded a range of release profiles. Three different barrier layers, $[GO\text{-}NH_2/Laponite]_{10}$, [Chitosan/ Lap-GO Hybrid]$_{10}$, and $[GO\text{-}NH_2/GO]_{10}$, were found to have distinct effects on siRNA release. SEM imaging of these barrier formulations revealed the formation of web-like sheets of GO; these structures likely contribute to preventing interlayer diffusion of siRNA. The incorporation of these barrier layers were found not only to modulate siRNA release, but also to increase siRNA loading.

Of these three formulations, the effects of the $[GO\text{-}NH_2/Laponite]_{10}$ barrier are noteworthy. This barrier layer induced sustained release of siRNA2 during the first week, followed by sustained release of siRNA1. This release profile roughly matches the physiological timeline of wound healing, with inflammation and proliferation generally occurring during the first week post-injury, followed by the remodeling stage afterward. A promising application of this work would be to coat a wound dressing with this LbL formulation for initial release of siRNA to address wound closure during the first week, followed by release of siRNA to address fibrosis.

In this chapter, we describe our discovery of LbL formulations and barrier layers that provide stratification of siRNA release. Apart from using these films for testing in animal wound models, recommendations for further work include efforts to tune delay of underlying siRNA1 by changing the number of bilayers used for the barrier. We hypothesize that increasing the number of bilayers would result in increased stratification of release. Further study may also include investigating different barrier layer compositions with GO and GO-NH_2. Partly initiated in the next chapter of this thesis, investigation into the effects of assembly parameters (eg. pH, concentrations, etc.) on siRNA loading, release, and efficacy is warranted as well. LbL formulations discovered in this work may apply to modulate sequential release of not only siRNA, but potentially also other therapeutic nucleic acids (eg. plasmid DNA, mRNA, miRNA mimics), growth factors, and antibiotics for controlled localized delivery.

2.5 References

(1) Alkekhia, D.; Hammond, P. T.; Shukla, A. Layer-by-Layer Biomaterials for Drug Delivery. *Annual Review of Biomedical Engineering* **2020**, *22* (1), null. https://doi.org/10.1146/annurev-bioeng-060418-052350.

(2) Borges, J.; Mano, J. F. Molecular Interactions Driving the Layer-by-Layer Assembly of Multilayers. *Chem. Rev.* **2014**, *114* (18), 8883–8942. https://doi.org/10.1021/cr400531v.

(3) Castleberry, S. A.; Almquist, B. D.; Li, W.; Reis, T.; Chow, J.; Mayner, S.; Hammond, P. T. Self-Assembled Wound Dressings Silence MMP-9 and Improve Diabetic Wound Healing In Vivo. *Advanced Materials* **2016**, *28* (9), 1809–1817. https://doi.org/10.1002/adma.201503565.

(4) Truong-Phuoc, L.; Christoforidis, K. C.; Vigneron, F.; Papaefthimiou, V.; Decher, G.; Keller, N.; Keller, V. Layer-by-Layer Photocatalytic Assembly for Solar Light-Activated Self-Decontaminating Textiles. *ACS Appl. Mater. Interfaces* **2016**, *8* (50), 34438–34445. https://doi.org/10.1021/acsami.6b12585.

(5) Jia, Z.; Xiu, P.; Roohani-Esfahani, S.-I.; Zreiqat, H.; Xiong, P.; Zhou, W.; Yan, J.; Cheng, Y.; Zheng, Y. Triple-Bioinspired Burying/Crosslinking Interfacial Coassembly Strategy for Layer-by-Layer Construction of Robust Functional Bioceramic Self-Coatings for Osteointegration Applications. *ACS Appl. Mater. Interfaces* **2019**, *11* (4), 4447–4469. https://doi.org/10.1021/acsami.8b20429.

(6) Chuang, H. F.; Smith, R. C.; Hammond, P. T. Polyelectrolyte Multilayers for Tunable Release of Antibiotics. *Biomacromolecules* **2008**, *9* (6), 1660–1668. https://doi.org/10.1021/bm800185h.

(7) Smith, R. C.; Riollano, M.; Leung, A.; Hammond, P. T. Layer-by-Layer Platform Technology for Small-Molecule Delivery. *Angewandte Chemie International Edition* **2009**, *48* (47), 8974–8977. https://doi.org/10.1002/anie.200902782.

(8) Shah, N. J.; Macdonald, M. L.; Beben, Y. M.; Padera, R. F.; Samuel, R. E.; Hammond, P. T. Tunable Dual Growth Factor Delivery from Polyelectrolyte Multilayer Films. *Biomaterials* **2011**, *32* (26), 6183–6193. https://doi.org/10.1016/j.biomaterials.2011.04.036.

(9) Saurer, E. M.; Jewell, C. M.; Kuchenreuther, J. M.; Lynn, D. M. Assembly of Erodible, DNA-Containing Thin Films on the Surfaces of Polymer Microparticles: Toward a Layer-by-Layer Approach to the Delivery of DNA to Antigen-Presenting Cells. *Acta Biomaterialia* **2009**, *5* (3), 913–924. https://doi.org/10.1016/j.actbio.2008.08.022.

(10) Almquist, B. D.; Castleberry, S. A.; Sun, J. B.; Lu, A. Y.; Hammond, P. T. Combination Growth Factor Therapy via Electrostatically Assembled Wound Dressings Improves Diabetic Ulcer Healing In Vivo. *Advanced Healthcare Materials* **2015**, *4* (14), 2090–2099. https://doi.org/10.1002/adhm.201500403.

(11) Min, J.; Braatz, R. D.; Hammond, P. T. Tunable Staged Release of Therapeutics from Layer-by-Layer Coatings with Clay Interlayer Barrier. *Biomaterials* **2014**, *35* (8), 2507–2517. https://doi.org/10.1016/j.biomaterials.2013.12.009.

(12) Min, J.; Choi, K. Y.; Dreaden, E. C.; Padera, R. F.; Braatz, R. D.; Spector, M.; Hammond, P. T. Designer Dual Therapy Nanolayered Implant Coatings Eradicate Biofilms and Accelerate Bone Tissue Repair. *ACS Nano* **2016**, *10* (4), 4441–4450. https://doi.org/10.1021/acsnano.6b00087.

(13) Janis, J. E.; Kwon, R. K.; Lalonde, D. H. A Practical Guide to Wound Healing. *Plastic and Reconstructive Surgery* **2010**, *125* (6). https://doi.org/10.1097/PRS.0b013e3181d9a0d1.

(14) Berger, A. G.; Chou, J. J.; Hammond, P. T. Approaches to Modulate the Chronic Wound Environment Using Localized Nucleic Acid Delivery. *Advances in Wound Care* **2020**. https://doi.org/10.1089/wound.2020.1167.
(15) Street, J.; Bao, M.; deGuzman, L.; Bunting, S.; Peale, F. V.; Ferrara, N.; Steinmetz, H.; Hoeffel, J.; Cleland, J. L.; Daugherty, A.; Bruggen, N. van; Redmond, H. P.; Carano, R. A. D.; Filvaroff, E. H. Vascular Endothelial Growth Factor Stimulates Bone Repair by Promoting Angiogenesis and Bone Turnover. *PNAS* **2002**, *99* (15), 9656–9661. https://doi.org/10.1073/pnas.152324099.
(16) Lynn, D. M.; Langer, R. Degradable Poly(β-Amino Esters): Synthesis, Characterization, and Self-Assembly with Plasmid DNA. *J. Am. Chem. Soc.* **2000**, *122* (44), 10761–10768. https://doi.org/10.1021/ja0015388.
(17) Kang, P.-L.; Chang, S. J.; Manousakas, I.; Lee, C. W.; Yao, C.-H.; Lin, F.-H.; Kuo, S. M. Development and Assessment of Hemostasis Chitosan Dressings. *Carbohydrate Polymers* **2011**, *85* (3), 565–570. https://doi.org/10.1016/j.carbpol.2011.03.015.
(18) Howard, K. A.; Rahbek, U. L.; Liu, X.; Damgaard, C. K.; Glud, S. Z.; Andersen, M. Ø.; Hovgaard, M. B.; Schmitz, A.; Nyengaard, J. R.; Besenbacher, F.; Kjems, J. RNA Interference in Vitro and in Vivo Using a Novel Chitosan/SiRNA Nanoparticle System. *Molecular Therapy* **2006**, *14* (4), 476–484. https://doi.org/10.1016/j.ymthe.2006.04.010.
(19) Liu, X.; Howard, K. A.; Dong, M.; Andersen, M. Ø.; Rahbek, U. L.; Johnsen, M. G.; Hansen, O. C.; Besenbacher, F.; Kjems, J. The Influence of Polymeric Properties on Chitosan/SiRNA Nanoparticle Formulation and Gene Silencing. *Biomaterials* **2007**, *28* (6), 1280–1288. https://doi.org/10.1016/j.biomaterials.2006.11.004.
(20) Chen, M.; Gao, S.; Dong, M.; Song, J.; Yang, C.; Howard, K. A.; Kjems, J.; Besenbacher, F. Chitosan/SiRNA Nanoparticles Encapsulated in PLGA Nanofibers for SiRNA Delivery. *ACS Nano* **2012**, *6* (6), 4835–4844. https://doi.org/10.1021/nn300106t.
(21) Akinc, A.; Anderson, D. G.; Lynn, D. M.; Langer, R. Synthesis of Poly(Beta-Amino Ester)s Optimized for Highly Effective Gene Delivery. *Bioconjug. Chem.* **2003**, *14* (5), 979–988. https://doi.org/10.1021/bc034067y.
(22) Gaharwar, A. K.; Mihaila, S. M.; Swami, A.; Patel, A.; Sant, S.; Reis, R. L.; Marques, A. P.; Gomes, M. E.; Khademhosseini, A. Bioactive Silicate Nanoplatelets for Osteogenic Differentiation of Human Mesenchymal Stem Cells. *Advanced Materials* **2013**, *25* (24), 3329–3336. https://doi.org/10.1002/adma.201300584.
(23) Gaharwar, A. K.; Schexnailder, P. J.; Kline, B. P.; Schmidt, G. Assessment of Using Laponite® Cross-Linked Poly(Ethylene Oxide) for Controlled Cell Adhesion and Mineralization. *Acta Biomaterialia* **2011**, *7* (2), 568–577. https://doi.org/10.1016/j.actbio.2010.09.015.
(24) Viseras, C.; Aguzzi, C.; Cerezo, P.; Bedmar, M. C. Biopolymer-Clay Nanocomposites for Controlled Drug Delivery. *Materials Science and Technology* **2008**, *24* (9), 1020–1026. https://doi.org/10.1179/174328408X341708.
(25) Takahashi, T.; Yamada, Y.; Kataoka, K.; Nagasaki, Y. Preparation of a Novel PEG–Clay Hybrid as a DDS Material: Dispersion Stability and Sustained Release Profiles. *Journal of Controlled Release* **2005**, *107* (3), 408–416. https://doi.org/10.1016/j.jconrel.2005.03.031.
(26) Dhieb, F. B.; Dil, E. J.; Tabatabaei, S. H.; Mighri, F.; Ajji, A. Effect of Nanoclay Orientation on Oxygen Barrier Properties of LbL Nanocomposite Coated Films. *RSC Adv.* **2019**, *9* (3), 1632–1641. https://doi.org/10.1039/C8RA09522A.

(27) Morton, S. W.; Poon, Z.; Hammond, P. T. The Architecture and Biological Performance of Drug-Loaded LbL Nanoparticles. *Biomaterials* **2013**, *34* (21), 5328–5335. https://doi.org/10.1016/j.biomaterials.2013.03.059.
(28) Serizawa, T.; Yamaguchi, M.; Akashi, M. Enzymatic Hydrolysis of a Layer-by-Layer Assembly Prepared from Chitosan and Dextran Sulfate. *Macromolecules* **2002**, *35* (23), 8656–8658. https://doi.org/10.1021/ma012153s.
(29) Serizawa, T.; Yamaguchi, M.; Kishida, A.; Akashi, M. Alternating Gene Expression in Fibroblasts Adhering to Multilayers of Chitosan and Dextran Sulfate. *Journal of Biomedical Materials Research Part A* **2003**, *67A* (3), 1060–1063. https://doi.org/10.1002/jbm.a.10150.
(30) Seabra, A. B.; Paula, A. J.; de Lima, R.; Alves, O. L.; Durán, N. Nanotoxicity of Graphene and Graphene Oxide. *Chem. Res. Toxicol.* **2014**, *27* (2), 159–168. https://doi.org/10.1021/tx400385x.
(31) Hong, J.; Shah, N. J.; Drake, A. C.; DeMuth, P. C.; Lee, J. B.; Chen, J.; Hammond, P. T. Graphene Multilayers as Gates for Multi-Week Sequential Release of Proteins from Surfaces. *ACS Nano* **2012**, *6* (1), 81–88. https://doi.org/10.1021/nn202607r.
(32) Chouhan, D. K.; Patro, T. U.; Harikrishnan, G.; Kumar, S.; Gupta, S.; Kumar, G. S.; Cohen, H.; Wagner, H. D. Graphene Oxide-Laponite Hybrid from Highly Stable Aqueous Dispersion. *Applied Clay Science* **2016**, *132–133*, 105–113. https://doi.org/10.1016/j.clay.2016.05.023.
(33) Yoo, J.; Lee, S. B.; Lee, C. K.; Hwang, S. W.; Kim, C.; Fujigaya, T.; Nakashima, N.; Shim, J. K. Graphene Oxide and Laponite Composite Films with High Oxygen-Barrier Properties. *Nanoscale* **2014**, *6* (18), 10824–10830. https://doi.org/10.1039/C4NR03429E.

CHAPTER 3.

Optimizing Layer-by-Layer Films for siRNA-Mediated Knockdown with Fractional Factorial Design

3.1 Introduction

Small interfering RNAs (siRNA) have great therapeutic potential for modulating protein expression at the post-transcriptional level. By associating with the endogenous RNA-induced silencing complex (RISC), siRNA cleaves mRNA of complementary sequence[1,2]. Thus, siRNA may be synthesized to theoretically target and knock down expression of any protein of choice, without concerns of integration and modification to the host DNA. FDA approvals have recently generated much excitement around siRNA therapies[3]. Potential applications are vast, ranging from inflammation management within a wound to personalized treatment of cancer[4,5].

Nonetheless, siRNA therapy is not without its challenges; naked siRNA administered intravenously is prone to nuclease degradation, rapid clearance, and rejection by the cellular membrane due to its negative charge[6]. Once in the cell, siRNA faces barriers of endosomal entrapment and lysosomal degradation. These hurdles must be overcome for effective siRNA treatment. Efforts to address these challenges in siRNA delivery have largely focused on nanoparticle delivery[7]. While there are undoubtedly benefits to intravenous delivery of siRNA nanoparticles, localized administration of siRNA may reduce both off-target effects and therapeutic load requirements. Moreover, localized delivery approaches hold promise across a variety of applications, such as treatment for bone repair, muscle regeneration, and fibrosis mitigation[8].

Research groups including our own have investigated using layer-by-layer (LbL) technology to coat orthopedic implants, wound dressings, and other medically relevant substrates with nucleic acids for local delivery[9–12]. Utilizing electrostatic interactions, LbL technology enables the assembly of conformal thin films exhibiting enhanced therapeutic loading and stability[13]. While reports have shown varied success in delivery of siRNA via LbL films, the effects of assembly conditions on efficacy remain unclear.

Hence we aim to elucidate LbL film fabrication for siRNA delivery. To complement the negatively charged siRNA in LbL assembly, we chose to use poly(β-amino ester) (PBAE), a polycation known for its biocompatibility and efficacy in gene delivery[14]. Studies have shown that

for nanoparticle delivery, therapeutic efficiency varies with the respective weight ratio (w/w ratio) of PBAE to siRNA[15]. In physiological conditions, a film containing PBAE degrades due to the hydrolyzable moieties of the polymer and releases its components for therapeutic activity[16,17]. A schematic for assembling our LbL films is shown in Figure 3.1a. LbL films were assembled on polyglactin 910 (Vicryl®) sutures. By alternately dipping the suture in solutions of PBAE and siRNA, with wash steps in between each deposition step, the bilayer film [PBAE/siRNA] was assembled on top of the sutures (Figure 3.1b). Here, we investigate the effects of LbL assembly parameters on PBAE incorporation, siRNA incorporation, and the resultant film's ability to induce protein silencing *in vitro*.

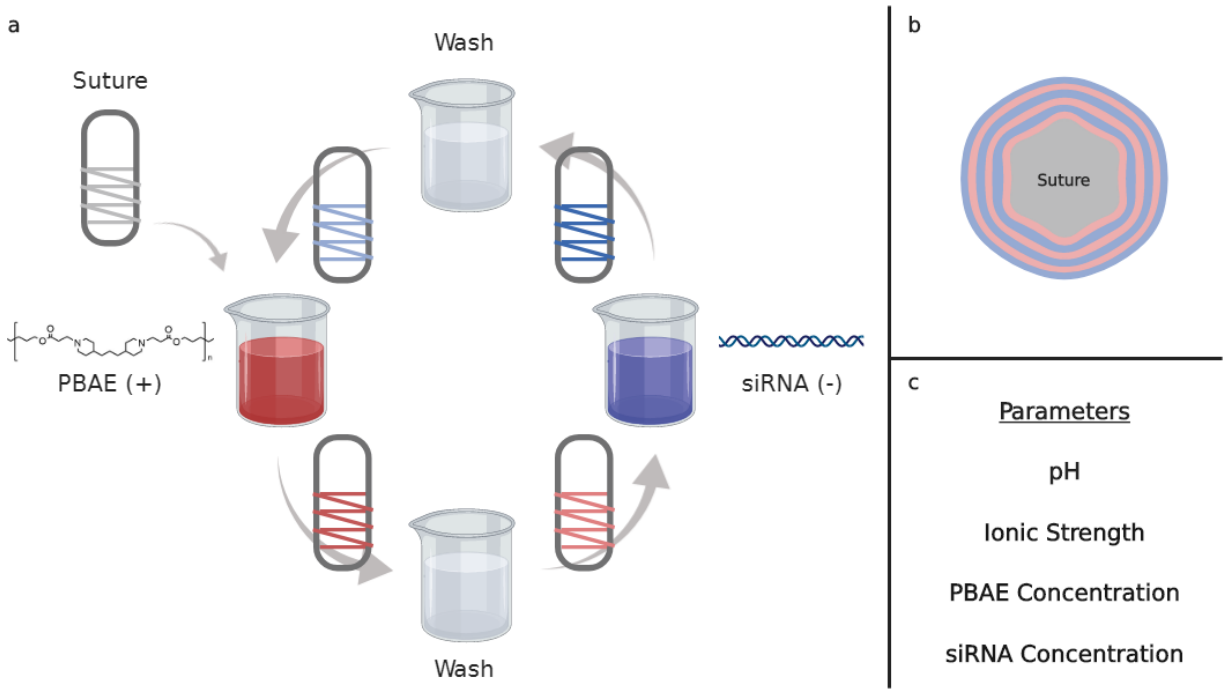

Figure 3.1 Layer-by-layer coating of suture and the parameters varied. (a) Schematic representation of dip LbL assembly for coating Vicryl 3-0 suture with [PBAE/siRNA] bilayers. (b) Cross-section depiction of a suture coated with 3 bilayers. Films assembled in this study consisted of 15 bilayers. (c) List of parameters varied in the fractional factorial design. The pH (pH 4.5 – pH 6.0) of the entire process, ionic strength (150 mM – 250 mM) and PBAE concentration (0.5 mg/mL – 2.0 mg/mL) of the PBAE bath, and the siRNA concentration (20 µg/mL – 30 µg/mL) of the siRNA bath were varied. Parameters are color coded to reference the affected steps: black for the entire process, red for the PBAE bath, and blue for the siRNA bath. Wash baths and the siRNA bath were buffered to 10 mM Sodium Acetate.

The assembly parameters that were studied consist of: pH, ionic strength, PBAE concentration, and siRNA concentration (Figure 3.1c). Experimental ranges were determined based on parameter values previously published by our lab[10,11,18]. Guided by Design of Experiment (DOE) principles, we conducted a Fractional Factorial Design to reduce the number of experiments required to determine statistically significant trends. Through this approach, we elucidated parameter effects and thereby optimized assembly conditions to establish an LbL film that, compared to previous efforts[11], induced greater knockdown while requiring fewer film layers.

3.2 Materials and Methods

3.2.1 Materials

siRNA targeting green fluorescent protein was purchased from Dharmacon (Lafayette, CO); Qiagen AllStars Neg. siRNA AF 647 Alexa Fluor 647-labeled siRNA was purchased from Qiagen (Valencia, CA). The GFP targeting siRNA has sequence 5'-GCA AGC TGA CCC TGA AGT TC–3'. Lipofectamine RNAiMAX transfection reagent was obtained from ThermoFisher Scientific (Waltham, MA). Ethicon 3-0 Vicryl sutures were purchased from Ethicon Inc. (Somerville, NJ). RNase free UltraPure water was purchased from Life Technologies (Carlsbad, CA). Sodium acetate buffer was purchased from Alfa Aesar (Haverhill, MA). 97% 4,4'-trimethylene dipiperidine and 99.9% anhydrous tetrahydrofuran (THF), inhibitor-free, were obtained from Sigma (St. Louis, MO). 99% 1,6-hexanediol diacrylate, stabilized with 90 ppm hydroquinone, was purchased from Alfa Aesar (Haverhill, MA). Hexane was purchased from Fisher Scientific (Waltham, MA). Chemicals were stored per manufacturer's instructions.

HeLa cervical cancer cells stably expressing a destabilized green fluorescent protein (GFP) (HeLa d2eGFP) were a gift from Professor Piyush Jain's Lab at the University of Florida. The plasmid construct used to express GFP in HeLa cells was CMV-d2eGFP-empty, which was a gift from Phil Sharp (Addgene plasmid # 26164). Media was Corning Dulbecco's Modified Eagle Medium (DMEM, Corning, NY) supplemented with Gibco 10% Fetal Bovine Serum (FBS, Waltham, MA) and Corning 1% Penicillin-Streptomycin (Corning, NY). The cells tested negative for mycoplasma on arrival, after thawing from storage, and periodically during culture, using a Lonza MycoAlert kit (Morristown, NJ).

3.2.2 Polymer synthesis

Synthesis of the PBAE polymer proceeded according to the literature[19]. Briefly, a 50 mL round bottom (RB) flask and stir bar were cleaned and dried in a drying oven. An oil bath was set to warm to 50°C with the stir rate set to 500 rpm. Meanwhile, 2.167 g (10.30 mmol, 1.02 equivalents) of 4,4'-trimethylene dipiperidine and 2.285 g (10.10 mmol, 1.0 equivs.) of 1,6-hexanediol diacrylate were massed to the nearest half milligram and added to the RB flask. A rubber stopper was used to cap the flask. Using the Schlenk line and dry nitrogen gas to maintain the solvent as anhydrous, a needle and syringe were used to draw up about 17 mL of THF, which was added to the RB flask. Dry nitrogen gas was bubbled into the reaction pot to purge any air, and the synthesis proceeded for 48 hours. The polymer was re-precipitated three times in ice-cold hexanes through a filter funnel, re-dissolving in THF between precipitations. The polymer was dried and stored at -20°C in a bag with desiccant. This synthesis has been successfully scaled up to three times the present synthesis, changing only the RB flask size to 250 mL.

3.2.3 Layer-by-layer film preparation

Layer-by-layer films were deposited on plasma treated Vicryl sutures. Sutures were cleaned with a 70% ethanol / 30% water mixture, rinsed with water, and consequently dried. Sutures were then wrapped around a stainless steel wire frame for ease in handling. Air plasma treatment was performed for 10 minutes on high setting in a plasma cleaner (PDC-32G, Harrick, USA). Sutures were then immediately immersed in a solution of PBAE for a duration of 1 hour. The PBAE was dissolved fresh daily using a rotating mixer due to its hydrolyzable nature and then filtered through a 0.2 μm cellulose acetate filter. Dissolution took a few hours. The concentration of PBAE, buffer pH, and ionic strength were defined by the design of experiments setup for each run.

A Carl Zeiss HMS-DS50 stainer (Oberkochen, Germany) was used to assemble the LbL films. Bilayer films were constructed through alternating adsorption steps. PBAE was adsorbed for 10 minutes, and siRNA was adsorbed for 15 minutes. Between the adsorption steps, the sutures were dipped in two wash baths of RNase free water for 30 seconds each. The fractional factorial design determined the pH of the entire process, the ionic strength of the PBAE bath, the PBAE concentration of the PBAE adsorption bath, and the siRNA concentration of the siRNA adsorption bath. All solutions were prepared in RNase free water, adjusted to the predetermined pH with

sodium acetate buffer. The wash baths and the siRNA baths were buffered to an ionic strength of 10 mM of sodium acetate.

3.2.4 LbL film characterization

Total PBAE and siRNA incorporation were measured by the following methods. Sutures coated with the LbL films were immersed in a 3 M NaCl solution. Sutures were incubated for 1 hour at 37°C then subjected to vigorous agitation for complete dissolution of the film. Releasate was split for quantification of PBAE and siRNA. The Pierce Micro BCA Protein Assay Kit (Thermo Scientific), typically used to measure protein concentration via detection of copper ion reduction[20], was repurposed to quantify the PBAE polycation in the releasate. To quantify siRNA, 100 µL releasate was first incubated with 50 µL 0.1 M NaOH for 1 hour at room temperature to hydrolyze the PBAE. Hydrolysis of the polymer was necessary, as we found that polymer complexation with siRNA interfered with RNA quantification. The releasate was then neutralized with an equal volume of 0.1 M HCl (50 µL), and the Quant-iT RiboGreen RNA Assay Kit (Invitrogen) was used to quantify the siRNA, following manufacturer's instructions. See Figure B.1 and Figure B.2 in Appendix B for standard curves and further rationale for these quantitation methods.

3.2.5 Polyplex Transfection Evaluation

HeLa d2eGFP cells in DMEM supplemented with 10% FBS and 1% penicillin-streptomycin were grown to confluence in a T75 flask at 37°C and 5% CO2. The cells were incubated for 10 minutes with Trypsin-EDTA solution to dissociate them. The dissociation was quenched with 5 mL of warm media, and the cells were pelleted at 1000 rpm in a centrifuge for 5 minutes at room temperature. The cells were resuspended in warm media and seeded at 5,000 per well in a 96-well plate. The next day, transfection was performed. 17 pmol siRNA (approx. 274 ng of labeled siRNA or 240 ng of GFP-targeting non-labeled siRNA) was mixed at varying w/w ratios with PBAE (dissolved at 1 mg/mL in 50 mM pH 5.2 sodium acetate buffer). 50 mM pH 5.2 sodium acetate buffer was added to a total volume of 85 µL. Additionally, 17 pmol siRNA was added to 85 µL 50 mM pH 5.2 sodium acetate buffer with 0.68 µL of RNAiMax to serve as a positive control. The cell media was replaced with 75 µL of OPTI-MEM, and 25 uL of the polyplexes was added to a well in the 96-well plate. This correlates to 50 nM siRNA in the final solution. Note that each stock solution therefore was plated in triplicate, with 10 µL to spare. Three

wells with just 100 μL of OPTI-MEM served as negative controls. The cells were returned to the incubator. After 6 hours, the media was replaced with warm DMEM supplemented with 10% FBS and 1% penicillin-streptomycin. The cells were incubated for three days after treatment at 37°C and 5% CO2 and then prepared for flow cytometry.

3.2.6 LbL Suture Transfection Evaluation

HeLa d2eGFP cells in DMEM supplemented with 10% FBS and 1% penicillin-streptomycin were grown to confluence in a T75 flask at 37°C and 5% CO2. The cells were incubated for 10 minutes with 5 mL Trypsin-EDTA solution to dissociate them. The dissociation was quenched with 5 mL of warm media, and the cells were pelleted at 1000 rpm in a centrifuge for 5 minutes at room temperature. The cells were resuspended in warm media and seeded at 7,000 per well in 48-well plates. The next day, transfection was performed. LbL coated sutures (cut into three 1 cm segments) were placed directly in culture with the cells in DMEM. The cells were incubated for three days after treatment at 37°C and 5% CO2 and then prepared for flow cytometry.

3.2.7 Flow Cytometry

Three days after treatment, cells were prepared for flow cytometry. The cells were dissociated with Trypsin-EDTA, as before, and the reaction was neutralized with warm media. The cells were spun down at 1000 rpm for 5 minutes at room temperature and the old media removed. The cells were resuspended in 50 μL of cold PBS with NucBlue Live Cell Stain (2 drops/mL per manufacturer's instructions) and incubated on ice, shielded from light for 30 minutes. The cells were centrifuged once again with the same conditions as before, and the PBS replaced with 150 μL of OPTI-MEM. Fluorescence was measured using a BD LSR II flow cytometer with a high throughput sampler attachment in the Swanson Biotechnology Center Flow Cytometry Facility at the Koch Institute for Integrative Cancer Research. NucBlue stain fluorescence was read with a 355 nm laser and 450/50 filter set, GFP fluorescence was read with a 488 nm laser and 530/30 filter set, and AlexaFluor647 labelled scrambled siRNA was read with a 640 nm laser and 660/20 filter set. 50 μL or up to 10000 live single cells, whichever came first, were read for each sample. Analysis was performed in BD FlowJo software (Ashland, OR). Live single-cell populations were analyzed for siRNA fluorescence, signaling uptake, and GFP expression, signaling siRNA-mediated knockdown for the polyplex data. For the suture data, only the NucBlue and GFP channels were read. The gating strategy can be found in Figure B.3.

3.2.8 Statistics

Each LbL film was assembled in triplicate (n = 3) and measurements were done in duplicate. Design of Experiment (DOE) was conducted with the assistance of JMP Pro 14 statistical software (SAS, Cary, NC). JMP was used to generate Runs 1-8 of the fractional factorial design. Runs 9-12 were added as center points for pH and PBAE. Assembly parameters pH, ionic strength, PBAE concentration, and siRNA concentration served as quantitative factors. Parameter ranges: pH (4.5 - 6.0), ionic strength (150 mM - 250 mM), PBAE concentration (0.5 mg/mL - 2 mg/mL), siRNA concentration (20 μg/mL - 30 μg/mL), were determined based on parameters previously published by our lab.[10,11,18] pH 5.2 and 1 mg/mL PBAE served as center points for their respective factors. JMP Pro software was used to run the standard least squares linear regression models. Statistical significance was pre-specified at the α=0.05 level.

3.3 Results and Discussion

3.3.1 Characterization of Films

LbL films were assembled on Polyglactin 910 (Vicryl®) sutures according to the fractional factorial design (Table 3.1). The siRNA used was designed to target the reporter gene, green fluorescent protein (GFP). Once sutures were coated, loading was characterized and *in vitro* knockdown studies were conducted as fully described in the methods section. Briefly, the Micro BCA assay and the RiboGreen assay were used to measure PBAE and siRNA incorporation respectively. The w/w ratio of loadings were also determined. To determine knockdown efficacy, HeLa cells expressing d2e-GFP were exposed to the coated sutures. Gene silencing was measured via flow cytometry. The PBAE loading, siRNA loading, w/w ratio, and knockdown are reported as mean with standard deviation in Table 3.1. No significant cytotoxicity was observed in cells treated with coated suture (Table B.1).

Table 3.1 Fractional factorial design parameters and response variable data. The parameters tested include pH, ionic strength, PBAE concentration, and siRNA concentration. Ranges were determined based on parameters previously published by our lab. Response variables of PBAE loading, siRNA loading, w/w ratio, and knockdown are reported as the mean and the standard deviation (SD). Cells are colored to depict differences in magnitude. JMP was used to determine Runs 1-8 for the fractional factorial design. Runs 9 – 12 were added as midpoints for pH and polymer concentration to test for non-linearity.

Run	pH	Ionic Strength (mM)	PBAE Conc. (mg/mL)	siRNA Conc. (µg/mL)	PBAE Loading (µg/cm)		siRNA Loading (µg/cm)		w/w ratio		Knockdown (%)	
					Mean	SD	Mean	SD	Mean	SD	Mean	SD
1	4.5	150	2.0	20	1.18	0.14	0.66	0.08	1.80	0.20	17.88	6.49
2	4.5	150	2.0	30	0.90	0.03	1.30	0.21	0.71	0.11	8.16	3.44
3	4.5	250	0.5	20	0.57	0.05	1.08	0.06	0.53	0.05	10.82	10.19
4	4.5	250	0.5	30	0.80	0.02	1.95	0.07	0.41	0.02	9.23	2.89
5	6.0	150	0.5	20	1.55	0.09	1.42	0.23	1.13	0.27	7.54	3.81
6	6.0	150	0.5	30	1.30	0.10	2.17	0.08	0.60	0.05	36.96	17.98
7	6.0	250	2.0	20	0.67	0.10	0.09	0.02	8.62	3.24	0.00	0.00
8	6.0	250	2.0	30	0.89	0.11	0.29	0.01	3.07	0.31	1.04	1.13
9	5.2	150	1.0	20	1.07	0.01	0.89	0.09	1.22	0.13	2.26	1.60
10	5.2	150	1.0	30	1.18	0.01	1.41	0.15	0.85	0.09	2.10	1.49
11	5.2	250	1.0	20	1.41	0.08	0.72	0.11	2.02	0.45	0.34	0.48
12	5.2	250	1.0	30	1.16	0.07	1.34	0.08	0.87	0.05	3.61	2.47

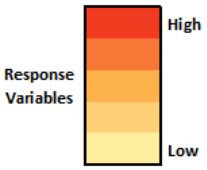

3.3.2 Least Squares Linear Regression Model

A standard least squares linear regression model was applied to PBAE and siRNA loadings, as well as their w/w ratio using the assembly parameters as the explanatory variables (Figure 3.2). Predicted values are plotted against actual values to visualize goodness-of-fit for each regression. Normalized coefficients, representing the correlation between the explanatory variable and the response, are reported for each parameter along with their p-values. While no significant trends ($p < 0.05$) were found for PBAE loading, several parameters were found to be statistically significant for the siRNA loading and the w/w ratio.

a PBAE Loading			b siRNA Loading			c PBAE:siRNA w/w Ratio		
Term	Norm. Coeff.	p-value	Term	Norm. Coeff.	p-value	Term	Norm. Coeff.	p-value
pH	+0.23 ↑	0.286	pH	-0.25 ↓	0.166	**pH**	**+2.51 ↑**	**0.033**
Ionic Strength	-0.28 ↓	0.129	**Ionic Strength**	**-0.39 ↓**	**0.021**	Ionic Strength	+1.53 ↑	0.088
PBAE Conc.	-0.19 ↓	0.370	**PBAE Conc.**	**-1.02 ↓**	**<0.001**	**PBAE Conc.**	**+2.95 ↑**	**0.016**
siRNA Conc.	-0.04 ↓	0.830	**siRNA Conc.**	**+0.60 ↑**	**0.003**	siRNA Conc.	-1.47 ↓	0.099

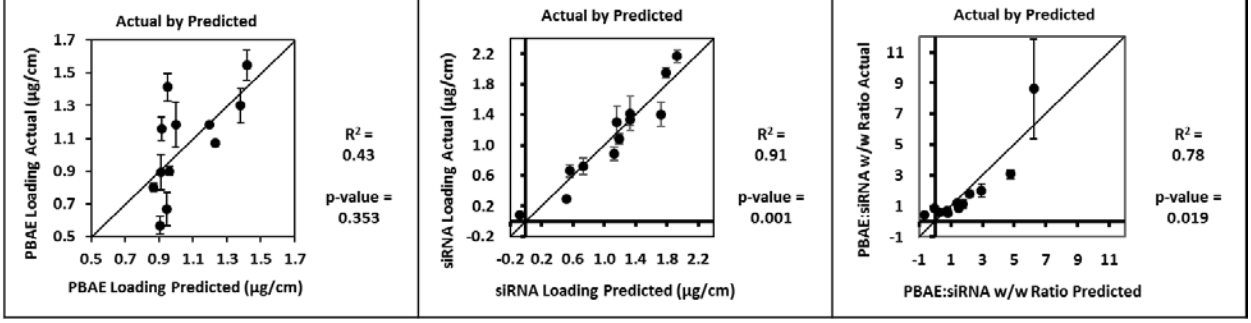

Figure 3.2 Standard Least Squares Fit of Parameters on Response Variables. A standard least squares fit was performed on the average values from each run for (a) PBAE loading, (b) siRNA loading, and (c) PBAE:siRNA w/w ratio. "Actual by Predicted" plots are shown with R^2 and p-values reported. The coefficients for each parameter were normalized by the range tested and p-values are reported. Parameter terms with correlation p-values < 0.05 are highlighted; significant positive coefficients are highlighted in red, negative coefficients are highlighted in blue. Error bars represent standard deviation.

3.3.3 Effects of pH

The assembly pH was not found to have a statistically significant effect on either the PBAE loading or the siRNA loading. Nonetheless, the slight positive correlation to PBAE loading compounded with the slight negative correlation to the siRNA resulted in a significant positive coefficient for the w/w ratio. This phenomenon is supported by previous research on the effect of pH in constructing LbL films[21]. As pH increases, the weak electrolyte PBAE becomes less positively charged. The decrease in charge leads to a loopier conformation during the adsorption of the polymer. The arrangement of dense loops may thus explain the increase in loading of PBAE. Since the phosphate groups on the RNA backbone have a pKa near 0, siRNA is completely ionized with a negative charge across the pH range in this study[17]. Furthermore, the stiff conformation of siRNA remains unchanged due to its short double helix structure. Nevertheless, the decrease in charge of the adsorbed PBAE results in a lower amount of siRNA required to neutralize the charge, and thus lesser adsorption.

3.3.4 Effects of Ionic Strength

The ionic strength of the PBAE deposition bath was not found to have a significant effect on PBAE loading within the experimental range. Previous studies have reported the thickness of a film to have a parabolic dependence on salt concentration, with the maximum thickness dependent on pH[22]. As the ionic strength within the PBAE deposition bath increases, ion exchange occurs to extrinsically compensate the PBAE charge with acetate ions while decreasing intrinsic charge compensation by the siRNA. Thus, loopier structures of PBAE would be formed, leading to greater incorporation of the polymer. However, if the salt concentration exceeds a certain point, the charge shielding of PBAE chains becomes so extensive that complexation to the LbL film no longer occurs. The ionic strength at which the maximum PBAE adsorption occurs is thus related to the ionization of the PBAE and therefore the solution pH. We have observed separately that at pH 4.5, ionic strength has a positive correlation with PBAE loading while at pH 6.0, the ionic strength has a negative correlation. As the pH shifts from 4.5 to 6.0, the measured PBAE pKa of 7.4 (Figure B.4) is approached and the degree of ionization decreases. This supports the observed phenomenon that the ionic strength at which maximum PBAE loading occurs decreases as the pH is increased. Due to this interaction between pH and ionic strength, the linear regression does not comprehensively capture the effects of ionic strength on PBAE loading.

The ionic strength of the PBAE deposition bath was found to be a significant term in only the siRNA loading. As the ionic strength increased, siRNA loading decreased. This suggests that across the pH levels tested, the increased ionic strength in the PBAE deposition bath induces swelling and partial decomposition of the film. At higher salt concentrations, extrinsic compensation occurs within the film, prompting ejection of some siRNA from the film into the PBAE bath.

3.3.5 Effects of PBAE Deposition Bath Concentration

In our experiments, the PBAE concentration did not have a significant effect on the PBAE loading in the film. This suggests that adsorption of PBAE is not diffusion limited in the range of concentrations tested. At the lowest concentration of 0.5 mg/mL PBAE, deposition equilibrium is already reached in the allotted dipping time of 10 minutes. Increase of PBAE concentration does not affect its loading.

Interestingly, the concentration of the PBAE deposition bath has a negative effect on siRNA loading. In separate experiments using fluorescently tagged siRNA, the fluorescent dye is

seen in the PBAE bath at the conclusion of film assembly when high PBAE concentrations are used (data not shown). This concentration-dependent stripping phenomena has been previously reported in LbL coating of nylon fibers[23]. Within the polycation bath during film assembly, polycation is typically deposited but polyanion may also be stripped from the surface[24]. As polyplexes are known to have greater stability in solution with excess of one of the polyelectrolyte species[25], a greater PBAE concentration within the deposition bath would promote stability of PBAE/siRNA complexes in solution. Coupling this effect with translational and configurational entropic gains of polyplex formation over film deposition[24], increasing the PBAE concentration within our experimental range leads to increased stripping of siRNA from the film. The negative correlation PBAE concentration has on siRNA loading contributes to the significant positive correlation with the w/w ratio.

3.3.6 Effects of siRNA Deposition Bath Concentration

The PBAE loading does not seem to be affected by the siRNA concentration. The lack of the aforementioned stripping effect may be due to the relatively low concentration of siRNA within the deposition bath.

The siRNA concentration exhibited a significant positive correlation to the siRNA loading. This suggests deposition of siRNA is diffusion limited in this concentration regime. As siRNA is the most expensive component of the assembly process, the concentrations used are admittedly much lower than those of the complementary PBAE. While the siRNA concentration of 20 μg/mL appears to be sufficient for adsorption and subsequent surface charge reversal for film formation, the greater concentration of 30 μg/mL indeed results in greater loading.

3.3.7 Optimization of Assembly Parameters for Knockdown

When the standard least squares linear regression was applied to the knockdown with the assembly parameters as the explanatory variables, significant terms were not identified (Figure B.5a). A regression using PBAE loading, siRNA loading, and w/w ratio as the explanatory variable produced a slightly better fit (Figure B.5b), albeit was still unable to determine significant effects.

Studies have shown that nanoparticle transfection of nucleic acids is dependent on the w/w ratio of its components[15,26,27]. *In vitro* transfection experiments with PBAE/siRNA polyplexes confirm that siRNA uptake and knockdown increased as w/w ratio increased (Figure B.6). To further investigate, we plotted the knockdown efficacy by the siRNA and PBAE loadings of each

individual suture in a bubble plot (Figure 3.3). In this visualization, we find that sutures that produce the greatest knockdown have the greatest siRNA loading. Furthermore, the sutures of high siRNA loading show greater knockdown if they also have high PBAE loading.

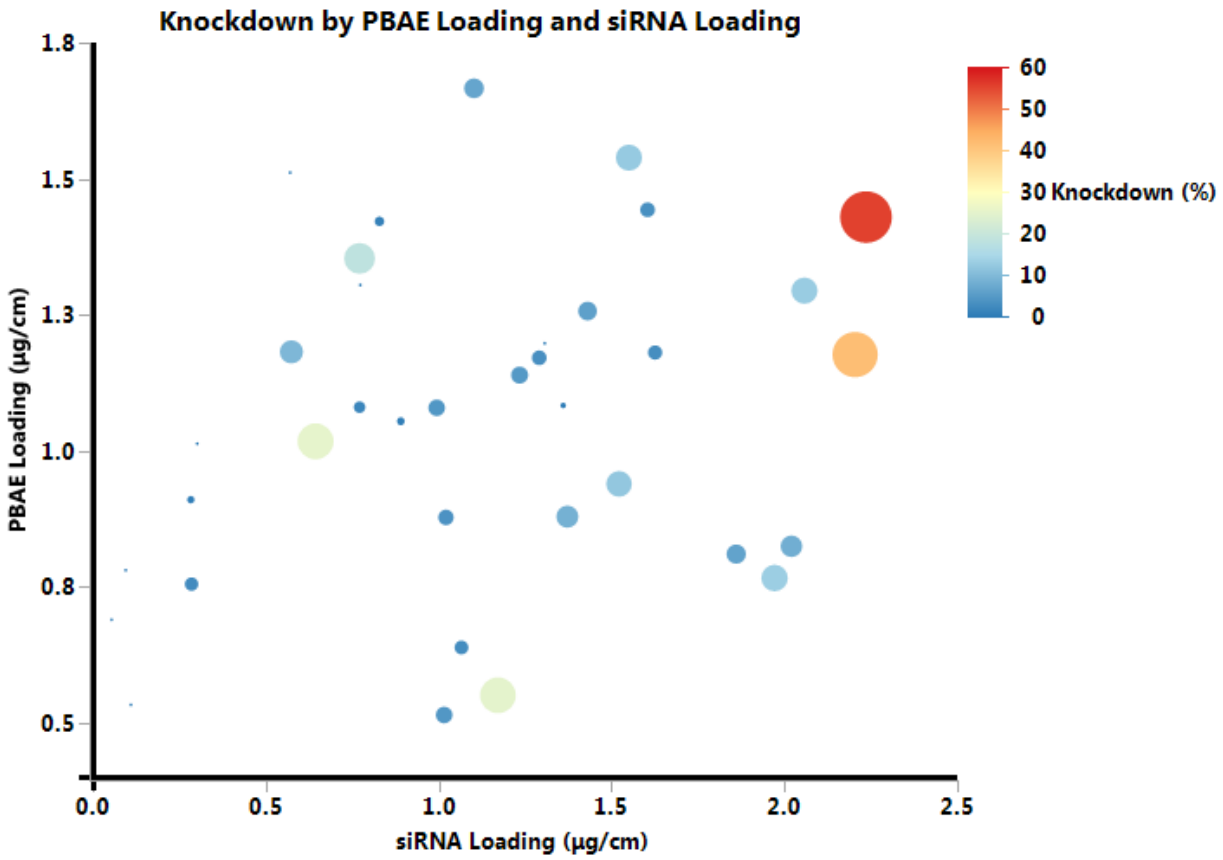

Figure 3.3 Bubble plot of *in vitro* knockdown by PBAE loading and siRNA loading. Resulting GFP knockdown data of all LbL films are represented with siRNA loading on the x-axis and PBAE loading on the y-axis. Each biological replicate is included as its own data point. LbL coated sutures that effected greater knockdown are represented with larger bubbles. The knockdown is also color coded with high knockdown in red and low knockdown in blue. Sutures that produce the greatest knockdown are seen to have the greatest siRNA loading. Sutures with high siRNA loading show greater knockdown if they also have high PBAE loading.

Informed by these experiments, we aimed to maximize knockdown by tuning assembly parameters to maximize siRNA loading while also maintaining an adequate w/w ratio. From the significant terms in the standard least squares fit, a low ionic strength and high siRNA concentration in our experimental range both contribute to greater siRNA loading. A high pH contributes to a greater w/w ratio. Since the polymer concentration is negatively correlated to siRNA loading and positively correlated to the w/w ratio, a moderate concentration was chosen.

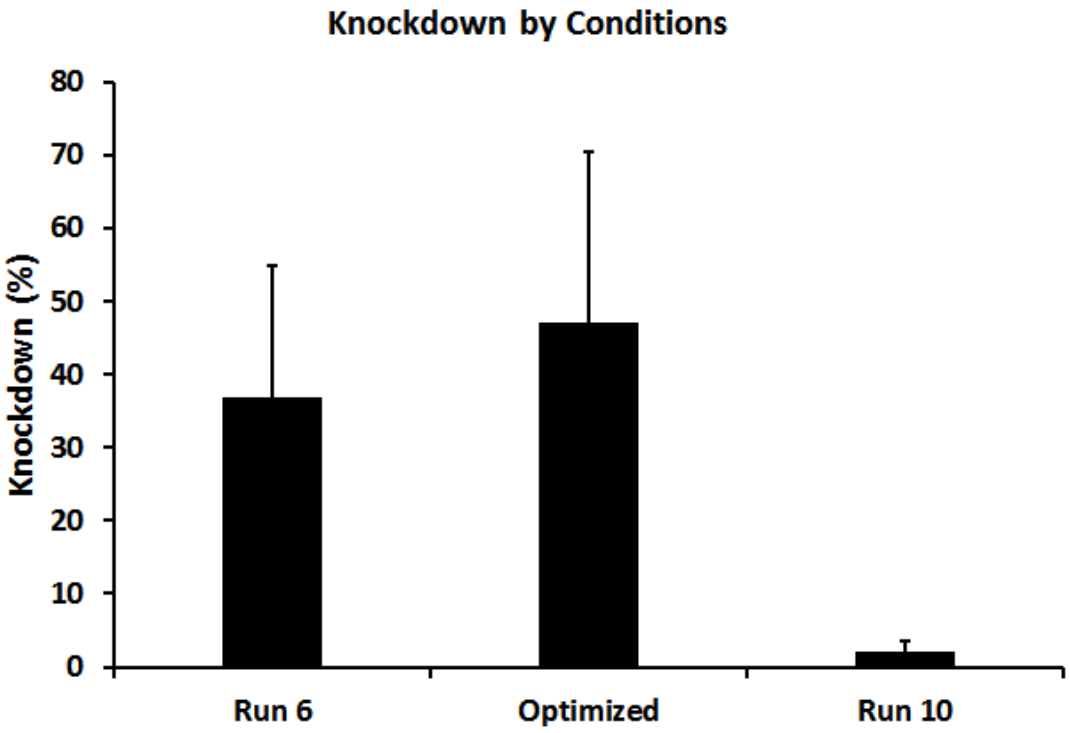

pH	6.0	6.0	5.2
Ionic Strength	150 mM	150 mM	150 mM
PBAE Conc.	0.5 mg/mL	1.0 mg/mL	1.0 mg/mL
siRNA Conc.	30 µg/mL	30 µg/mL	30 µg/mL

Figure 3.4 Knockdown comparison of optimized formulation vs. runs with neighboring conditions. The optimized LbL parameters of pH 6, ionic strength of 150 mM, PBAE concentration of 1.0 mg/mL, and siRNA concentration of 30 µg/mL was found to achieve *in vitro* knockdown of 47%. Run 6 (37% knockdown) and Run 10 (2% knockdown) from the fractional factorial design both neighbor these conditions with a single parameter varied. Colors denote high (red), moderate (yellow), and low (blue) values of parameters within the experimental range of the design.

Within our parameter space, the assembly conditions were thus optimized as follows: pH 6.0, ionic strength of 150 mM, PBAE concentration of 1.0 mg/mL, and siRNA concentration of 30 µg/mL. An LbL film was constructed on sutures with these conditions and *in vitro* knockdown was evaluated (Figure 3.4). As hypothesized, the optimized conditions resulted in greater knockdown than all the runs from the fractional factorial design. The optimized conditions neighbor two of the runs from the design: Run 6 and Run 10. The increase in PBAE deposition bath concentration compared to Run 6 (the run that produced the highest knockdown from the fractional factorial design) resulted in 10% greater gene silencing efficiency. This reflects the beneficial trade-off between siRNA loading and w/w ratio in that regime.

Previous efforts from our lab in incorporating siRNA on sutures involve a hierarchical LbL structure with a [PBAE/Dextran Sulfate]$_{20}$ degradable layer deposited first, followed by a [Chitosan/siRNA]$_{25}$ bilayer[11]. 37% knockdown was achieved in HeLa cells after three days of transfection. The optimized conditions determined here results in a film that is simpler in construction (bilayer formulation vs. hierarchical structure of two bilayers), requires fewer film layers (15 bilayers vs. a total of 45 bilayers), and produces greater knockdown (47% vs. 37%).

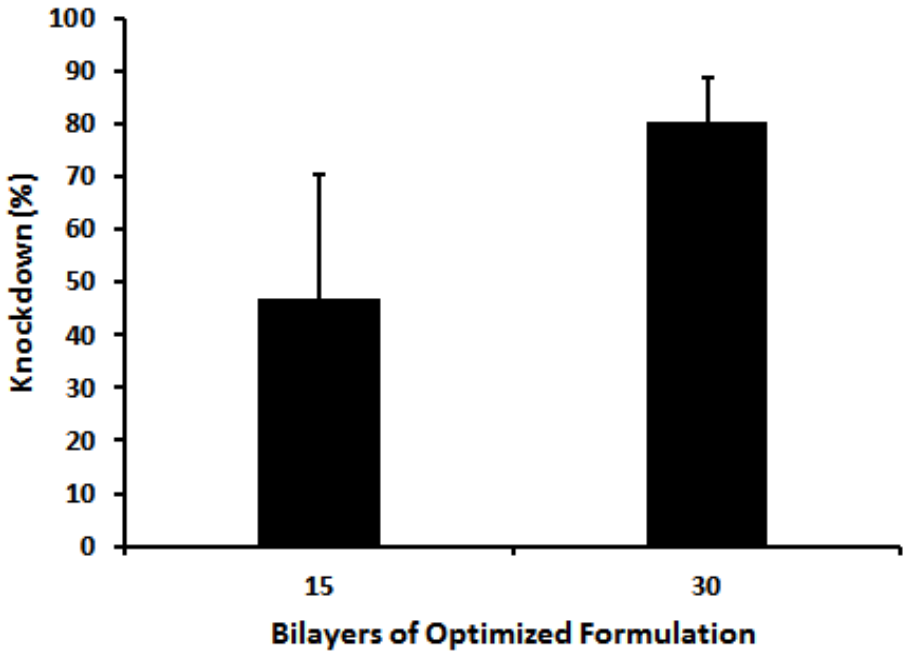

Figure 3.5 Knockdown of LbL films with optimized parameters. As the number of bilayers is increased to 30, over 80% of siRNA knockdown is achieved.

In further investigation of these optimized conditions, films of 30 bilayers were constructed on the Vicryl sutures and *in vitro* efficacy was evaluated (Figure 3.5). The increase of knockdown with 30 bilayers compared to 15 bilayers reveals the dose-responsiveness of the cells to the LbL film. With 30 bilayers, the optimal assembly conditions resulted in over 80% knockdown.

3.4 Conclusions

In this study we have investigated the incorporation of siRNA in LbL thin films for local delivery. By conducting a fractional factorial design, we determined the effects of assembly parameters: pH, ionic strength, PBAE concentration, and siRNA concentration on the loadings of PBAE, siRNA, and their w/w ratio in an LbL film assembled on commercially available polyglactin 910 (Vicryl®) sutures. The significant effects drawn from a standard least squares

linear regression model are corroborated from theory and findings from past studies on films assembled with weak polyelectrolytes. Adjusting the conditions to maximize siRNA loading and w/w ratio, we determined a set of optimized assembly conditions that achieved greater *in vitro* knockdown compared to all runs from the experimental design. Compared to previously published siRNA LbL films from our lab[11], films identified in this study are simpler in construction and require fewer film layers to achieve similar siRNA efficacy *in vitro*. The reduction of required film layers could translate to savings in time and materials in therapeutic LbL film production. The discussed effects of assembly conditions on LbL formulation suggests that investigation of values outside the parameter ranges of this study may yield even more efficient films. We believe that this work demonstrates the applicability of DOE principles to optimize LbL assembly conditions for maximizing siRNA efficacy. This work has potential applications in designing films to optimize efficacy of other therapeutic nucleic acids.

3.5 References

(1) Ameres, S. L.; Martinez, J.; Schroeder, R. Molecular Basis for Target RNA Recognition and Cleavage by Human RISC. *Cell* **2007**, *130* (1), 101–112. https://doi.org/10.1016/j.cell.2007.04.037.

(2) Rand, T. A.; Petersen, S.; Du, F.; Wang, X. Argonaute2 Cleaves the Anti-Guide Strand of SiRNA during RISC Activation. *Cell* **2005**, *123* (4), 621–629. https://doi.org/10.1016/j.cell.2005.10.020.

(3) Commissioner, O. of the. FDA approves first-of-its kind targeted RNA-based therapy to treat a rare disease https://www.fda.gov/news-events/press-announcements/fda-approves-first-its-kind-targeted-rna-based-therapy-treat-rare-disease (accessed May 25, 2020).

(4) Chakraborty, C.; Sharma, A. R.; Sharma, G.; Doss, C. G. P.; Lee, S.-S. Therapeutic MiRNA and SiRNA: Moving from Bench to Clinic as Next Generation Medicine. *Molecular Therapy - Nucleic Acids* **2017**, *8*, 132–143. https://doi.org/10.1016/j.omtn.2017.06.005.

(5) Berger, A. G.; Chou, J. J.; Hammond, P. T. Approaches to Modulate the Chronic Wound Environment Using Localized Nucleic Acid Delivery. *Advances in Wound Care* **2020**. https://doi.org/10.1089/wound.2020.1167.

(6) Whitehead, K. A.; Langer, R.; Anderson, D. G. Knocking down Barriers: Advances in SiRNA Delivery. *Nat Rev Drug Discov* **2009**, *8* (2), 129–138. https://doi.org/10.1038/nrd2742.

(7) Tatiparti, K.; Sau, S.; Kashaw, S. K.; Iyer, A. K. SiRNA Delivery Strategies: A Comprehensive Review of Recent Developments. *Nanomaterials* **2017**, *7* (4), 77. https://doi.org/10.3390/nano7040077.

(8) Sarett, S. M.; Nelson, C. E.; Duvall, C. L. Technologies for Controlled, Local Delivery of SiRNA. *Journal of Controlled Release* **2015**, *218*, 94–113. https://doi.org/10.1016/j.jconrel.2015.09.066.

(9) Song, W.; Song, X.; Yang, C.; Gao, S.; Klausen, L. H.; Zhang, Y.; Dong, M.; Kjems, J. Chitosan/SiRNA Functionalized Titanium Surface via a Layer-by-Layer Approach for in Vitro Sustained Gene Silencing and Osteogenic Promotion. *Int J Nanomedicine* **2015**, *10*, 2335–2346. https://doi.org/10.2147/IJN.S76513.

(10) Castleberry, S. A.; Almquist, B. D.; Li, W.; Reis, T.; Chow, J.; Mayner, S.; Hammond, P. T. Self-Assembled Wound Dressings Silence MMP-9 and Improve Diabetic Wound Healing In Vivo. *Advanced Materials* **2016**, *28* (9), 1809–1817. https://doi.org/10.1002/adma.201503565.

(11) Castleberry, S. A.; Golberg, A.; Sharkh, M. A.; Khan, S.; Almquist, B. D.; Austen, W. G.; Yarmush, M. L.; Hammond, P. T. Nanolayered SiRNA Delivery Platforms for Local Silencing of CTGF Reduce Cutaneous Scar Contraction in Third-Degree Burns. *Biomaterials* **2016**, *95*, 22–34. https://doi.org/10.1016/j.biomaterials.2016.04.007.

(12) Hossfeld, S.; Nolte, A.; Hartmann, H.; Recke, M.; Schaller, M.; Walker, T.; Kjems, J.; Schlosshauer, B.; Stoll, D.; Wendel, H.-P.; Krastev, R. Bioactive Coronary Stent Coating Based on Layer-by-Layer Technology for SiRNA Release. *Acta Biomaterialia* **2013**, *9* (5), 6741–6752. https://doi.org/10.1016/j.actbio.2013.01.013.

(13) Alkekhia, D.; Hammond, P. T.; Shukla, A. Layer-by-Layer Biomaterials for Drug Delivery. *Annual Review of Biomedical Engineering* **2020**, *22* (1), null. https://doi.org/10.1146/annurev-bioeng-060418-052350.

(14) Akinc, A.; Anderson, D. G.; Lynn, D. M.; Langer, R. Synthesis of Poly(Beta-Amino Ester)s Optimized for Highly Effective Gene Delivery. *Bioconjug. Chem.* **2003**, *14* (5), 979–988. https://doi.org/10.1021/bc034067y.
(15) Vandenbroucke, R. E.; Geest, B. G. D.; Bonné, S.; Vinken, M.; Haecke, T. V.; Heimberg, H.; Wagner, E.; Rogiers, V.; Smedt, S. C. D.; Demeester, J.; Sanders, N. N. Prolonged Gene Silencing in Hepatoma Cells and Primary Hepatocytes after Small Interfering RNA Delivery with Biodegradable Poly(β-Amino Esters). *The Journal of Gene Medicine* **2008**, *10* (7), 783–794. https://doi.org/10.1002/jgm.1202.
(16) Wood, K. C.; Boedicker, J. Q.; Lynn, D. M.; Hammond, P. T. Tunable Drug Release from Hydrolytically Degradable Layer-by-Layer Thin Films. *Langmuir* **2005**, *21* (4), 1603–1609. https://doi.org/10.1021/la0476480.
(17) Chuang, H. F.; Smith, R. C.; Hammond, P. T. Polyelectrolyte Multilayers for Tunable Release of Antibiotics. *Biomacromolecules* **2008**, *9* (6), 1660–1668. https://doi.org/10.1021/bm800185h.
(18) Castleberry, S.; Wang, M.; Hammond, P. T. Nanolayered SiRNA Dressing for Sustained Localized Knockdown. *ACS Nano* **2013**, *7* (6), 5251–5261. https://doi.org/10.1021/nn401011n.
(19) Lynn, D. M.; Langer, R. Degradable Poly(β-Amino Esters): Synthesis, Characterization, and Self-Assembly with Plasmid DNA. *J. Am. Chem. Soc.* **2000**, *122* (44), 10761–10768. https://doi.org/10.1021/ja0015388.
(20) Smith, P. K.; Krohn, R. I.; Hermanson, G. T.; Mallia, A. K.; Gartner, F. H.; Provenzano, M. D.; Fujimoto, E. K.; Goeke, N. M.; Olson, B. J.; Klenk, D. C. Measurement of Protein Using Bicinchoninic Acid. *Anal. Biochem.* **1985**, *150* (1), 76–85. https://doi.org/10.1016/0003-2697(85)90442-7.
(21) Shiratori, S. S.; Rubner, M. F. PH-Dependent Thickness Behavior of Sequentially Adsorbed Layers of Weak Polyelectrolytes. *Macromolecules* **2000**, *33* (11), 4213–4219. https://doi.org/10.1021/ma991645q.
(22) Dubas, S. T.; Schlenoff, J. B. Polyelectrolyte Multilayers Containing a Weak Polyacid: Construction and Deconstruction. *Macromolecules* **2001**, *34* (11), 3736–3740. https://doi.org/10.1021/ma001720t.
(23) Dubas, S. T.; Limsavarn, L.; Iamsamai, C.; Potiyaraj, P. Assembly of Polyelectrolyte Multilayers on Nylon Fibers. *Journal of Applied Polymer Science* **2006**, *101* (5), 3286–3290. https://doi.org/10.1002/app.23826.
(24) Sui, Z.; Salloum, D.; Schlenoff, J. B. Effect of Molecular Weight on the Construction of Polyelectrolyte Multilayers: Stripping versus Sticking. *Langmuir* **2003**, *19* (6), 2491–2495. https://doi.org/10.1021/la026531d.
(25) Dautzenberg, H.; Kriz, J. Response of Polyelectrolyte Complexes to Subsequent Addition of Salts with Different Cations. *Langmuir* **2003**, *19* (13), 5204–5211. https://doi.org/10.1021/la0209482.
(26) Lavertu, M.; Méthot, S.; Tran-Khanh, N.; Buschmann, M. D. High Efficiency Gene Transfer Using Chitosan/DNA Nanoparticles with Specific Combinations of Molecular Weight and Degree of Deacetylation. *Biomaterials* **2006**, *27* (27), 4815–4824. https://doi.org/10.1016/j.biomaterials.2006.04.029.
(27) Mao, S.; Sun, W.; Kissel, T. Chitosan-Based Formulations for Delivery of DNA and SiRNA. *Advanced Drug Delivery Reviews* **2010**, *62* (1), 12–27. https://doi.org/10.1016/j.addr.2009.08.004.

CHAPTER 4.

Development of *In Vivo* Model to Evaluate siRNA Layer-by-Layer Film Efficacy

4.1 Introduction

The overall goal of this thesis work is to develop layer-by-layer (LbL) films for controlled localized delivery of siRNA to modulate gene expression in wound healing. In Chapter 3, we presented our work in maximizing siRNA-mediated knockdown via coated sutures *in vitro* by tuning LbL assembly parameters. The next step is to assess the ability of these LbL coated sutures to achieve gene knockdown *in vivo*.

Previous work has been performed to evaluate siRNA-mediated knockdown from LbL coated sutures in a third-degree burn model in rats[1]. While Castleberry et al. was able to show gene reduction of approximately 36% compared to controls, we sought to develop a simpler model to evaluate gene knockdown. Wound repair is a highly intricate process involving various cell types, growth factors, and chemokines[2]. Though application in wound healing is the ultimate goal, we decided that developing a simple *in vivo* model, without the complexities of a wound environment, to validate siRNA efficacy would be beneficial.

Here we describe our efforts in developing a simple *in vivo* mouse model to test siRNA knockdown efficacy of LbL coated polyglactin 910 (Vicryl) sutures. We present findings from a pilot study using film coatings constructed with conditions similar to the optimized LbL assembly parameters determined in Chapter 3.

4.2 Materials and Methods

4.2.1 Materials

siRNA targeting green fluorescent protein was purchased from Dharmacon (Lafayette, CO); the GFP targeting siRNA has sequence 5'-GCA AGC TGA CCC TGA AGT TC–3'. Qiagen AllStars Neg. siRNA AF 647 Alexa Fluor 647-labeled siRNA was purchased from Qiagen (Valencia, CA). Lipofectamine RNAiMAX transfection reagent was obtained from ThermoFisher Scientific (Waltham, MA). Ethicon 3-0 Vicryl sutures (with 60 mm KS needle) were purchased from Ethicon Inc. (Somerville, NJ). RNase free UltraPure water was purchased from Life Technologies (Carlsbad, CA). Sodium acetate buffer pH 6.0 was purchased from Teknova

(Hollister, CA). 97% 4,4'-trimethylene dipiperidine, 99% ReagentPlus diethylenetriamine (DETA), and 99.9% anhydrous tetrahydrofuran (THF), inhibitor-free, were obtained from Sigma (St. Louis, MO). 99% 1,6-hexanediol diacrylate, stabilized with 90 ppm hydroquinone, and 3-amino-1-propanol, 99% were purchased from Alfa Aesar (Haverhill, MA). Hexane was purchased from Fisher Scientific (Waltham, MA). Chemicals were stored per manufacturer's instructions.

HeLa cervical cancer cells stably expressing a destabilized green fluorescent protein (GFP) (HeLa d2eGFP) were a gift from Professor Piyush Jain's Lab at the University of Florida. The plasmid construct used to express GFP in HeLa cells was CMV-d2eGFP-empty, which was a gift from Phil Sharp (Addgene plasmid # 26164). Media was Corning Dulbecco's Modified Eagle Medium (DMEM, Corning, NY) supplemented with Gibco 10% Fetal Bovine Serum (FBS, Waltham, MA) and Corning 1% Penicillin-Streptomycin (Corning, NY). The cells tested negative for mycoplasma on arrival, after thawing from storage, and periodically during culture, using a Lonza MycoAlert kit (Morristown, NJ).

4.2.2 Poly 2-30%C3OH-DETA (P2C3OHD) Synthesis

Synthesis of the poly(β-amino ester) (PBAE) polymer proceeded according to the literature[3,4]. Briefly, a 250 mL round bottom (RB) flask and stir bar were cleaned and dried in a drying oven. An oil bath was set to warm to 50°C with the stir rate set to 500 rpm. The reaction ratio is designed so that the total moles of amine-functionalized monomer to acrylate-functionalized monomer is 1.02. The total amine-functionalized monomer is comprised of 70% 4,4'-trimethylene dipiperidine and 30% 3-amino-1-propanol, by moles. Thus, 4.555 g (21.63 mmol, 0.714 equivalents) of 4,4'-trimethylene dipiperidine, 0.697 g (9.27 mmol, 0.306 equivalents) 3-amino-1-propanol, and 6.856 g (30.30 mmol, 1.00 equivalents) were massed. The 4,4'-trimethylene dipiperidine was added first to the RB flask. Using the Schlenk line and dry nitrogen gas to maintain the solvent as anhydrous, a needle and syringe were used to draw up about 50 mL of THF, about 10 mL of which was added to the RB flask. The 4,4'-trimethylene dipiperidine monomer was left to dissolve, at which point 3-amino-1-propanol was added to the RB flask. Finally, 1,6-hexanediol diacrylate was added to the RB flask along with the remainder of the THF. A rubber stopper was used to cap the flask. Dry nitrogen gas was bubbled into the reaction pot to purge any air. The synthesis proceeded for 48 hours. A balloon filled with dry nitrogen gas provided nitrogen to the reaction environment throughout the course of the synthesis. The resulting polymer is a Poly 2 modified with 30% 3-amino-1-propanol feed which we termed

Poly 2-30%C3OH (P2C3OH). The polymer was re-precipitated in ice-cold hexanes through a filter funnel and then dried.

The P2C3OH polymer was end-capped with diethylenetriamine (DETA) following a procedure from the literature[4]. In this work, a ratio of 4 mmol DETA was used for end-capping per 1 g of dried polymer. Weighing to the nearest half milligram, as before, 1 g of polymer was massed along with 0.413 g (4 mmol) diethylenetriamine. The reagents were mixed in an RB flask with 20 mL anhydrous THF. The RB flask was capped with a rubber stopper, bubbled with dry nitrogen gas, and equipped with a nitrogen-filled balloon. The reaction proceeded for 24 hours at 50°C with stir set to 500 rpm. After 24 hours, the polymer was re-precipitated as before using ice-cold hexanes and a filter funnel. We termed the resulting end-capped polymer as Poly 2-30%C3OH-DETA (P2C3OHD). The polymer was dried and stored at -20°C in a bag with desiccant.

4.2.3 Layer-by-layer Film Preparation

P2C3OHD was prepared at 1.0 mg/mL in RNase free water buffered to an ionic strength of 150 mM with pH 6.0 sodium acetate. The P2C3OHD was dissolved fresh daily using a rotating mixer due to its hydrolyzable nature and then filtered through a 0.2 µm cellulose acetate filter. Dissolution took a few hours.

Layer-by-layer films were deposited on plasma treated Vicryl sutures. Sutures were cleaned with a 70% ethanol / 30% water mixture, rinsed with water, and consequently dried. Sutures were then wrapped around a stainless-steel wire frame for ease in handling. Sutures for *in vivo* experiments were coated with the needle attached. Care was taken to retain sharpness of the needles during handling of the sutures. Air plasma treatment was performed for 10 minutes on high setting in a plasma cleaner (PDC-32G, Harrick, USA). Sutures were then immediately immersed in the solution of P2C3OHD for a duration of 1 hour.

A Carl Zeiss HMS-DS50 stainer (Oberkochen, Germany) was used to assemble the LbL films. Bilayer films were constructed through alternating adsorption steps. P2C3OHD was adsorbed for 10 minutes, and siRNA (25 ug/mL) was adsorbed for 15 minutes. Between the adsorption steps, the sutures were dipped in two wash baths of RNase free water for 30 seconds each. The wash baths and the siRNA baths were buffered to an ionic strength of 10 mM of pH 6.0 sodium acetate.

4.2.4 LbL Suture In Vitro *Evaluation*

HeLa d2eGFP cells in DMEM supplemented with 10% FBS and 1% penicillin-streptomycin were grown to confluence in a T75 flask at 37°C and 5% CO2. The cells were incubated for 10 minutes with 5 mL Trypsin-EDTA solution to dissociate them. The dissociation was quenched with 5 mL of warm media, and the cells were pelleted at 1000 rpm in a centrifuge for 5 minutes at room temperature. The cells were resuspended in warm media and seeded at 6,000 per well in 48-well plates. The next day, transfection was performed. LbL coated sutures (cut into three 1 cm segments) were placed directly in culture with the cells in DMEM. The cells were incubated for three days after treatment at 37°C and 5% CO2 and then prepared for flow cytometry. The cells were dissociated with Trypsin-EDTA. Fluorescence was measured using a BD LSR II flow cytometer with a high throughput sampler attachment in the Swanson Biotechnology Center Flow Cytometry Facility at the Koch Institute for Integrative Cancer Research. GFP fluorescence was read with a 488 nm laser and 530/30 filter set. 50 μL or up to 10000 live single cells, whichever came first, were read for each sample.

4.2.5 LbL Suture In Vivo *Evaluation*

All animal studies were approved by the MIT Institutional Animal Care and Use Committee (IACUC). Animals were housed and cared for in the USDA-inspected MIT Animal Facility under federal, state, local, and NIH guidelines for animal care. C57BL/6-Tg(UBC-GFP)30Scha/J mice were purchased from Jackson Labs (Bar Harbor, ME). Two groups of mice were used: (1) GFP siRNA suture treated and (2) negative control Alexa Fluor 647-labeled siRNA suture treated. Each group consisted of 3 mice total.

One day before suture implantation, mice were anesthetized with 1-4% isoflurane in oxygen. The backs of the mice were shaved and Nair product was used to carefully remove hair from the implantation area. The next day, suture implantation was performed with mice under anesthesia. Marker and ruler were used to mark insertion and exit points (4 cm apart) on both the right and left sides of the dorsum. Coated suture was inserted on the left side, pushed through the subcutaneous space, and exited 4 cm from the insertion point. Excess suture was cut and tissue glue was applied. Unmodified suture was similarly inserted on the right side as an internal control. The mice were imaged daily for 3 days post suture implantation.

4.2.6 In Vivo *Fluorescence Imaging*

IVIS Spectrum In Vivo Imaging System was used to image and measure fluorescence of the mice. GFP fluorescence was quantified at 465 ex / 540 em wavelengths. Fluorescence of Alexa Fluor 647-labeled siRNA was quantified at 640 ex / 700 em wavelengths. Living Image software (PerkinElmer) was used to measure radiant efficiency. Regions of interest (ROI) were drawn on the left and right sides to encompass the corresponding implanted suture. The ROI drawn were of similar size and shape across all mice.

4.2.7 Statistics

Sutures were constructed in triplicate. Three mice were used in each group. Values are represented mean ± standard deviation (SD).

4.3 Results and Discussion

4.3.1 Modified Poly 2 for LbL Film Incorporation

In Chapter 3, we describe our efforts in optimizing film assembly parameters to maximize knockdown efficacy of LbL films composed of Poly 2 and siRNA. Poly 2 is a type of poly(β-amino ester) (PBAE), a synthetic polycation known for its biocompatibility as well as its efficacy in gene delivery[5]. In the work presented here, we chose to use a modified Poly 2 as the polycation to complement siRNA.

Poly 2 was synthesized with a 30% feed of 3-amino-1-propanol to incorporate a propanol side chain within the polymer. Studies have shown that the addition of hydrophobic alkyl side chains improves transfection efficacy of PBAEs[6]. Furthermore, diethylenetriamine (DETA) was used to endcap the polymer in efforts to enhance binding interaction with RNA and transfection efficiency[4]. A scheme of the synthesis of the resulting polymer, Poly 2-30%C3OH-DETA (P2C3OHD), is shown in Figure 4.1. The synthesis of this polymer is described in greater detail in the Materials and Methods section.

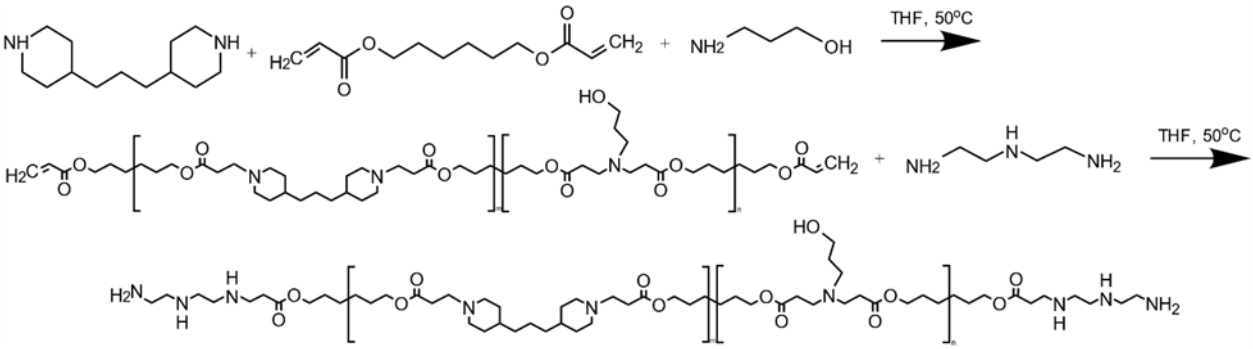

Figure 4.1 Synthesis of Poly 2-30%C3OH-DETA. Poly 2 was constructed with 30% feed of 3-amino-1-propanol. It was then endcapped with diethylenetriamine.

4.3.2 Layer-by-Layer Film Assembly

Layer-by-layer films were assembled onto Vicryl sutures as previously described. Briefly, Vicryl sutures were cleaned, wrapped around a stainless-steel wire frame, and plasma treated. Films were assembled by alternately dipping the suture in solutions of P2C3OHD (1 mg/mL) and siRNA (25 μg/mL) with wash baths in between (Figure 4.2a). Assembly parameters are similar to those determined in Chapter 3 and are detailed in the Materials and Methods section.

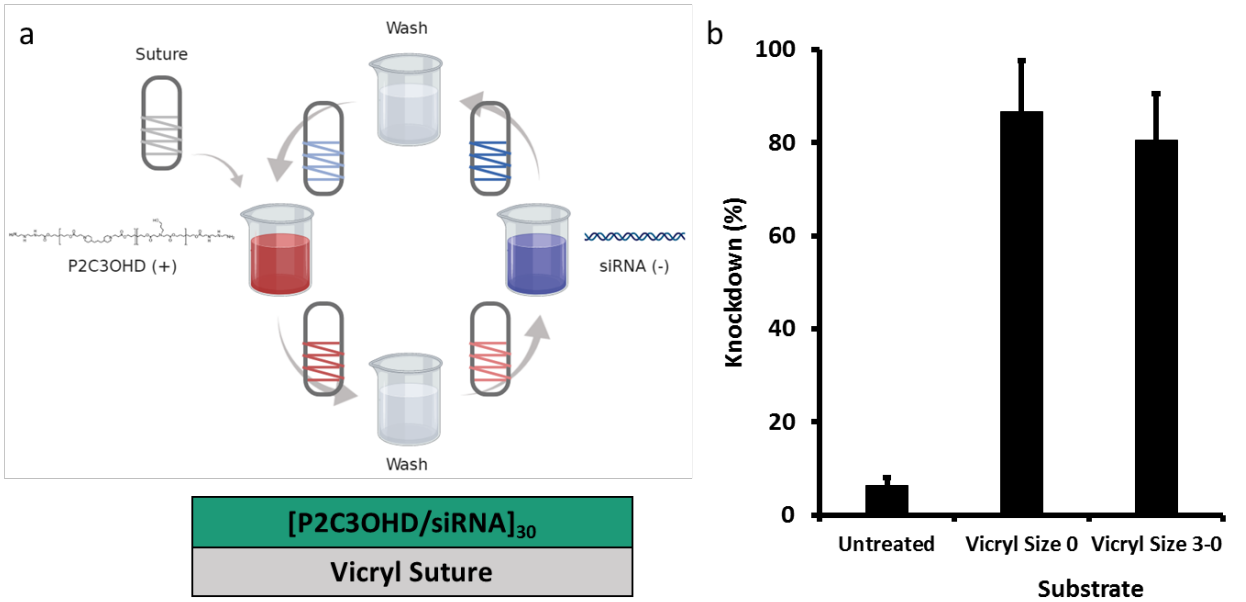

Figure 4.2 (a) Schematic of $[P2C3OHD/siRNA]_{30}$ assembly on Vicryl sutures. (b) *In Vitro* knockdown of GFP from sutures with the $[P2C3OHD/siRNA]_{30}$ film relative to treatment of uncoated suture. Error bars represent standard deviation.

4.3.3 In Vitro *Knockdown from LbL Coated Sutures*

In vitro knockdown efficacy was characterized for these LbL films as described previously. Briefly, HeLa cells expressing d2e-GFP, a destabilized GFP protein, were seeded at a density of 6,000 cells per well in 48-well plates a day before transfection in DMEM. The next day, transfection was performed. LbL coated sutures (cut into three 1 cm segments) were placed directly in culture with the cells. The siRNA used in the film coatings was designed to silence the GFP gene. After three days of transfection, flow cytometry was used to measure cell fluorescence.

These films were found to achieve considerable knockdown *in vitro*. Films coated on Vicryl sutures with USP size designation of 0 were found to achieve 86.7 ± 10.8% knockdown relative to treatment with uncoated suture. Vicryl sutures of size 3-0 coated with the LbL film were found to achieve 80.5 ± 10.1% knockdown. With this remarkable knockdown achieved *in vitro*, we proceeded with evaluating knockdown in a simple mouse model.

4.3.4 In Vivo *Model to Evaluate LbL Coated Sutures*

For our pilot studies, we used C57BL/6-Tg(UBC-GFP)30Scha/J mice, which are transgenic mice that express the GFP reporter gene. One day before suture implantation, the dorsum of each mouse was shaved and Nair was used to remove any remaining hair in the area. A ruler was used to mark suture entrance and exit points 4 cm apart on the right and left sides of each mouse. For suture implantation, LbL coated sutures with 60 mm KS needle intact were used. The sutures were of USP size designation 3-0. The needle was inserted, and passed through the subcutaneous space along the spine, and consequently exited at the marked locations. The suture was clipped at the entrance and exit points near the skin to leave as little suture for the mice to interact with. Tissue glue was used at both entrance and exit locations to secure the suture. The protocol is described in (Figure 4.3). For this pilot study, two treatment groups were investigated: (1) suture coated with siRNA targeting GFP (siGFP) and (2) negative control siRNA (siCon) labeled with Alexa Fluor 647 dye. Each group consisted of three mice. Coated sutures were implanted on the left side of each mouse. Uncoated sutures were implanted on the right side of each mouse as an internal control.

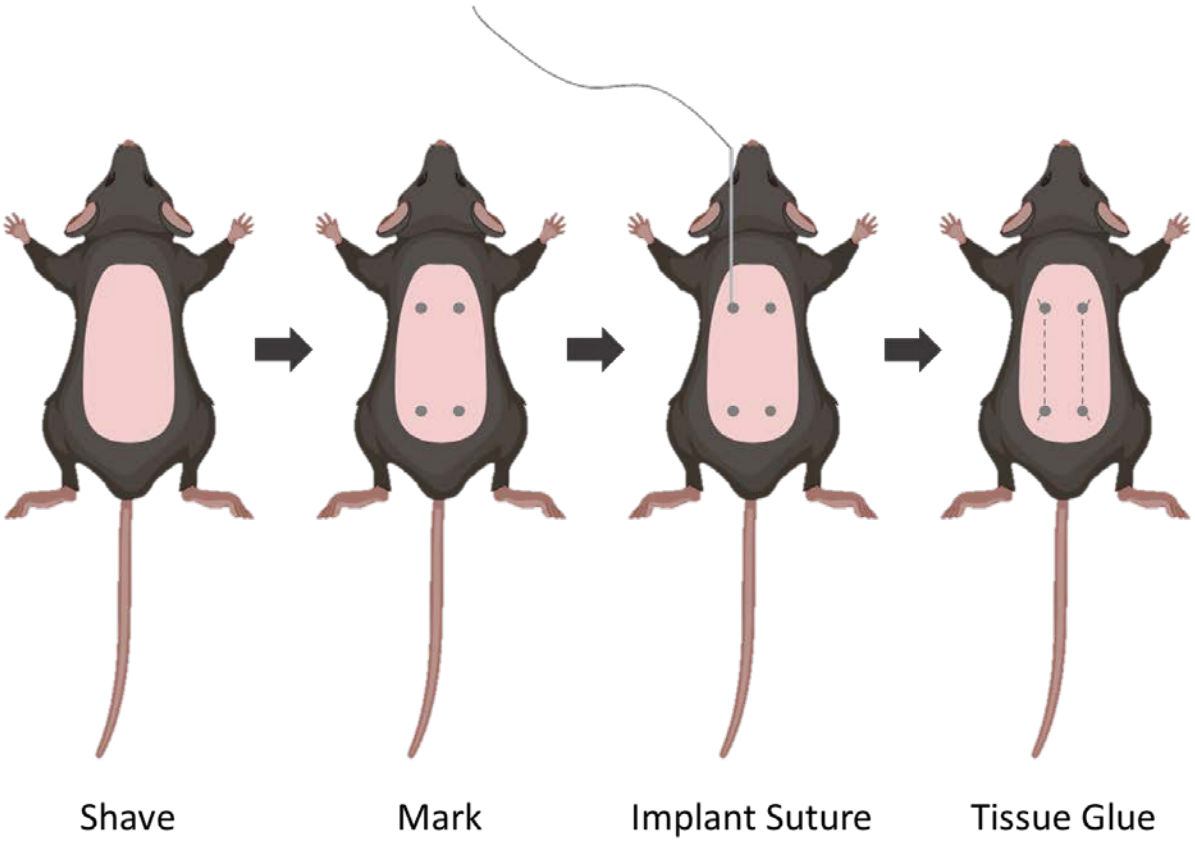

Figure 4.3 Implantation of LbL Coated Suture in Mice. Mice were shaved and suture entrance and exit points were marked. LbL coated suture was implanted in the subcutaneous space and tissue glue was used to secure the suture.

4.3.5 In Vivo *GFP Imaging of Mice*

To evaluate siRNA activity of the LbL coated, IVIS Spectrum In Vivo Imaging System was used to image the mice immediately before suture implantation, after implantation, and daily for three days post implantation (Figure 4.4a). Regions of interest (ROI) were drawn around the suture implantation site and radiant efficiency was measured. To quantify GFP fluorescence, 465 ex / 540 em wavelengths were used.

During the course of the study, two of the mice in the siGFP group were not imaged on both Day 2 and Day 3 due to complications that arose with the mice. From the IVIS imaging, no significant differences of GFP were seen between the left (treatment) and right (uncoated control) sides of the mice. Nonetheless, a trend may be appreciated when plotting the averaged GFP signal for both groups (Figure 4.4b).

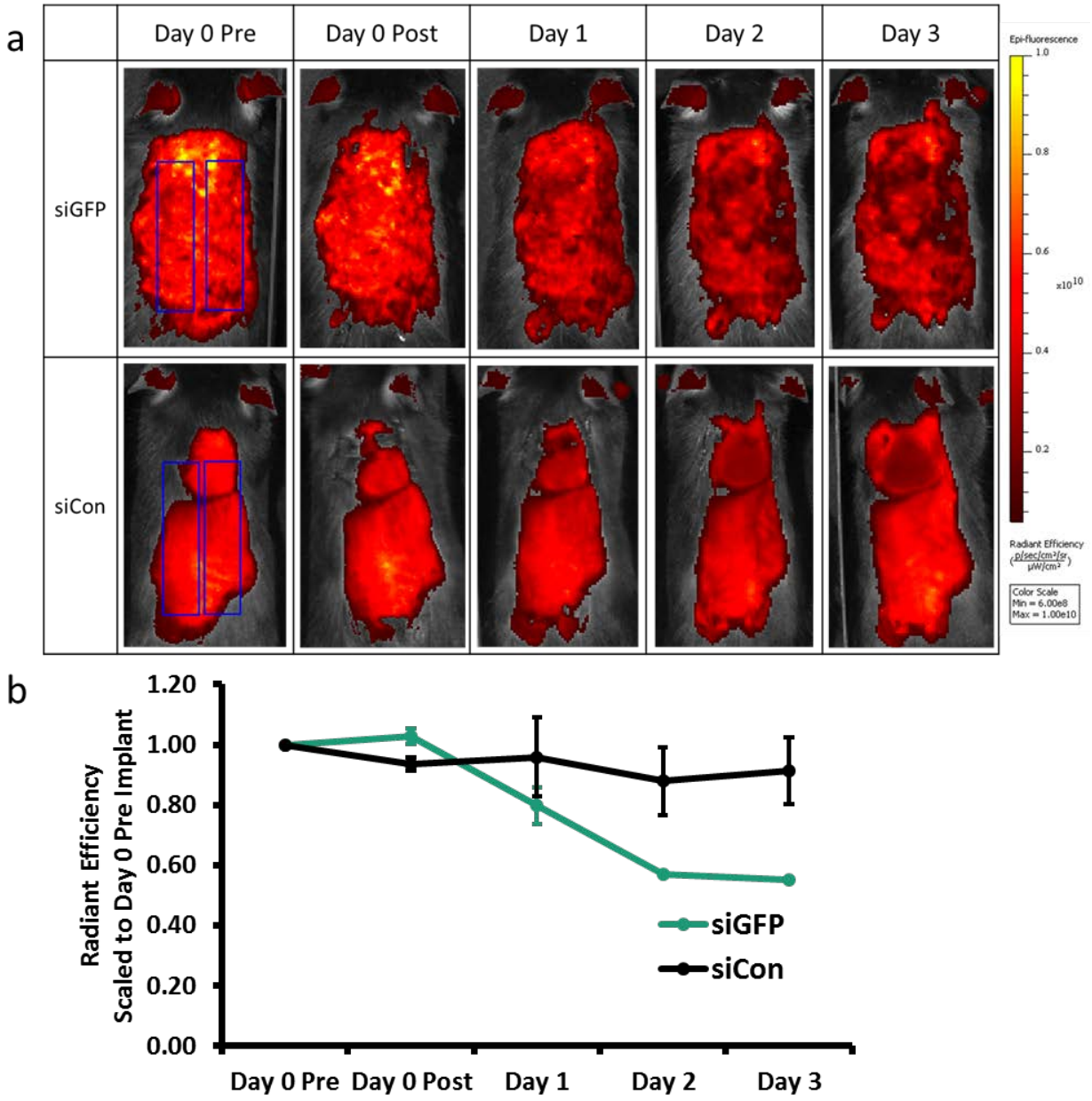

Figure 4.4 *In Vivo* GFP Fluorescence (a) GFP Fluorescence Imaging of Mice Treated with siRNA Coated Sutures. IVIS was used to image GFP fluorescence at 465 ex / 540 em. Images were taken pre-implantation, post-implantation, and then daily for three days. Regions of interest (ROI) were drawn to cover the area around the sutures. Coated sutures were implanted on the left; uncoated sutures were implanted on the right. Representative mice from each treatment group are presented. (b) Average radiant efficiency of GFP over time. Radiant efficiency was averaged over both left and right ROIs for each mouse. Data for mice treated with suture coated with GFP-targeting siRNA (siGFP) are shown in green. Data for mice treated with negative control siRNA (siCon) are shown in black. Error bars represent standard error.

While statistical significance could not be claimed due to only imaging a single mouse on Day 2 and Day 3, it does appear that treatment with siGFP may produce some effect. Mice treated with siCon displayed relatively constant GFP signal over the course of the study. Mice treated with siGFP began to show reduction in signal on Day 1. On the following days, the single imaged mouse showed continued reduction of GFP fluorescence, with approximately 45% reduction of radiant efficiency on Day 3 compared to pre-implantation.

4.3.6 In Vivo *Tracking of Fluorescently Tagged siRNA*

The negative control siRNA used in this *in vivo* pilot study was tagged with Alexa Fluor 647 to track the siRNA after implantation. IVIS images taken at 640 ex / 700 em confirm loading and release of siRNA in the mice (Figure 4.5). Images taken Day 0 immediately after implantation show bright signal of the fluorescent siRNA on and surrounding the suture. The signal confirms retention of coated siRNA on the suture after being drawn through the subcutaneous space in the dorsum. On Day 1, the reduction of signal indicates near complete release of siRNA from the implanted sutures within 24 hours.

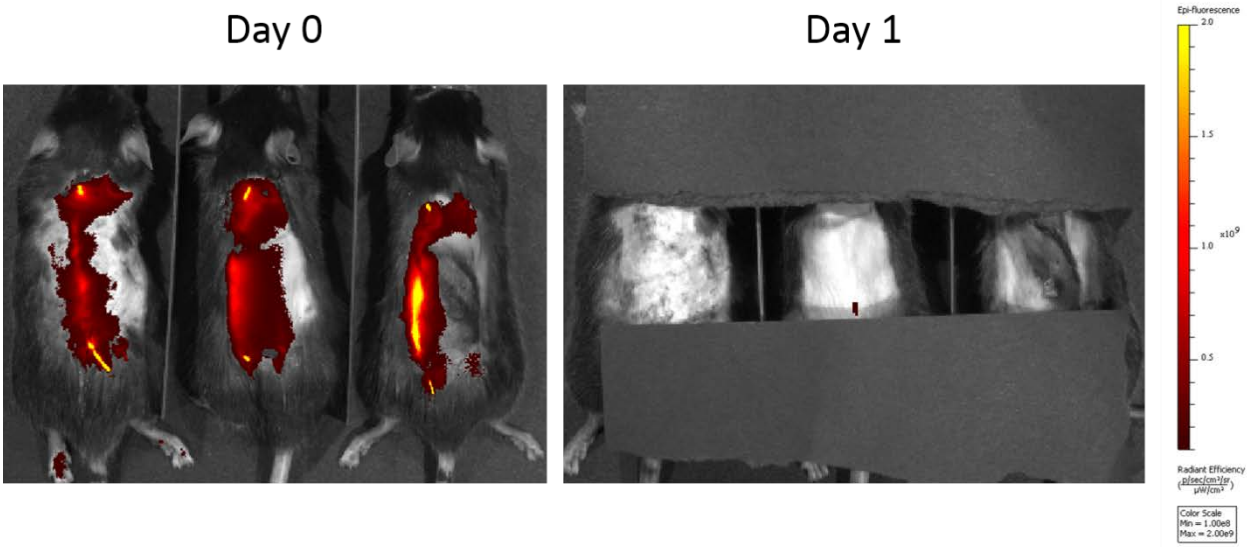

Figure 4.5 In Vivo Release of Fluorescently Tagged siRNA. Negative control siRNA tagged with Alexa Fluor 647 was imaged at 640 ex / 700 em. Images taken immediately post implantation (left) reveal retention of siRNA on the suture after the procedure was performed. Images taken on Day 1 (right) show that near complete release of siRNA is released within 24 hours from implantation.

4.4 Conclusions and Recommendations

Local siRNA delivery has great potential for application in treating various pathologies including bone repair, muscle regeneration, inflammation, and fibrosis mitigation[7]. Here we describe our work in developing a mouse model for proof-of-concept validation of *in vivo* efficacy of siRNA delivered via LbL coated sutures. The model is a non-wounding model to remove confounding factors associated with the complex microenvironment of a wound. Mice ubiquitously expressing GFP were used to detect real-time knockdown of the reporter gene with *in vivo* fluorescence imaging.

The LbL films used in this study had the architecture of $[P2C3OHD/siRNA]_{30}$. The PBAE, Poly 2, was modified with a propanol side chain and DETA endcap to form P2C3OHD. The modifications were made in efforts to increase transfection efficacy. Polyglactin 910 (Vicryl) sutures were used as the substrate. *In vitro* evaluations of sutures coated with the LbL films show achievement of over 80% siRNA-mediated knockdown of GFP.

In our *in vivo* pilot study, these sutures were implanted into GFP expressing mice. IVIS technology was successfully used to image GFP fluorescence of shaved mice over time. Furthermore, fluorescently tagged siRNA was successfully monitored in the treated mice with IVIS.

Though complications within the pilot experiment led to only one mouse in the siGFP group being imaged on Day 2 and Day 3, some trends may be appreciated; reduction of GFP signal is seen in this group compared to mice treated with siCon. We were also able to visualize delivery of fluorescently tagged siRNA; near complete release from the suture is achieved within 24 hours of implantation.

After imaging on Day 3, mice were sacrificed and the tissue surrounding the suture implant were taken for cryosectioning. Lab shutdown due to COVID-19 response prevented us from sufficiently analyzing these samples. Analysis of GFP expression from the surrounding tissue may provide deeper insight to the efficacy of the siRNA released from the coated suture implants.

From this pilot experiment, we formed the following recommendations for future work involving this model:

- Locked nucleic acid (LNA) modification of siRNA has been shown to increase biostability and efficacy, while reducing off-target effects[8]. Using LNA modified siRNA to target the

GFP gene may be more effective in evaluating silencing potential for therapeutic application.

- Complications arose for two of the mice in the pilot study. Autopsy of these mice revealed puncturing of the peritoneum from the suture needle. Great care must be taken during suture implantation to keep the implant in the subcutaneous space, avoiding piercing of the peritoneum.
- Tissue glue application seemed to cause irritation on the mouse dorsum. In some mice, we noticed areas of skin treated with tissue glue were clawed off. During IVIS imaging, the tissue glue was also found to exhibit background radiation. For future studies, we recommend against the use of tissue glue, or using a very sparing amount if necessary.
- To prevent other mice from disturbing the suture implant, we recommend single housing of each mouse during this study.
- To better evaluate siRNA efficacy, a greater dose of siRNA may be needed. Implanting multiple strands of coated suture in parallel across a concentrated area may be prudent for observing siRNA knockdown.
- While reduction of GFP was noticed for the single siGFP-treated mouse imaged over the course of the three days, this may in fact be due to regrowth of hair in the area quenching the GFP signal. Care must be taken to completely remove the hair by shaving and application of Nair to the area before suture implantation. If regrowth of hair is noticed post-implantation, the hair must be shaven to prevent interference with IVIS fluorescence imaging.

4.5 References

(1) Castleberry, S. A.; Golberg, A.; Sharkh, M. A.; Khan, S.; Almquist, B. D.; Austen, W. G.; Yarmush, M. L.; Hammond, P. T. Nanolayered SiRNA Delivery Platforms for Local Silencing of CTGF Reduce Cutaneous Scar Contraction in Third-Degree Burns. *Biomaterials* **2016**, *95*, 22–34. https://doi.org/10.1016/j.biomaterials.2016.04.007.

(2) Shaw, T. J.; Martin, P. Wound Repair at a Glance. *Journal of Cell Science* **2009**, *122* (18), 3209–3213. https://doi.org/10.1242/jcs.031187.

(3) Lynn, D. M.; Langer, R. Degradable Poly(β-Amino Esters): Synthesis, Characterization, and Self-Assembly with Plasmid DNA. *J. Am. Chem. Soc.* **2000**, *122* (44), 10761–10768. https://doi.org/10.1021/ja0015388.

(4) Wu, C.; Li, J.; Wang, W.; Hammond, P. T. Rationally Designed Polycationic Carriers for Potent Polymeric SiRNA-Mediated Gene Silencing. *ACS Nano* **2018**, *12* (7), 6504–6514. https://doi.org/10.1021/acsnano.7b08777.

(5) Akinc, A.; Anderson, D. G.; Lynn, D. M.; Langer, R. Synthesis of Poly(Beta-Amino Ester)s Optimized for Highly Effective Gene Delivery. *Bioconjug. Chem.* **2003**, *14* (5), 979–988. https://doi.org/10.1021/bc034067y.

(6) Eltoukhy, A. A.; Chen, D.; Alabi, C. A.; Langer, R.; Anderson, D. G. Degradable Terpolymers with Alkyl Side Chains Demonstrate Enhanced Gene Delivery Potency and Nanoparticle Stability. *Advanced Materials* **2013**, *25* (10), 1487–1493. https://doi.org/10.1002/adma.201204346.

(7) Sarett, S. M.; Nelson, C. E.; Duvall, C. L. Technologies for Controlled, Local Delivery of SiRNA. *Journal of Controlled Release* **2015**, *218*, 94–113. https://doi.org/10.1016/j.jconrel.2015.09.066.

(8) Elmén, J.; Thonberg, H.; Ljungberg, K.; Frieden, M.; Westergaard, M.; Xu, Y.; Wahren, B.; Liang, Z.; Ørum, H.; Koch, T.; Wahlestedt, C. Locked Nucleic Acid (LNA) Mediated Improvements in SiRNA Stability and Functionality. *Nucleic Acids Res* **2005**, *33* (1), 439–447. https://doi.org/10.1093/nar/gki193.

CHAPTER 5.
Conclusions and Future Directions

5.1 Summary

RNA interference is a promising technology for treatment of a number of diseases involving dysregulated gene expression. This thesis presents our work in exploiting layer-by-layer (LbL) self-assembly technology to construct thin films for controlled localized delivery of siRNA. We investigated films for sequential release of siRNA, optimized LbL assembly parameters to maximize siRNA efficacy *in vitro*, and developed a non-wounding mouse model to evaluate *in vivo* efficacy of LbL films constructed on sutures.

In Chapter 1, we describe the potential of siRNA as a therapeutic to modulate gene expression. The barriers to siRNA delivery are discussed and LbL technology is presented as a method for controlled localized delivery of siRNA. Wound healing is introduced as a promising field for the application of this siRNA therapy. The three overlapping stages of the wound healing process are described in detail and the complications of dysregulated healing are discussed. Thus, context is provided for the work presented in this thesis.

In Chapter 2, we present our work in constructing LbL films for sequential release of siRNA. The tetralayer film $[\text{Chitosan/siRNA/Poly 2/Laponite}]_{25}$ was identified as an architecture exhibiting sustained release of siRNA for over 14 days in PBS. This architecture served as the base tetralayer in our work developing dual release films. We investigated effects of molecular weight and number of bilayers on the effectiveness of the barrier $[\text{Chitosan/Laponite}]_x$ to prevent siRNA interlayer diffusion between tetralayers of similar composition. These studies led us to discover the hierarchical structure of layering the $[\text{Chitosan/siRNA2/Poly 2/Dextran Sulfate}]_{25}$ tetralayer over the $[\text{Chitosan/siRNA1/Poly 2/Laponite}]_{25}$ tetralayer. This film exhibited staggered release of siRNA without the assistance of a barrier layer. Various barrier layers containing GO and/or GO-NH_2 were investigated and found to modulate sequential siRNA release of the films even further. The $[\text{GO-NH}_2\text{/Laponite}]_{10}$ barrier layer was found to induce sustained release of siRNA2 over the course of the first seven days of incubation, followed by sustained release of siRNA1.

In Chapter 3, we analyze the effects of assembly parameters on composition and *in vitro* knockdown efficacy of LbL films containing siRNA. Polyglactin 910 (Vicryl) sutures were coated with a bilayer consisting of Poly 2, a PBAE, and siRNA. A library of films were constructed on

sutures under varying LbL conditions. A fractional factorial design was employed to determine the assembly parameters of pH, ionic strength of the PBAE bath, PBAE concentration, and siRNA concentration. Significant effects of these assembly parameters on PBAE loading, siRNA loading, and their respective weight ratios were elucidated and corroborated with theory from previously published studies. Informed by these findings, assembly parameters were tuned to maximize siRNA knockdown efficacy. Films constructed with the optimized conditions were found to achieve over 80% knockdown *in vitro*.

In Chapter 4, we describe our work in developing a non-wounding mouse model to evaluate *in vivo* knockdown from LbL coated sutures. The LbL films used in this study were constructed similarly to the optimized films presented in Chapter 3. The polycation used was a Poly 2 modified with a propanol side chain and endcapped to increase transfection efficacy. We decided upon using mice that ubiquitously expressed the reporter gene GFP. Vicryl sutures coated with the LbL film were implanted subcutaneously in the dorsum of the mice. In our preliminary pilot study, we were able to track GFP fluorescence in the mice over the course of three days. Though significance in knockdown could not be determined, the results proved promising. Fluorescence of control siRNA tagged with Alexa Fluor 647 were found to be released from implanted sutures within 24 hours of implantation. A number of recommendations for future studies were drawn from this pilot study.

5.2 Future Directions

5.2.1 Optimizing Efficacy of Dual-Release siRNA Films

In this thesis, we have studied the construction of LbL films for delivery of siRNA. We have discovered film architectures that exhibit sequential release of siRNA with the assistance of barrier layers; we have also determined assembly conditions to optimize knockdown from the bilayer film $[PBAE/siRNA]_x$. A natural follow-up to this work would be an investigation of assembly conditions to improve knockdown efficacy of the sequential release siRNA films. Though a systematic study to tune the tetralayer assemblies within the hierarchical structure of the dual-release films will require a much more extensive effort compared the optimization study of the single-release bilayer, this work would be crucial to the development of sequential release siRNA films. Multi-therapy films with tunable release of siRNAs would show greater promise in the treatment of pathologies such as bone regeneration and wound repair.

5.2.2 LbL Delivery of Other Therapeutic Nucleic Acids

Apart from siRNA, other nucleic acids have been widely researched for therapeutic use. These therapeutic nucleic acids (TNAs) include plasmid DNA, microRNA mimics, anti-microRNA oligonucleotides, messenger RNA, and antisense oligonucleotides. Each of these TNAs operate with different mechanisms and have their own unique benefits in modulating gene expression. While similarities in composition and charge provide a common basis for LbL incorporation of the various TNAs, differences in shape, size, and mechanism of the TNAs present distinct challenges in achieving effective transfection from LbL films. A systematic approach, such as the fractional factorial design presented in Chapter 3, may be used to optimize LbL film assembly for delivery of alternate TNAs.

5.2.3 Further Development of Non-Wounding Animal Model

As detailed in Chapter 4, we conducted a pilot experiment involving the implant of siRNA coated sutures in a GFP-expressing mice. Further development of this model may be prudent for verification of *in vivo* siRNA efficacy without the complexities associated with the wound environment. As described in the conclusion of Chapter 4, recommendations for future work with this model include using locked nucleic acid (LNA) modified siRNA to increase biostability, single housing of mice, implanting multiple strands of suture, and greater care in suture implantation tissue glue application, and hair removal.

APPENDIX A.

Troubleshooting LbL Knockdown

In this section, we present our efforts in troubleshooting knockdown from LbL films. These experiments were performed to follow up on the research presented in Chapter 2.

A.1 In Vitro Cell Line Experiments

To test the dual siRNA systems developed in Chapter 2, we sought to use a cell line with two reporter genes. The cell line that was investigated was an MDA-MB-435 melanoma cell line that expresses both green fluorescent protein (GFP) and red fluorescent protein (RFP). siRNAs against both fluorescent reporter genes were obtained and validated (Figure A.1). Treatment of a single siRNA using Lipofectamine RNAiMAX was able to achieve knockdown of the associated reporter gene without affecting expression of the other reporter gene. Treatment of both siRNAs was shown to achieve knockdown of both genes.

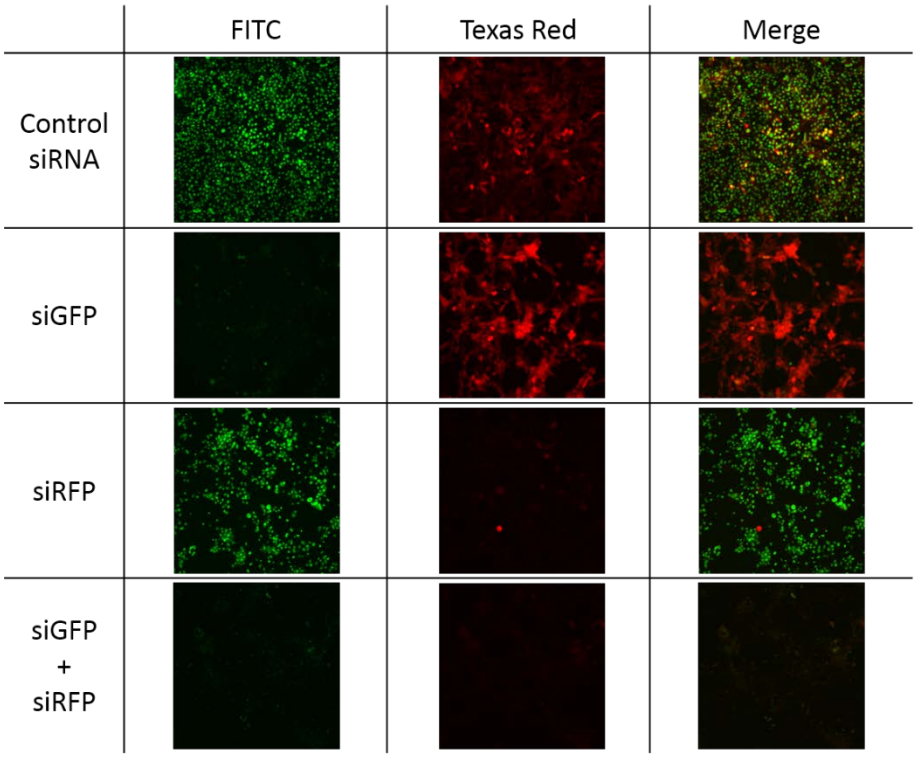

Figure A.1 Validation of siRNAs for Dual-Reporter MDA-MB-435 Cells siRNAs for GFP and RFP were validated for the cell line. Treatment of a single siRNA resulted in the exclusive knockdown of the corresponding reporter gene. Treatment with both siRNAs resulted in knockdown of both reporter genes.

A.2 Troubleshooting Knockdown

Before testing the sequential knockdown from our dual release films, we investigated whether or not the LbL architecture with a single siRNA can knockdown a single reporter gene. For these experiments, we used HeLa cells expressing d2e-GFP, a destabilized GFP with a shorter half-life. Films constructed on silicon chips were incubated in Opti-MEM (a reduced serum medium) at 37°C for either 2 or 3 days. The GFP-expressing cells were then exposed to the releasate in a 96-well plate. Flow cytometry was performed 2 days later.

The first film tested was the bottom siRNA-containing layer of the previously investigated architecture: $[\text{Chitosan/siGFP/Poly2/Laponite}]_{25}$. Previous work in the Hammond lab has shown this film to effect up to 45% knockdown. However, despite all our efforts in troubleshooting, knockdown from this film architecture was not reproduced. When the commercially available transfection reagent Lipofectamine RNAiMAX was added with the releasate, approximately 70% knockdown was achieved. This suggests that the siRNA released from the film is not degraded and is still active. However, the lack of knockdown suggests that either the siRNA complexes are not able to enter the cell, or the complexes have entered but are not able to escape the endosomes.

Many different architectures were then tested to investigate which, if any, were able to effect knockdown of GFP. The results are tabulated in Table A.1.

Table A.1 LbL Architectures Built on Silicon Chips Tested for In Vitro Knockdown. Films were assembled with 25 tetralayers.

Polycation	Polyanion	Polycation	Polyanion	pH	Knock-down?	KD with lipo RNAiMAX	Elution Time (Days)
Chitosan	siRNA	25 kDa Poly 2	Laponite Clay	4.5	No	~80%	2
Chitosan	siRNA	15 kDa Poly 2	Laponite Clay	4.5	No	~90%	2
Chitosan	siRNA	10 kDa Poly 2	Laponite Clay	4.5	No	~70%	2
Chitosan	siRNA	10 kDa Poly 2	Dextran Sulfate	4.5	No	~20%	2
10 kDa Poly 2	siRNA	10 kDa Poly 2	siRNA	4.5	No	~35%	2
10 kDa Poly 2	siRNA	10 kDa Poly 2	Laponite Clay	4.5	No	~20%	2
10 kDa Poly 2	siRNA	10 kDa Poly 2	Dextran Sulfate	4.5	No	No	2
40 kDa LPEI	siRNA	25 kDa Poly 2	Laponite Clay	4.5	No	~70%	3
40 kDa LPEI	siRNA	10 kDa Poly 2	Laponite Clay	4.5	No	~100%	3
40 kDa LPEI	siRNA	40 kDa LPEI	Laponite Clay	4.5	No	~100%	3
40 kDa LPEI	siRNA	10 kDa Poly 2	siRNA	4.5	No	~100%	3
40 kDa LPEI	siRNA	10 kDa Poly 2	Dextran Sulfate	4.5	No	~25%	3
Chitosan	siRNA	Poly 2 / LPEI	Laponite Clay	4.5	No	~95%	3
Chitosan	siRNA	10 kDa Poly 2	Laponite Clay	5.2	No	~95%	3

Of the fourteen different LbL architectures listed in this table, not a single film's releasate from its silicon chip substrate produced any GFP knockdown. However, when Lipofectamine RNAiMAX is added, significant knockdown is achieved for many of the films. This indicates that for those films, active siRNA is indeed released, but unable to effect knockdown without the aid of the additional transfection reagent. The complexes released by the film itself are not sufficient.

Several more experiments were performed with Vicryl Rapide PLGA sutures. Sutures were coated with LbL films. The sutures were then cut into approximately 1 cm pieces. Three pieces of suture were placed directly in culture with GFP-expressing cells in a 48-well plate. siRNA against GFP and a fluorescently-tagged negative control siRNA were used. Flow cytometry was performed 3 days after initial incubation. Several of the formulations and their results are tabulated in Table A.2.

Table A.2 LbL Architectures Built on PLGA Suture Tested for In Vitro Knockdown. Films were assembled with 25 tetralayers.

Polycation	Polyanion	Polycation	Polyanion	pH	Knock-down?	Labeled siControl Signal	Release Time (Days)
Chitosan	siRNA	25 kDa Poly 2	Laponite Clay	4.5	No	~90%	3
Chitosan	siRNA	10 kDa Poly 2	Laponite Clay	4.5	No	~95%	3
10 kDa Poly 2	siRNA	10 kDa Poly 2	Laponite Clay	4.5	No	N/A	3
10 kDa Poly 2	siRNA	10 kDa Poly 2	siRNA	4.5	~10%	~99%	3
40 kDa LPEI	siRNA	40 kDa LPEI	siRNA	4.5	No	~15%	3
40 kDa LPEI	siRNA	10 kDa Poly 2	siRNA	4.5	~20%	~90%	3
40 kDa LPEI	siRNA	10 kDa Poly 2	Laponite Clay	4.5	No	~75%	2

From the suture experiments, there were two formulations that achieved siRNA-specific knockdown. The [10 kDa Poly 2/siRNA] bilayer film resulted in approximately 10% knockdown. The [40 kDa LPEI/siRNA/10 kDa Poly 2/siRNA] tetralayer film resulted in 20% knockdown. Yet remarkably, cells exhibited much greater signal of the labeled control siRNA. This is seen in films that resulted in no appreciable GFP knockdown as well. This suggests that the siRNA is indeed entering the cells; however, once inside, knockdown is not achieved. This may be explained by failure of the complexes to escape the endosome.

Confocal imaging was performed to further investigate how the LbL releasate interacts with the cell. Vicryl Rapide suture was coated with the bilayer [Poly 2/siRNA]$_{30}$. The siRNA used was a negative control siRNA labeled with Alexa-Fluor 647. The suture was placed directly in culture with HeLa cells expressing d2eGFP. Imaging with Nikon A1R was performed 3 days post incubation. Hoechst staining was used to stain for the nucleus. A representative image is shown below in Figure A.2. The nucleus is stained in blue. The GFP is shown in green. The siRNA is shown in red. Many of the cells are seen to have taken up the siRNA. However, the punctate fluorescence suggests that the siRNA is indeed trapped in endosomes.

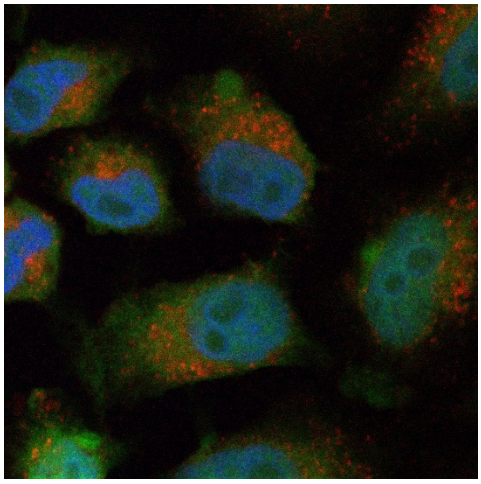

Figure A.2 Confocal Imaging of LbL Treated Cells. HeLa cells expressing d2eGFP were exposed to PLGA sutures coated with a [Poly 2/siRNA]$_{30}$ LbL coating. The nuclei is stained in blue with Hoechst. The GFP is shown in green. The siRNA is labeled with Alexa-Fluor 647 and is shown in red. The punctate fluorescence suggests the siRNA is trapped in endosomes.

To further troubleshoot the knockdown problem, we investigated deeper into the LbL coating process of the sutures. We monitored the siRNA concentration in the dipping bath. From previous studies performed in the lab, the concentration of the siRNA in the bath was set to 20 μg/mL at the beginning of the dipping process. During the coating process of 30 bilayers, the siRNA bath was found to be depleted at an unanticipated rate. Taking into account coating of the suture and the wire frame, the concentration in the siRNA bath, and transfer into other baths, still a considerable amount of siRNA remains unaccounted for. Due to the newfound depletion of siRNA, we investigated the effects of replenishing the siRNA multiple times throughout the dipping process. The effects on the concentration of the siRNA bath are shown in Figure A.3. In each case, the decrease in siRNA concentration appears to be first order. This may be expected; the amount of siRNA adsorbed onto the suture may follow the concentration of siRNA in the bath.

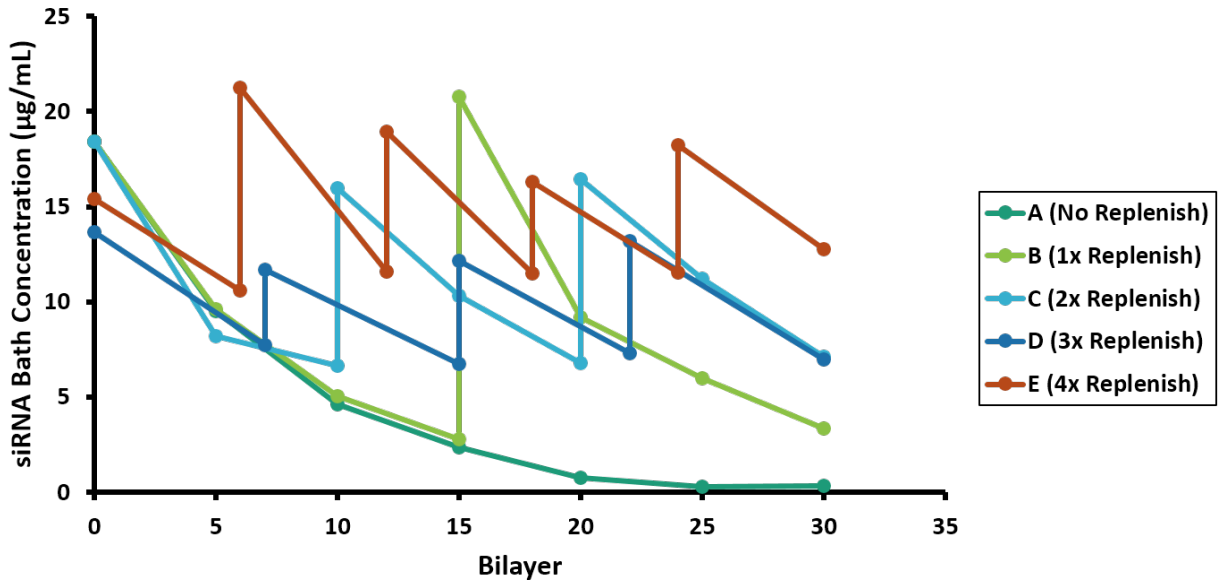

Figure A.3 Effect of Replenishing siRNA on Concentration in Bath Over Dipping Process. The concentration of the siRNA bath was monitored over the course of bilayer coating of [Poly 2/siRNA]$_{30}$ on PLGA sutures. The amount of siRNA added was predetermined in an estimate to bring the concentration back to the initial level of approximately 18 µg/mL. There appears to be a first order decrease in the concentration for each case.

The effect of replenishing on the siRNA loading on the sutures was also investigated, as shown in Figure A.4a. The ability for these sutures to effect GFP knockdown was also measured, as shown in Figure A.4b. As the number of replenishments increases, the amount of siRNA incorporated into the LbL coating on the suture generally increases. However, this does not directly correlate with the ability to achieve knockdown *in vitro*. The film that effected the most knockdown came from the process that included a single replenishment of siRNA midway through dipping. Approximately 20% GFP knockdown was seen with this film. Films that included more replenishment, and therefore greater siRNA loading, in fact effected less knockdown.

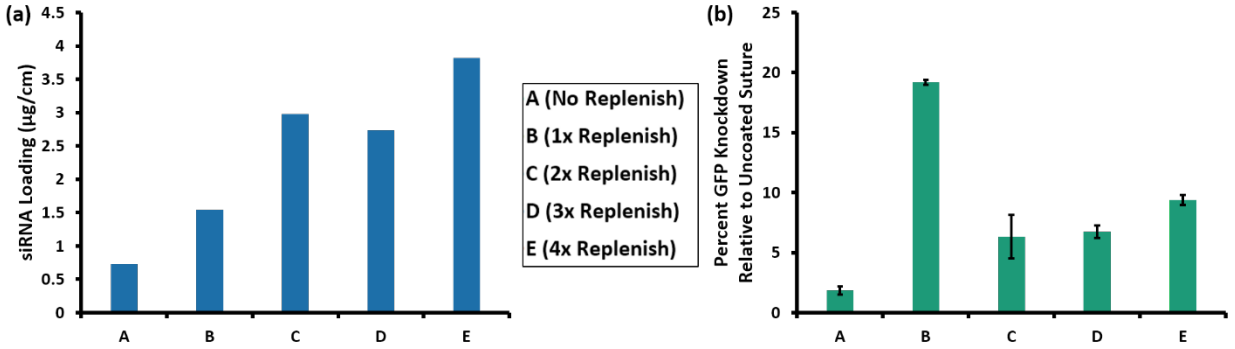

Figure A.4 Effects of Replenishing siRNA on siRNA Loading and Effecting Knockdown (a) siRNA loading generally increases as the number of replenishments increases. Approximately 4 µg/cm loading is achieved when siRNA is replenished four times throughout LbL coating. (b) The film that resulted in the greatest GFP knockdown is when siRNA is replenished once, midway through dipping. Almost 20% knockdown is achieved with this film.

We then further investigated the coating that included a single replenishment of siRNA as it effected the greatest knockdown. We looked at the effect of putting different amount of suture pieces into the wells with the cells. This can be seen in Figure A.5. Generally, as the number of suture pieces applied to the wells increased, GFP knockdown increased. With the data produced in Figure A.4b, this suggests that an increase in siRNA dosing alone will not effect greater knockdown. The N:P ratio of the LbL releasate is likely a more appropriate metric of ability to effect knockdown. With more replenishment, more siRNA is loaded; however, we hypothesize the composition of the film becomes less conducive for knockdown. Yet with a more optimal composition from a single replenishment, an increase of dosing does indeed effect greater knockdown.

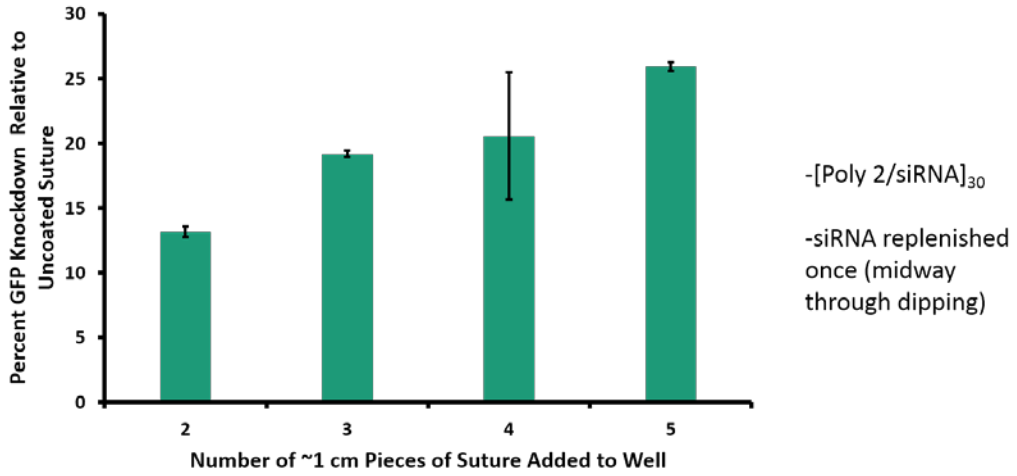

Figure A.5 Effect of Number of Pieces of Suture on GFP Knockdown. HeLa cells were treated with sutures coated with $[Poly\ 2/siRNA]_{30}$ bilayers. The siRNA bath was replenished midway through the dipping process. Generally, as the number of pieces of suture applied to each well increases, the GFP knockdown increases. Over 25% knockdown was achieved with 5 pieces of suture.

These findings on the importance of N:P ratio as well as dose on achieving *in vitro* knockdown prompted the work presented in Chapter 3. Assembly parameters were investigated in their effects on film composition and consequent knockdown.

APPENDIX B.

Supporting Information for Chapter 3

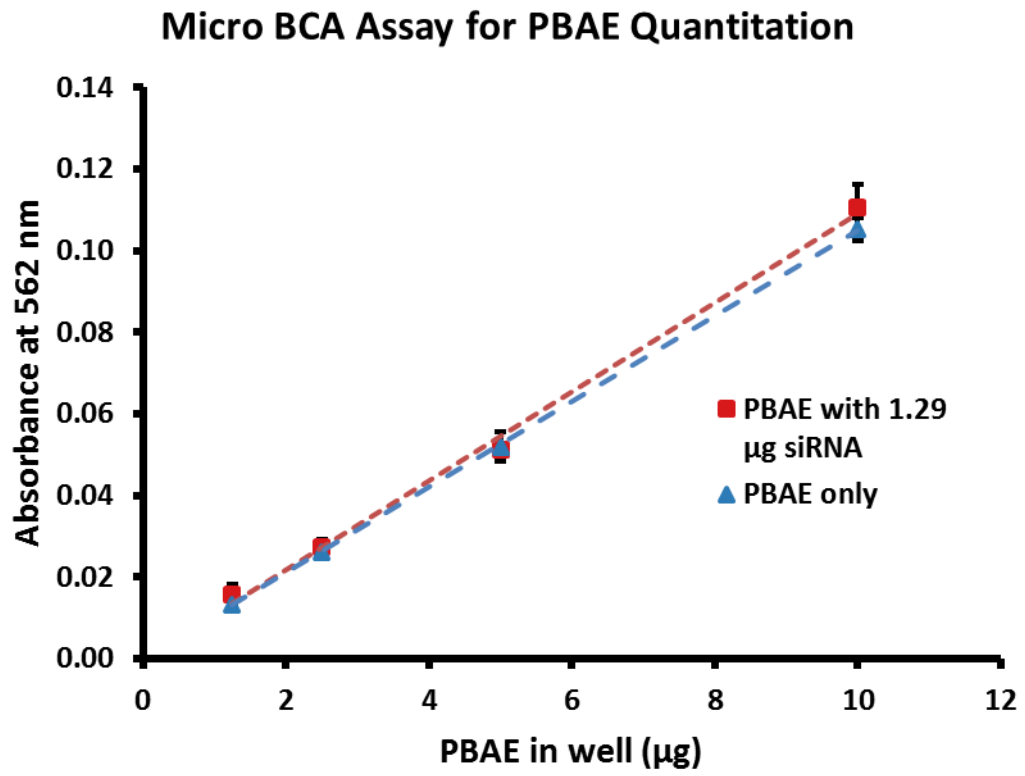

Figure B.1 Micro BCA Assay for PBAE Quantitation. Serial two-fold dilutions of PBAE were made with siRNA (red squares) and without siRNA (blue triangles). The Micro BCA assay was performed following manufacturer's instructions. The linear regressions (represented by dashed lines) show that the presence of siRNA does not affect Micro BCA assay readings. We found that the Micro BCA assay can be appropriately repurposed to quantify PBAE loading in the LbL film.

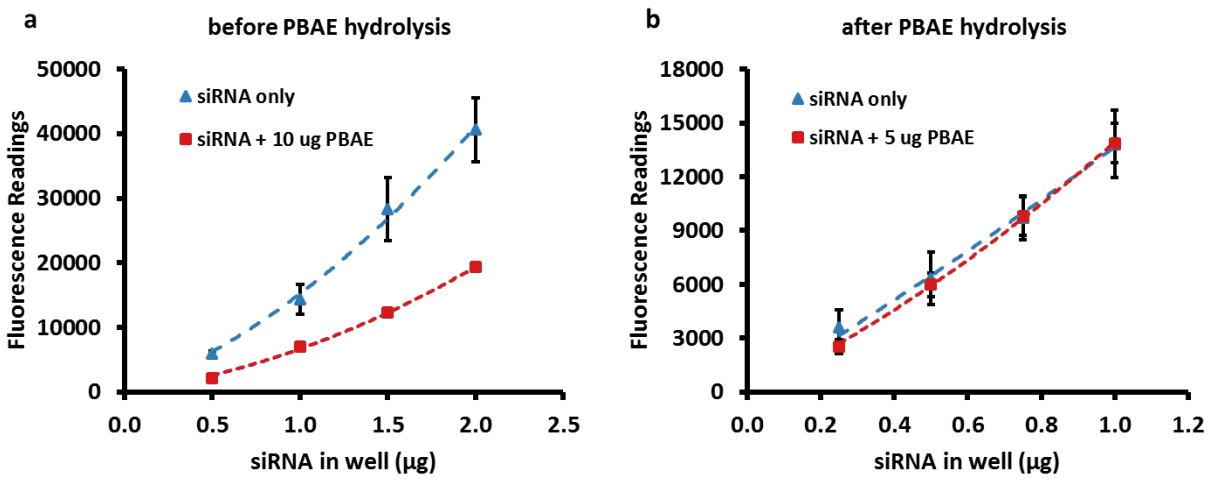

Figure B.2 Ribogreen Assay for siRNA Quantitation. Standard curves with known siRNA amounts were made with PBAE (red squares) and without PBAE (blue triangles). The Ribogreen assay was performed following manufacturer's instructions. Without modification (a), the presence of PBAE quenches the Ribogreen fluorescent signal considerably. To address the quenching, the PBAE was hydrolyzed as detailed in the experimental section. After hydrolysis of the PBAE (b), interference from the PBAE is shown to be minimized.

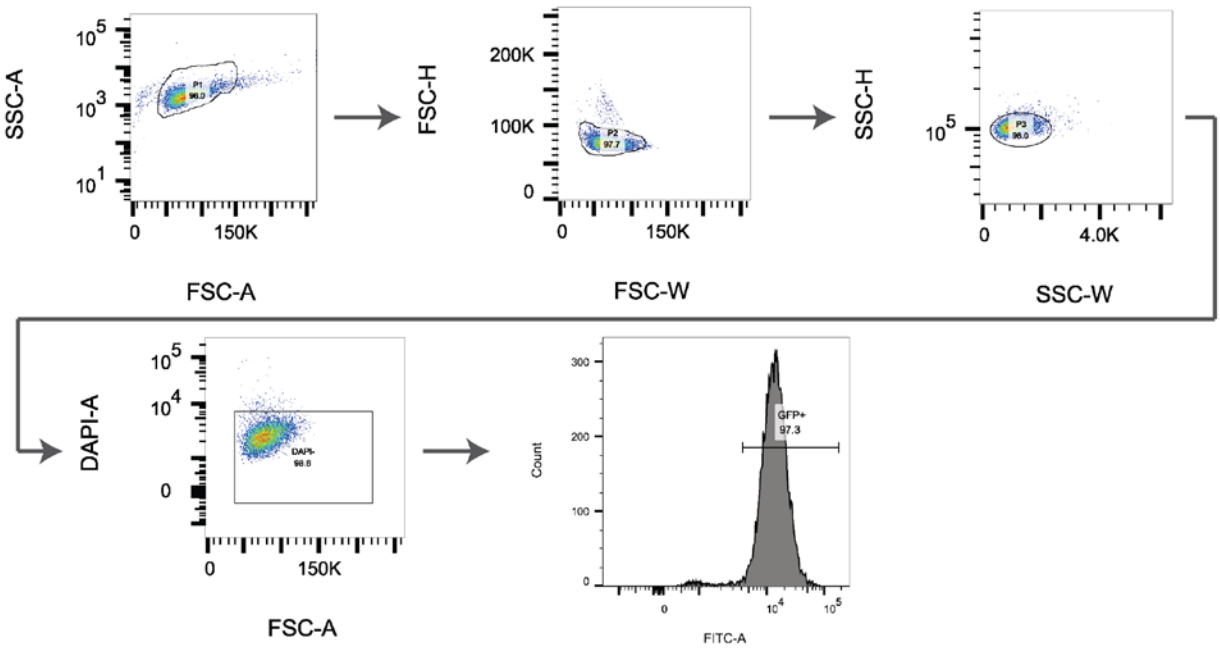

Figure B.3 Gating Strategy for Flow Cytometry

Table B.1 Fractional factorial design parameters and response variable data. The parameters tested include pH, ionic strength, PBAE concentration, and siRNA concentration. Ranges were determined based on parameters previously published by our lab. Response variables of PBAE loading, siRNA loading, w/w ratio, knockdown, and viability are reported for each replicate. Cells are colored to depict differences in magnitude. JMP was used to determine Runs 1a - 8c for the fractional factorial design. Runs 9a – 12c were added as midpoints for pH and polymer concentration to test for non-linearity.

Run	pH	Ionic Strength (mM)	PBAE Conc. (mg/mL)	siRNA Conc. (µg/mL)	PBAE Loading (µg/cm)	siRNA Loading (µg/cm)	w/w ratio	Knockdown (%)	Viability (%)
1A	4.5	150	2.0	20	1.02	0.64	1.58	25.52	90.0
1B	4.5	150	2.0	20	1.18	0.57	2.06	9.65	95.8
1C	4.5	150	2.0	20	1.35	0.77	1.76	18.46	96.9
2A	4.5	150	2.0	30	0.88	1.37	0.64	8.61	87.4
2B	4.5	150	2.0	30	0.88	1.02	0.86	3.73	94.9
2C	4.5	150	2.0	30	0.94	1.52	0.62	12.14	86.1
3A	4.5	250	0.5	20	0.64	1.07	0.60	2.80	95.3
3B	4.5	250	0.5	20	0.52	1.02	0.51	4.46	92.7
3C	4.5	250	0.5	20	0.55	1.17	0.47	25.21	97.1
4A	4.5	250	0.5	30	0.77	1.97	0.39	13.17	93.0
4B	4.5	250	0.5	30	0.83	2.02	0.41	8.20	95.9
4C	4.5	250	0.5	30	0.81	1.86	0.44	6.33	87.4
5A	6.0	150	0.5	20	1.44	1.60	0.90	3.32	88.8
5B	6.0	150	0.5	20	1.54	1.55	0.99	12.55	88.8
5C	6.0	150	0.5	20	1.67	1.10	1.51	6.74	83.6
6A	6.0	150	0.5	30	1.43	2.24	0.64	56.02	87.4
6B	6.0	150	0.5	30	1.29	2.06	0.63	12.86	81.2
6C	6.0	150	0.5	30	1.18	2.20	0.53	42.01	79.1
7A	6.0	250	2.0	20	0.69	0.05	12.76	0.00	92.0
7B	6.0	250	2.0	20	0.78	0.09	8.24	0.00	95.7
7C	6.0	250	2.0	20	0.53	0.11	4.86	0.00	95.4
8A	6.0	250	2.0	30	1.01	0.30	3.36	0.00	95.6
8B	6.0	250	2.0	30	0.91	0.28	3.22	0.50	93.1
8C	6.0	250	2.0	30	0.76	0.29	2.65	2.62	89.4
9A	5.2	150	1.0	20	1.08	0.99	1.09	4.42	97.9
9B	5.2	150	1.0	20	1.05	0.89	1.18	0.60	91.5
9C	5.2	150	1.0	20	1.08	0.77	1.40	1.77	94.4
10A	5.2	150	1.0	30	1.20	1.31	0.92	0.00	95.7
10B	5.2	150	1.0	30	1.18	1.63	0.73	3.04	93.7
10C	5.2	150	1.0	30	1.17	1.29	0.91	3.25	90.1
11A	5.2	250	1.0	20	1.31	0.77	1.69	0.00	89.5
11B	5.2	250	1.0	20	1.42	0.83	1.72	1.03	93.3
11C	5.2	250	1.0	20	1.51	0.57	2.65	0.00	97.2
12A	5.2	250	1.0	30	1.14	1.23	0.92	4.74	87.5
12B	5.2	250	1.0	30	1.26	1.43	0.88	5.91	89.6
12C	5.2	250	1.0	30	1.08	1.36	0.80	0.18	58.8

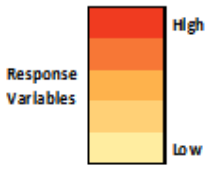

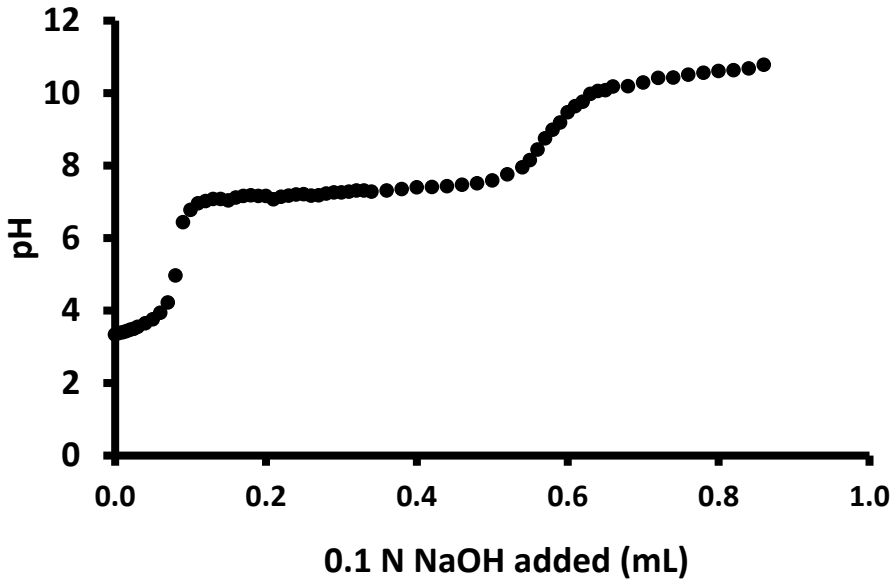

Figure B.4 pH Titration of PBAE. 10.1 mg PBAE was dissolved at 1 mg/mL in water with 75 µL of 1 M HCl. 0.1 N NaOH was used for titration. The pKa of the PBAE was found to be 7.4.

a	Knockdown	
Term	Norm. Coeff.	p-value
pH	+0.33 ↑	0.967
Ionic Strength	-8.31 ↓	0.233
PBAE Conc.	-7.03 ↓	0.389
siRNA Conc.	+3.71 ↑	0.579

b	Knockdown	
Term	Norm. Coeff.	p-value
PBAE Loading	+1.83 ↑	0.862
siRNA Loading	+25.24 ↑	0.118
w/w Ratio	+7.16 ↑	0.662

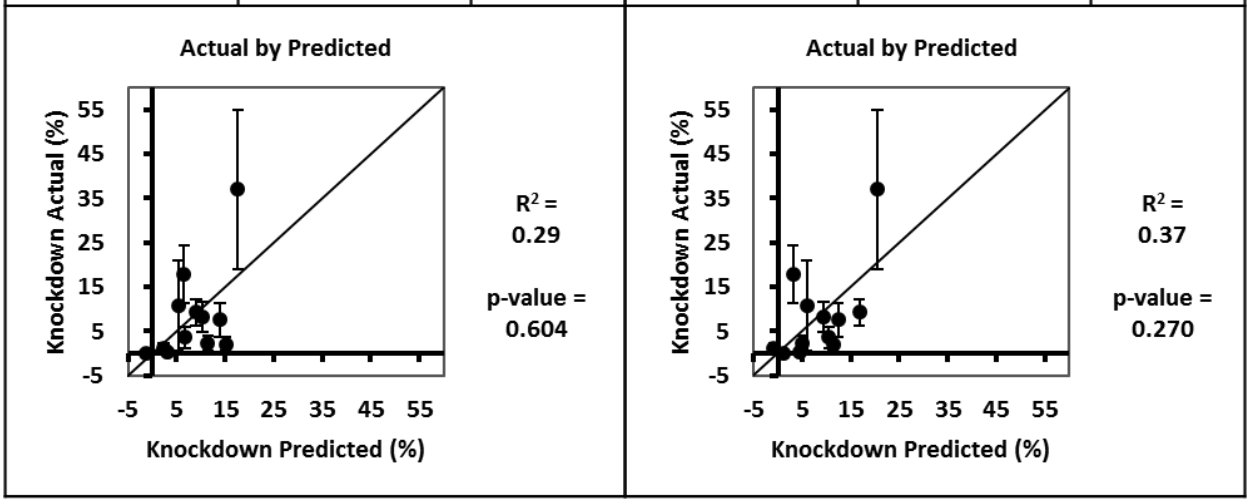

Figure B.5 Standard Least Squares Fit on Knockdown. A standard least squares fit was performed for *in vitro* knockdown with (a) assembly parameters as explanatory variables and (b) PBAE loading, siRNA loading, and w/w ratio as explanatory variables. "Actual by Predicted" plots are shown with R^2 and p-values reported. The coefficients for each parameter were normalized by the ranges of the explanatory variables and p-values are reported. No significant parameter terms were identified for either regression (correlation p-value < 0.05). Error bars represent standard deviation.

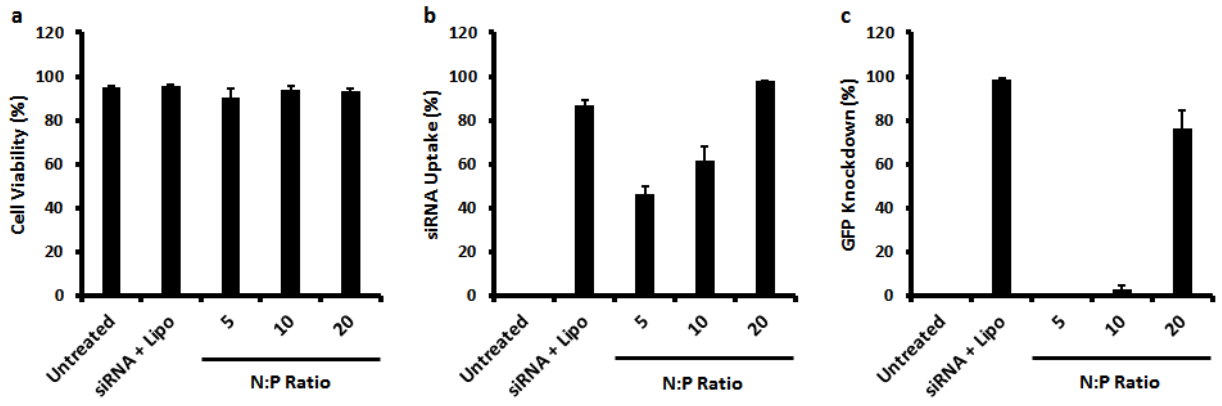

Figure B.6 Polyplex transfection studies. Polyplexes were formed by mixing PBAE and siRNA together at predetermined ratios. HeLa cells expressing d2e-GFP were treated with polyplexes. Flow cytometry was performed three days after treatment. (a) NucBlue assay was used to measure viability. (b) Alexa Fluor 647-labeled siRNA was used to track siRNA uptake. (c) GFP-targeting siRNA was used in studies of siRNA knockdown efficacy. Untreated cells served as negative controls. For positive controls, cells were treated with siRNA + Lipofectamine RNAiMAX.

Polyplexes were assembled by mixing PBAE and siRNA at predetermined N:P ratios of 5, 10, and 20. (A 1:1 weight ratio of PBAE to siRNA roughly equates to an N:P ratio of 2.) HeLa cells expressing destabilized GFP were treated with these polyplexes, and cell viability, siRNA uptake, and GFP silencing were measured through flow cytometry.

The polyplexes were shown to have minimal cytotoxicity in the range of N:P ratios tested. As the N:P ratio increases, uptake of fluorescent siRNA increases steadily. Accordingly, GFP knockdown also increases with N:P ratio.

APPENDIX C.

Supporting Information for Chapter 4

Here we detail some of the work that led us to the LbL film formulation used in Chapter 4

C.1 P2C3OHD vs. Poly 2

The bilayer [P2C3OHD/siRNA]$_{30}$ was constructed on PLGA sutures in a similar manner as with Poly 2 to achieve the greatest knockdown, with a pH of 6.0, 20 μg/mL siRNA bath, and a single replenishment of siRNA midway through dipping (as described in Appendix A). At this point in our research, we had not yet begun to monitor ionic strength. With three pieces of suture placed into culture with HeLa cells expressing d2eGFP, approximately 50% knockdown was achieved with this formulation. This is greater knockdown than what was observed previously with the [Poly 2/siRNA] bilayers. The resulting GFP expression relative to uncoated suture for the [Poly 2/siRNA] film and the [P2C3OHD/siRNA] film is seen in Figure C.1.

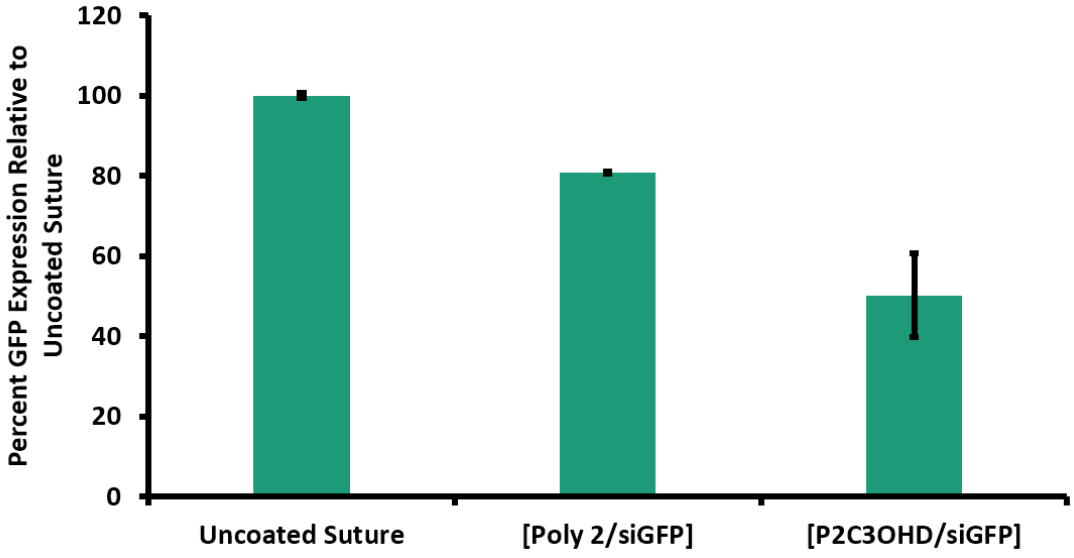

Figure C.1 GFP Knockdown of [P2C3OHD/siRNA] vs. [Poly 2/siRNA] The [Poly 2/siGFP] coated suture was able to effect approximately 20% knockdown. The [P2C3OHD/siGFP] suture was able to effect approximately 50% knockdown. Error bars represent standard error.

C.2 Evaluation of Various Substrates

This [P2C3OHD/siRNA] formulation was also applied to various other substrates. These substrates effected different responses in GFP knockdown. Figure C.2 shows the knockdown achieved by the same LbL coating on different substrates. The variation in knockdown seems to indicate that the substrate itself has an effect on transfection efficiency. Once hypothesis to why the Vicryl Rapide suture may lead to greater knockdown is that its relatively quick degradation rate leads to the breaking up of the LbL film into smaller fragments which may be more easily endocytosed by cells and may contribute to greater endosomal escape. Other hypotheses to the variation in knockdown include differences in diameters of the sutures as well as differences in construction (ie. woven vs. monofilament sutures).

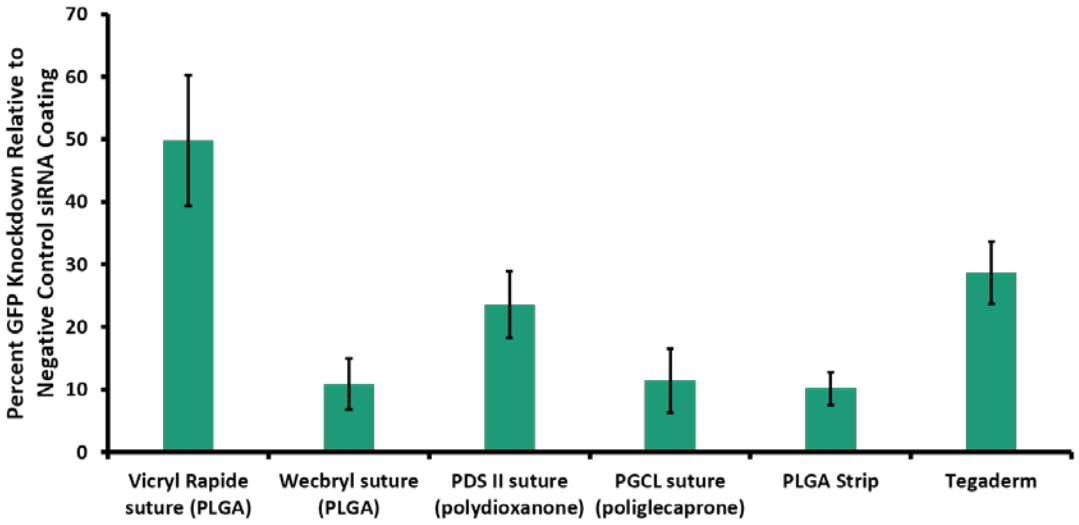

Figure C.2 GFP Knockdown from [P2C3OHD/siRNA] Film from Various Substrates. The [P2C3OHD/siGFP] bilayer was constructed on Vicryl Rapide Suture, Webcryl suture, PDS II suture, PLGA strips, and Tegaderm. Knockdown ranges from 10% to 50%. The distinct abilities to effect knockdown indicates that the substrate may have an effect on transfection. Error bars represent standard error.

C.3 Polyplex Evaluation of P2C3OHD

To better understand the mechanism of transfection from the LbL coatings, we performed some studies with simple polyplexes of P2C3OHD and siRNA. For a range of weight ratios, zeta potential and knockdown efficiency measurements were taken. These data are shown in Figure C.3. We see that as the weight ratio of P2C3OHD to siRNA increases, the zeta potential increases as expected. As the weight ratio increases above 10, the zeta potential levels off around +22 mV. A similar phenomenon is seen in the knockdown study. As the weight ratio increases, greater knockdown is achieved. The knockdown efficiency starts to level off after above a weight ratio of 10.

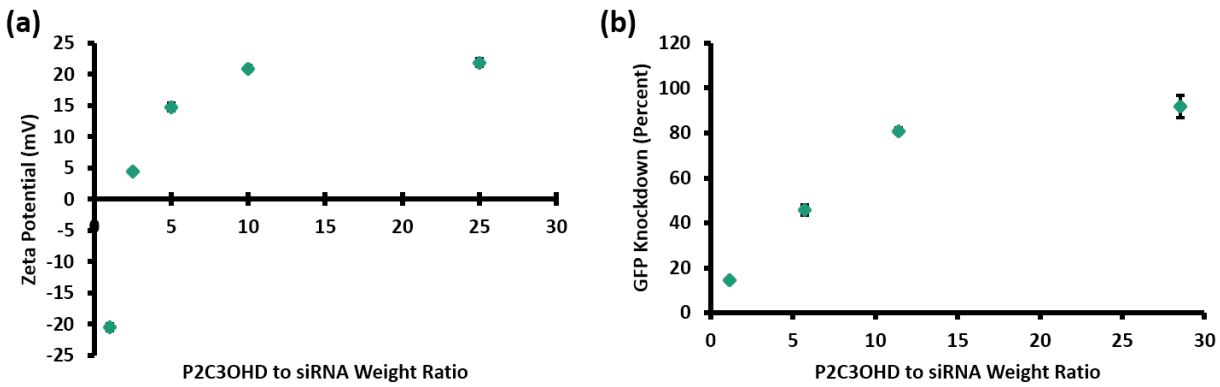

Figure C.3 Analysis of P2C3OHD siRNA Polyplexes (a) Zeta potential vs. P2C3OHD to siRNA weight ratio plot. Generally, as the weight ratio of P2C3OHD to siRNA increases, the zeta potential increases. As the weight ratio increases above 10, the zeta potential levels off around +22 mV. (b) GFP Knockdown vs. P2C3OHD to siRNA weight ratio plot. As the weight ratio increases, greater knockdown is effected. The knockdown efficiency starts to level off after above a weight ratio of 10. Error bars represent standard deviation.

Sutures coated with $[P2C3OHD/siRNA]_{30}$ in the same manner as before were incubated in water. The releasate was analyzed by DLS and was found to have an average size of 150 nm and an average zeta potential of -10.1 mV. Correlating to Figure C.3a, this would suggest that the releasate may have a weight ratio around 1.5. Correlating this ratio with Figure C.3b, we can recognize that the expected knockdown for this weight ratio is slightly above 20%. This agrees with the average knockdown seen across the substrates in Figure C.2.

C.4 Dose Studies of [P2C3OHD/siRNA] Bilayer

Studies were then performed to determine effects of pH and ionic strength on siRNA and P2C3OHD loading (data not shown). Assembly at pH 6.0 with an ionic strength of 150 mM in the P2C3OHD bath was found to result in a high weight ratio of P2C3OHD to siRNA with good siRNA loading. At this point, the assembly conditions that were chosen were the following: pH 6.0, 150 mM ionic strength, 1 mg/mL P2C3OHD, and 20 μg/mL siRNA. With these conditions, we analyzed the effect of suture dose and number of bilayers on *in vitro* knockdown.

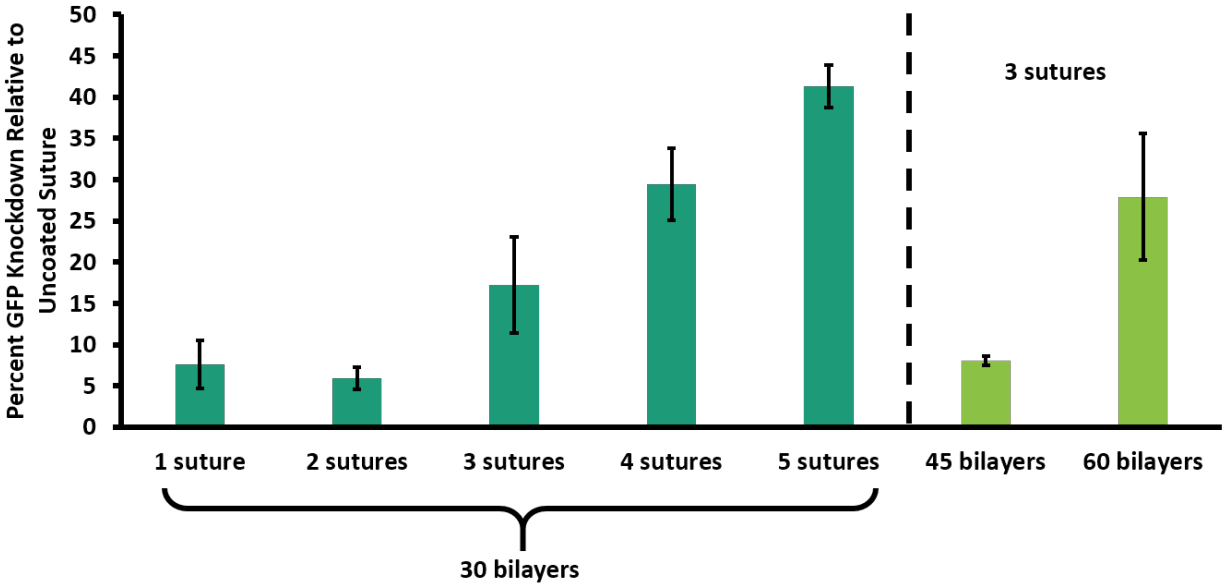

Figure C.4 Knockdown by Varying Suture Number and Bilayers. The [P2C3OHD/siGFP] bilayer was constructed on size 5-0 Vicryl Rapide Suture. The concentration of the P2C3OHD bath was 1 mg/mL, the concentration of the siRNA was 20 µg/mL. The dipping pH was 6.0 and the concentration of buffer in the PBAE bath was 150 mM. The number of sutures applied to each well and the number of bilayers coated were varied. Knockdown was normalized to cells treated with uncoated suture. Error bars represent standard error.

Vicryl Rapide sutures of size 5-0 were coated with $[P2C3OHD/siGFP]_x$ with varying number of bilayers. GFP-expressing HeLa cells were treated with these sutures, and at various doses of suture coated with 30 bilayers (Figure C.4). One suture dose corresponds to a 1 cm piece of suture placed in the well. As expected and previously seen in Appendix A, the increased dose of coated suture resulted in greater knockdown. Over 40% knockdown is achieved when 5 sutures were used. When 60 bilayers were assembled on the suture, greater knockdown was seen compared to 30 bilayers when 3 suture pieces were used. Curiously, the 45 bilayer formulation resulted in less knockdown, this warrants further investigation.

C.5 Loading Studies by Bilayer and Suture Size

We then investigated the difference in loadings with 30 bilayers compared to 60 bilayers. For this study, BCA assay was used to quantify the P2C3OHD (PBAE) and siRNA was quantified by its fluorescent tag. (Later we found that the fluorescent tag affects the BCA reading. While the following data may not reflect completely accurate loadings, we believe comparisons of magnitude are still valid. See Chapter 3 and Appendix B for refined methods in quantification.) While an increase of loadings is seen with 60 bilayers compared to 30 bilayers, the loadings were far from double as initially hypothesized (Figure C.5).

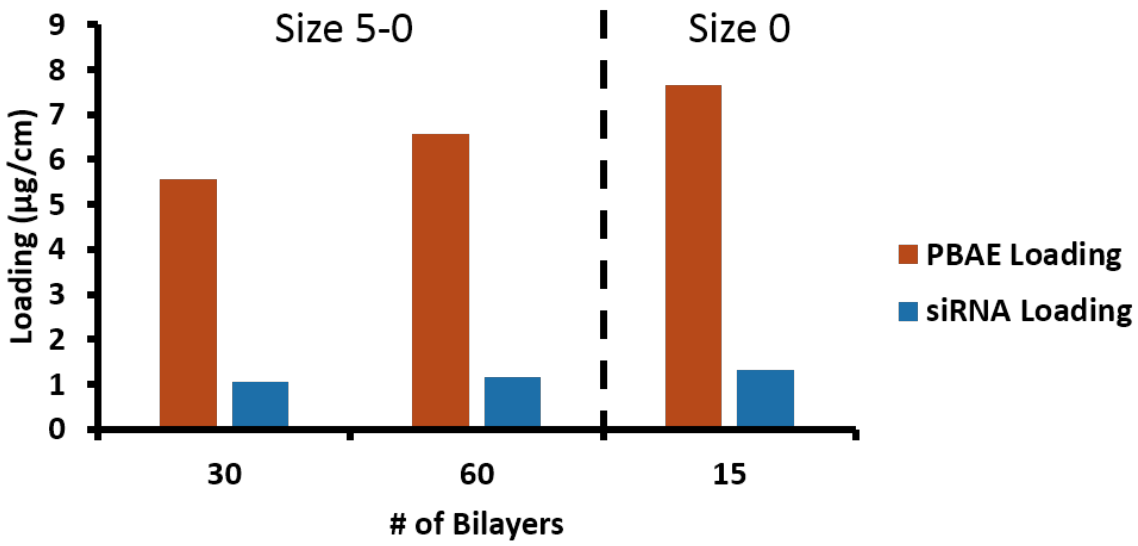

Figure C.5 Loading on Sutures of Varying Sizes and Varied Bilayers The [P2C3OHD/siGFP] bilayer was constructed on size 5-0 Vicryl Rapide Suture and size 0 Vicryl Suture. The concentration of the P2C3OHD (PBAE) bath was 1 mg/mL, the concentration of the siRNA was 20 µg/mL. The dipping pH was 6.0 and the concentration of buffer in the PBAE bath was 150 mM. PBAE and siRNA loading were measured with BCA assay and fluorescence reading respectively.

To further increase loading on a suture, we investigated coating sutures of thicker gauge. A Size 0 Vicryl suture was used. The diameter of the 0 gauge suture is 0.35 mm while the diameter of the 5-0 gauge suture is 0.1 mm. The larger suture was coated with 15 bilayers. With 15 bilayers on the Size 0 suture, loadings exceeded Size 5-0 sutures coated with 30 bilayers, and even with 60 bilayers.

C.6 Final Approach to Assembly Conditions

Taking into account these considerations on size and availability of straight needles, the Vicryl 3-0 suture with a KS 60 mm straight needle was decided upon for the *in vivo* pilot experiments. Further experiments revealed that increasing the siRNA bath concentration leads to increase of siRNA loading and subsequent *in vitro* knockdown. Thus the assembly conditions of pH 6.0, 150 mM ionic strength, 1 mg/mL P2C3OHD, and 25 µg/mL siRNA with size 3-0 Vicryl sutures as the substrate were determined for the work presented in Chapter 4.